Synthetic and Structural Studies on Cyclic π-Systems Surrounded by Rigid σ-Frameworks

Tohru Nishinaga

Division of Energy and Hydrocarbon Chemistry
Graduate School of Engineering
Kyoto University

1995

Contents

Chapter 1 General Introduction 1

Chapter 2 Synthesis, Structure, and Reduction of the Cyclooctatetraene Tetra-Annelated with Bicyclo[2.2.2]octene Frameworks 10

Chapter 3 Properties of the Cation Radical and the Dication of Tetrakis(bicyclo[2.2.2]octeno)cyclooctatetraene 34

Chapter 4 A Polycyclic Pentamer of Bicyclo[2.2.2]octene. A Hydrocarbon Molecule with a Long C-C Single Bond Connecting Two Cofacially Disposed Cyclopentadiene Rings 64

Chapter 5 1,1-Dimethylsila-, -germa-, and -stannacycloheptatrienes Fully Annelated with Bicyclo[2.2.2]octene: Syntheses, Structures, and Properties 86

Chapter 6 A Novel Carbodication Composed of Two Tris(bicyclo[2.2.2]octeno)tropylium Units Connected by a Triple Bond: Synthesis, Structure, and Properties 119

Chapter 7 Syntheses, Properties, and Redox Behaviors of 7-Phenyl-1,2:3,4:5,6-tris(bicyclo[2.2.2]octeno)tropylium Ion and the Dications Composed of Two 1,2:3,4:5,6-Tris(bicyclo[2.2.2]octeno)tropylium Units Connected by *para*- and *meta*-Phenylene Spacers 147

Chapter 8 General Conclusion 167

List of Publications 172

Acknowledgment 173

Chapter 1

General Introduction

Cyclic π-conjugated systems constitute one of the most important classes of compounds in the fields from fundamental to applied chemistry. Today, their various properties are utilized in application as functional materials such as the photo- and thermo-chromic materials, photosensitive materials, liquid crystals, nonlinear optical materials and so on.

The fundamental chemistry of cyclic π-systems, which has influenced the molecular design of these materials, had a turning point at the successful theoretical interpretation of "aromaticity" by E. Hückel in 1930's.[1] Then, the chemistry has developed, keeping pace with the progress of syntheses and theories, and has produced many non-benzenoid aromatic compounds, represented by cyclopropenylium ion (**1**),[2] cyclopentadienide ion (**2**),[3] tropylium ion (**3**),[4] cyclooctatetraene dianion (**4**),[5] and the higher annulenes.[6] Needless to say, it is the π-electron that plays the dominant role in the chemistry of aromatic compounds. One of the main issues in the study in this field has been therefore structural modification of the π-systems for creation of novel electronic properties. Most of such modification includes a structural change in the mode of π conjugation, that is, extension of the π-system by linear or cross-conjugation or by condensation with another π-system. Another effective method of structural modification is the introduction of hetero atoms as typically shown by the example of tetrathiafulvalene (**5**)[7] in comparison of heptafulvalene. On the other hand, the main role of σ-frameworks is considered to control the shape of π-electronic systems. Then, what would happen to the properties of the original π-conjugated system when it is surrounded by rigid σ-frameworks? Not only the inductive effects but the σ–π conjugative

effects would operate to give the π-system new electronic properties. The following findings constitute the background of the present study.

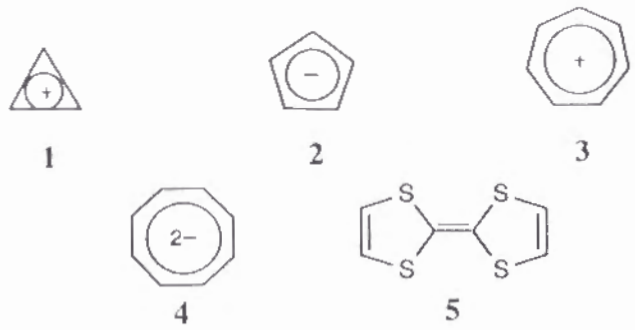

1 2 3 4 5

For stabilization of a cyclopropenylium ion, the substitution with cyclopropyl groups was shown to be far more effective than that with simple alkyl groups which were expected to exert their inductive electron donation.[8] The π-conjugation with phenyl groups were proved to be less effective than the contribution of alkyl groups.[9] These facts indicate that the σ–π conjugation with the cyclopropyl groups is quite important in stabilization of this cationic species. In a series of substituted tropylium ions, the same order of substituent effects was observed. However, there was observed some saturation effect for stabilization as the number of cyclopropyl groups increased.[10]

This is apparently due to the possible free rotation of the cyclopropyl group: as the cation becomes more stabilized, the cyclopropyl group tends to be less confined to the stabilizing bisected conformation. Thus, prior to the present study, an examination had been made concerning the effect of annelation of a tropylium ion with rigid σ-frameworks which can provide the σ-bonds fixed at the position nearly parallel to the 2p-orbitals of the π-systems. As shown in Table 1, the tropylium ion **8** annelated with a highly strained bicyclic system, bicyclo-[2.1.1]hexene, however, was destabilized compared with 1,4-di-*t*-butyl- (**6**) or 1,4-dicyclopropyl derivative (**7**) due to the increased angle strain caused by such a

Table 1. Comparison of pK_{R+} Value and Reduction Potential (E_{red}) for Representative Disubstituted Tropylium Ions.

Tropylium ion	 **3**[a]	 **6**[a]	 **7**[a]	 **8**[b]	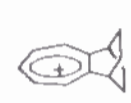 **9**[b]
pK_{R+} (CH_3CN–H_2O (1:1))	3.88	5.42	7.63	5.10	7.80
E_{red} (CH_3CN) V vs Ag/Ag^+	–0.51	–0.72	–0.76	–0.71	–0.77
Substituent Effects	None	Inductive	σ-conjugative	σ-conjugative *minus* angle strain	σ-conjugative *plus* Inductive

[a] ref. 10. [b] ref. 11.

strained system.[11] In contrast, annelation with a much less strained bicyclo[2.2.2]octene (BCO) unit, as in the cation **9**, was found to be nearly as effective as substitution with two cyclopropyl groups in stabilizing the cation. These findings led to the synthesis of a tropylium ion tris-annelated with BCO units **10**, which exhibited an extraordinary stability (pK_{R+} ~ 13.0).[12]

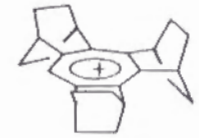

10

The synthesis of cation **10** started with a linear combination of BCO units. As shown in Scheme 1, 2,3–dibromobicyclo[2.2.2]octene (**11**) was made to react with *n*–butyllithium at −78 °C in THF to give a series of the BCO oligomers **13** (*n* = 2–5) by a rather unexpected reaction involving a highly strained acetylene **12** as an intermediate. The reductive cyclization of **13** (*n* = 3) afforded a highly symmetrical benzene **14** in good yield,[13] which was then converted to **10** via ring expansion and hydride abstraction.[12]

Scheme I

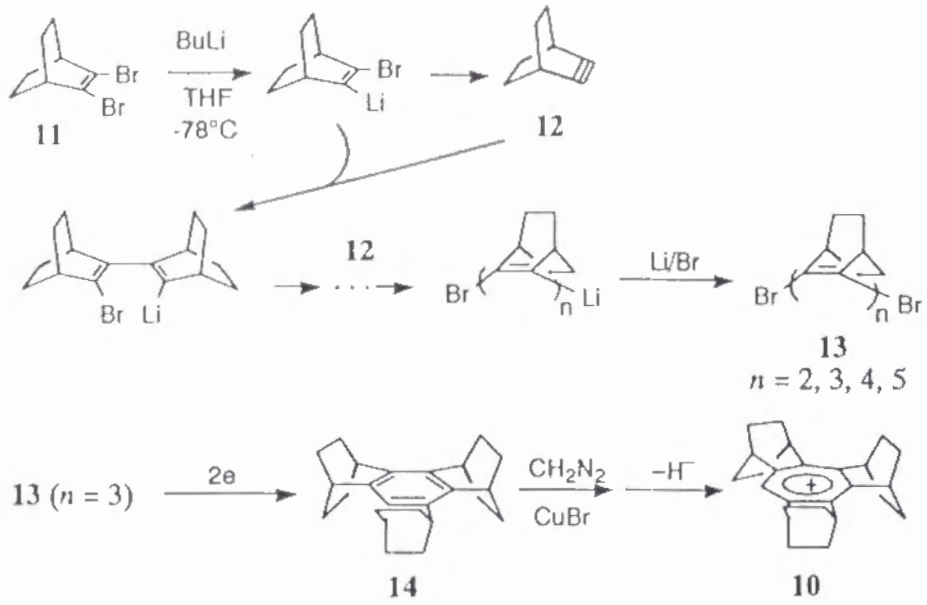

Such full annelation with BCO units was effective in stabilizing not only the cationic closed-shell compound but also the cationic open-shell species. The electrolytically generated cation radical of benzene **14** was stable even at room temperature under an inert atmosphere.[13] This remarkable stability is attributed to both the electronic and steric effects of the rigid σ-frameworks. Particularly effective is the so-called "Bredt's rule protection",[14] since the supposedly most labile α-hydrogen of the σ-frameworks is protected from deprotonation according to "Bredt's rule".

Based on these results of the foregoing research, the chemistry of cyclic π-systems fully annelated with the BCO unit has been further extended in the present study. The following two chapters are concerned with the products obtained by the reductive cyclization of tetramer **13** (n = 4), that is, the cyclooctatetraene (COT) tetra-annelated with BCO frameworks (**15**). Thus, in Chapter 2, the synthesis of COT **15** is described. Its tub-shape structure was clarified by X-ray crystallographic study, and the rigidity of the central eight-membered ring of **15** was confirmed by both experimental and theoretical approaches. In order to inspect the possibility of formation of the planar conformation, the generation of the 10π aromatic dianion was investigated using the NMR technique.

15

As described above, the annelation with BCO frameworks is quite effective for the stabilization of both closed- and open-shell cationic systems. The properties of the cation radical and the dication of **15** are of particular interest, since only little is known about cation radical[15] and dication[16] of COT in spite of their theoretical importance. In Chapter 3 are described the structure of $\mathbf{15}^{\cdot+}SbCl_6^-$ determined by X-ray crystal analysis and the structure of the 6π aromatic dication $\mathbf{15}^{2+}$ observed by variable-temperature ^{13}C NMR. The former is the first example of a COT cation radical ever isolated as a stable crystal and its X-ray structure determined. Dication $\mathbf{15}^{2+}$ is also the first example of a COT dication that is stable at room temperature in solution. These two species are the most typical examples which represent the effectiveness of BCO annelation in stabilization of cationic π-systems. Theoretical interpretations of electronic states and electronic spectra of these species are also made.

In Chapter 4, the product of the reductive cyclization of BCO pentamer **13** (n = 5) is described. The product is not a cyclodecapentaene derivative, which would have been formed by cyclization occurring at both ends of pentamer **13** (n = 5), but a bicyclo[2.2.2]octane having two spiro-connected cyclopentadiene rings at the vicinal carbons, i.e., hydrocarbon **16**. The most remarkable feature of the

X-ray structure of **16** is unusual elongation of the central C–C bond connecting the two cofacially disposed cyclopentadiene rings. The major contributing factor of the bond elongation is discussed based on the theoretical consideration with the aid of molecular mechanics and molecular orbital calculations.

16

Chapter 5 deals with syntheses, crystal structures and properties of the silepin (**17**), germepin (**18**) and stannepin (**19**) tris-annelated with the BCO frameworks. Previously silepins were studied in search for a possibility of cyclic (p–d)π conjugation.[17] Also stannepins have attracted interest as a precursor of borepins.[18] Interest in silepins and borepins is mainly derived from a possibility of the tropylium-like stabilization effect by the cyclic delocalization of six π-electrons over the whole ring system. As has been mentioned above, the heterepins **17, 18** and **19** have the structural characteristics suitable for stabilizing tropylium ion.[12] For discussion of such π-electron delocalization in this class of compounds, it is important to estimate the stability of the central seven-membered ring in a planar conformation. However, none of such experimental data have been obtained in spite of several attempts.[17,19] In this chapter, the results of first successful X-ray determination of the structures of heterepins containing Group 14 elements are discussed together with the barrier for ring inversion in solution.

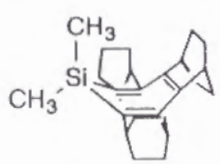

17

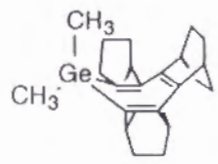

18

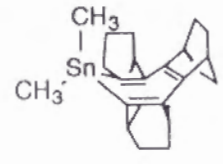

19

The next two chapters are concerned with the newly synthesized carbodications which are composed of two units of the tropylium ion **10** connected by several different π-conjugative spacers. In Chapter 6 is described the dication composed of the two units of **10** connected by acetylene (**20**) and in Chapter 7 the similar dication connected by *para*-(**21**) and *meta*-(**22**) phenylene spacers.

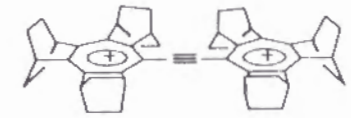

20

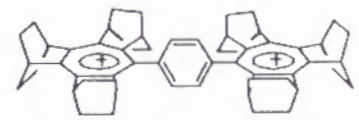

21

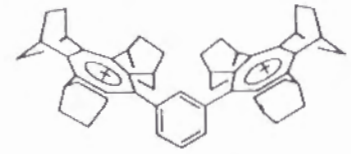

22

As to the parent tropylium ion substituted with an ethynyl group, the arylethynyl derivatives are known,[20] but there has been no report on the dication with two tropylium units at both sides of acetylene. This seems to be ascribed to the extreme instability of a possible precursor, ethynylcycloheptatriene. The use of BCO-annelated cycloheptatriene is therefore advantageous because of kinetic stability due to the bulky and rigid σ-frameworks. On the other hand, the parent dication with two tropylium units connected by phenylene spacer have already been prepared,[21] but no properties except some NMR data have been examined. It is of particular interest to investigate the one- and two-electron reduction of these novel carbodications. The full annelation with BCO units could stabilize the formed tropyl radical owing to severe steric hindrance for dimerization and also due to lack of any hydrogen atom that could be abstracted from the radical. It should also be discussed whether the singlet or triplet state would be formed upon

two-electron reduction of dications **20**, **21** and **22**. From these viewpoints, there are described the synthesis, full characterization of these dications, their thermodynamic stability, and redox behaviors observed by cyclic voltammetry and ESR in Chapter 6 and 7.

In the last chapter, the concluding remarks throughout these studies are given.

References and Notes

(1) (a) Hückel, E. *Physik.* **1931**, *70*, 204. (b) Hückel, E. *Physik.* **1937**, *76*, 204. (c)Hückel, E. *Electrochem.* **1937**, *43*, 752.

(2) For example, Breslow, R; Groves, J. T. *J. Am. Chem. Soc.*, **1970**, *92*, 984.

(3) For example, Webster, O. W. *J. Am. Chem. Soc.*, **1966**, *88*, 3046.

(4) Doering, W. von E.; Knox, L. H. *J. Am. Chem. Soc.*, **1954**, *76*, 3203.

(5) Katz, T. J. *J. Am. Chem. Soc.*, **1960**, *82*, 3784.

(6) Sondheimer, F. *Acc. Chem. Res.*, **1972**, *5*, 81.

(7) Wudl, F.; Wobschall, D.; Hufnagel, E. J. *J. Am. Chem. Soc.*, **1972**, *94*, 670.

(8) (a) Kerber, R. C.; Hsu, C-M. *J. Am. Chem. Soc.*, **1973**, *95*, 3239. (b) Komatsu, K.; Tomiokla, I. Okamoto, K. *Tetrahedron Lett.*, **1980**, *21*, 947. (c) Moss, R. A.; Munjal, R. C. *Tetrahedron Lett.*, **1980**, *21*, 1221. (d) Moss, R. A.; Schen, S.; Krogh-Jespersen, K.; Potenza, J. A.; Schugar, H. J.; Munjar, R. C. *J. Am. Chem. Soc.*, **1986**, *108*, 134.

(9) Breslow, R.; Hover, H.; Chang, H. W. *J. Am. Chem. Soc.*, **1962**, *84*, 3168.

(10) Komatsu, K.; Takeuchi, K.; Arima, M.; Waki, Y.; Shirai, S. Okamoto, K. *Bull, Chem, Soc, Jpn.*, **1982**, *55*, 3257.

(11) Komatsu, K.; Akamatsu, H.; Okamoto, K. *Tetrahedron Lett.*, **1987**, *28*, 5889.

(12) (a) Komatsu, K.; Akamatsu, H.; Jinbu, Y.; Okamoto, K. *J. Am. Chem. Soc.*, **1988**, *110*, 633. (b) Komatsu, K.; Akamatsu, H.; Aonuma, S.; Jinbu, Y.; Maekawa, N. *Tetrahedron*, **1991**, *47*, 6951.

(13) Komatsu, K.; Aonuma, S.; Jinbu, Y.; Tsuji, R.; Hirosawa, C.; Takeuchi, K. *J. Org. Chem.*, **1991**, *56*, 195.

(14) (a) Nelsen, S. F.; Kessel, C. R. *J. Am. Chem. Soc.*, **1979**, *101*, 2503. (b) Nelsen, S. F.; Kessel, C. R.; Brien, D. J. *J. Am. Chem. Soc.*, **1980**, *102*, 702.

(15) (a) Desseau, R. M. *J. Am. Chem. Soc.* **1970**, *92*, 6356-6358. (b) Shida, T.; Iwata, S. *J. Am. Chem. Soc.* **1973**, *95*, 3473-3483. (c) Dai, S.; Wang, J. T.; Williams, F. *J. Am. Chem. Soc.* **1990**, *112*, 2837-2839.

(16) Olah, G. A.; Staral, J. S.; Liang, G.; Paquette, L. A.; Melega, W. P.; Carmody, M. J. *J. Am. Chem. Soc.* **1977**, *99*, 3349-3355.

(17) (a) Cartledge, F. K.; Mollere, P. D. *J. Organomet. Chem.*. **1971**, *26*, 175–181. (b) Barton, T. J.; Volz, W. E.; Johnson, J. L. *J. Org. Chem.*. **1971**, *36*, 3365–3367. (c) Barton, T. J.; Kippenhan, Jr., R. C.; Nelson, A. J. *J. Am. Chem. Soc.* **1974**, *96*, 2272–2273.

(18) Sugihara, Y.; Yagi, T.; Murata, I. *J. Am. Chem. Soc.* **1992**, *114*, 1479–1481, and references are cited therein.

(19) (a) Corey, J. Y.; Corey, E. R. *Tetrahedron Lett.*. **1972**, 4669–4672. (b) Nakadaira, Y.; Sato, R.; Sakurai, H. *Organometallics*, **1991**, *10*, 435–442.

(20) Jutz, C.; Voithenleitner, F. *Chem. Ber.* **1964**, *97*, 1337-1348.

(21) (a) Murray, R. W.; Kaplan, M. L. *Tetrahedron Lett*. **1965**, 2903-2909.(b) Murray, R. W.; Kaplan, M. L. *Tetrahedron Lett*. **1967**, 1307-1312.

Chapter 2

Synthesis, Structure, and Reduction of the Cyclooctatetraene Tetra-Annelated with Bicyclo[2.2.2]octene Frameworks

Abstract

A new cyclooctatetraene (COT) fully annelated with bicylo[2.2.2]octene (BCO) units, tetrakis(bicyclo[2.2.2]octeno)cyclooctatetraene (**4**) was synthesized by reductive cyclization of the α,ω-dibromide of BCO tetramer **3** (n = 4) with 2–3 equiv sodium naphthalenide in THF at room temperature, in 20% yield. The main product of this reaction was tris(bicyclo[2.2.2]octeno)benzene (**1**) formed by elimination of one BCO unit in 40 % yield. The X-ray structure of **4** showed that the central COT ring has a tub-structure with the external dihedral angle for bending of the tub-structure ranging from 41.3° to 44.9°. The ^{13}C NMR spectrum of **4** at room temperature showed signals for one olefinic carbon, one bridgehead carbon, and two types of methylene carbons, indicating that the COT **4** is fixed at D_{2d} symmetric tub-structure in an NMR time scale. No line broadening was observed for any of these ^{13}C NMR signals at 22.5 MHz in nitrobenzene–d_5 at the temperature up to 150 °C; the barrier for ring inversion is calculated to be larger than 24 kcal mol^{-1} at least. The molecular mechanics calculations also predicted that the structure with the planar eight-membered ring would be destabilized by 53.9 kcal mol^{-1}. Nevertheless, COT **4** was readily reduced to the planar dianion $\mathbf{4}^{2-}$ with potassium mirror in THF–d_8 at room temperature, clearly demonstrating the aromatic stabilization of 10π electron system.

Introduction

Cyclooctatetraene (COT) drew attention as the vinylog of benzene when it was first prepared by Willstätter in 1911.[1] This interest was further intensified by Hückel's proposal[2] in 1937 that a 4n π-electron cyclic system should possess an unfavorable electronic delocalization in contrast to the stability in 4n+2 π-electron system. That COT itself could exist as a stable molecule in spite of the presence of 8π-electrons was made explicable by its structural characterization as a non-planar "tub" form[3] possessing alternating double and single bonds.[4] This structural feature enables COT to have two possibilities for its structural change. Ring inversion (eq. 1) proceeds via a planar transition state with alternating bonds. Extensive measurements on inversion barriers of COTs have been made.[5] The value of the inversion barriers reflects a structural flexibility of the COT ring. The second possibility, the bond shifting (eq. 2), usually requires a higher activation energy than simple ring inversion because the transition state involves a cyclic conjugation of 8π-electrons which is highly destabilized as a typical antiaromatic system.[5,6] On the other hand, recent work by Paquette[7] has implicated a pseudo rotation mechanism that avoids the antiaromatic nature of a fully conjugated transition state for the bond shifting process.

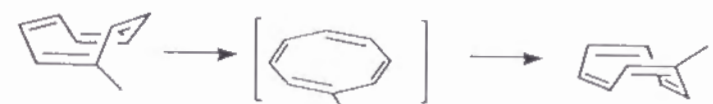
(eq. 1)

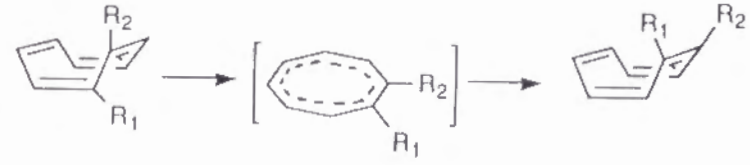

(eq. 2)

Two-electron reduction of COT gives the COT dianion (eq. 3),[8] which is a stable 10π-aromatic compound possessing a planar geometry in most cases. The X-ray structure of the 1,3,5,7-tetramethylcyclooctatetraene dianion has experimentally verified the planarity of the central ring.[9] However, the dianions of di- and tribenzo-COT derivatives were shown to have a non-planar COT ring.[10] Thus, the essentially planar structure of the COT dianion seems to be severely influenced by the steric effect around the COT ring.

(eq. 3)

On the other hand, it has previously been shown that the combination of steric and electronic effects of specially arranged σ-frameworks can endow new properties to the original π-systems especially when they are positively charged as in the case of cation radical of benzene **1**[11b] and tropylium ion **2**.[12] However, no such effects have been examined for carbanionic systems. For the synthesis of benzene derivative **1**, reductive cyclization of the trimeric dibromide **3** (n = 3)[11b] was found to be quite successful.[11] In this chapter is described, the synthesis of a new cyclooctatetraene **4** tetra-annelated with BCO units using the same method as in **1** together with its structural properties and two-electron reduction to the dianion.

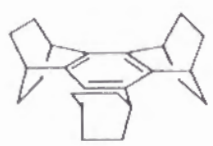

1

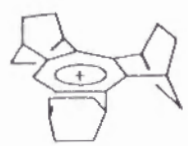

2

3

4

Results and Discussion

MM2 Calculations on the Favored Conformations of BCO Oligomers. The starting material for this work, that is, the dibromide of BCO-tetramer, **3** (n = 4), was isolated from a mixture of oligomers **3** (n = 2–5), which were obtained via generation of bicyclo[2.2.2]octyne by lithiation of monomeric dibromide **3** (n = 1) followed by LiBr elimination (see Scheme 1 in Chapter 1).[11b]

In the previous work, two-electron reduction of the terminal dibromide of BCO trimer **3** (n = 3) with sodium naphthalenide was shown to give benzene **1** in high yield (89%).[11] As to the cyclization mechanism of **3** (n = 3), the key reaction was considered to be an intramolecular cyclization of a σ-radical **5** (Scheme 1) formed by "dissociative electron-transfer",[13] i.e., one-electron reduction with concomitant elimination of the bromide ion. In order to rationalize the occurrence of such a cyclization, the conformation of a series of BCO oligomers was examined by molecular mechanics calculations using the MM2 method.[14]

Scheme 1

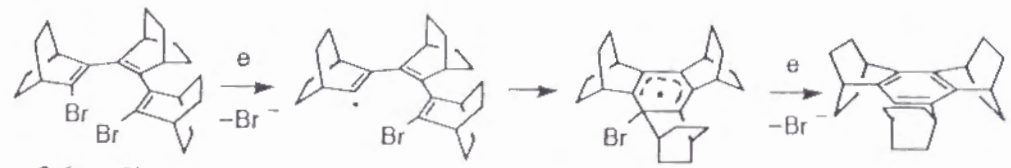

3 (n = 3) **5** **1**

Since some of the parameters needed for full manipulation of bromo-substituted compounds were not available in the MM2 program,[14] calculations were conducted on oligomeric hydrocarbons **6** instead. The MM2 calculations were carried out to obtain the optimized geometry as well as the steric energies for all the possible conformers of each of

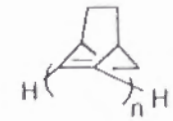

6

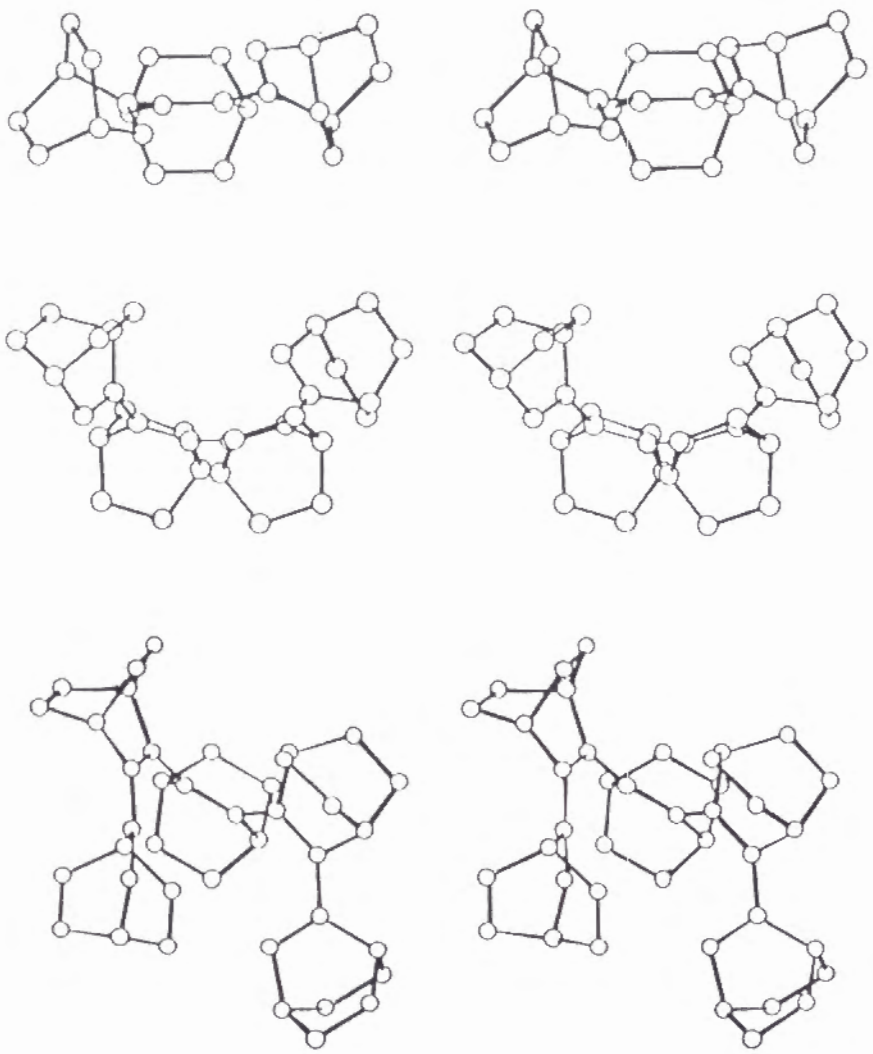

Figure 1. Stereoviews of MM2-minimized structures for the most stable conformation of **6** (n = 3), **6** (n = 4) and **6** (n = 5) from the top. Hydrogens are omitted for clarity.

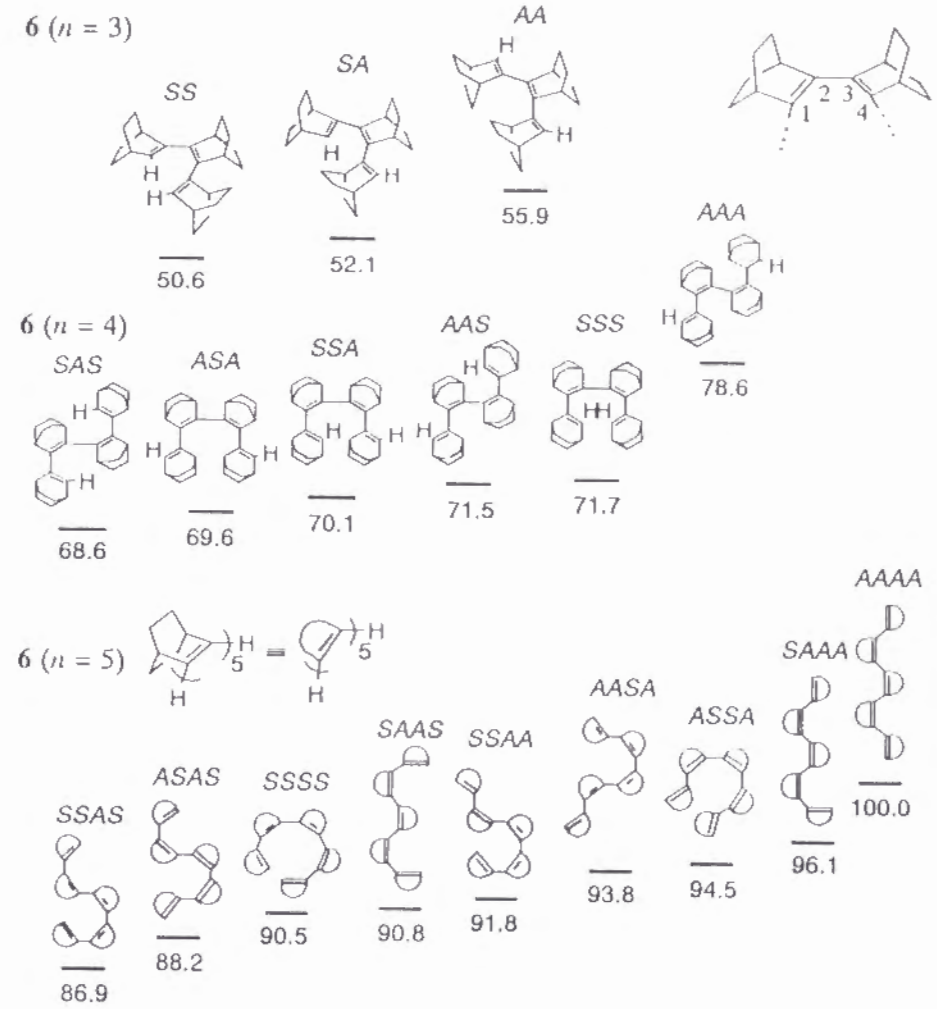

Figure 2. Schematic presentation of the possible conformers and steric energies (kcal mol^{-1}) calculated for the MM2-minimized structure of each conformation of **6** (n = 3,4 and 5). Combination of the relative conformation with respect to each single bond is shown on each structure: *S* refers to *syn* ($-90° < \theta < 90°$), and *A* to *anti* ($-180° < \theta < -90°$ or $90° < \theta < 180°$), where θ is the dihedral angle −1234 shown at the top. For the value of θ calculated for each conformer, see the Experimental Section.

the oligomers **6** (n = 3, 4 and 5). The results are shown in Figure 1 and schematically in Figure 2. Although the rotational barrier is quite small for each of the connecting single bonds,[15] and the molecules should be quite flexible, there seems to be a preference for specific conformations for each of the oligomers due to intramolecular nonbonded interactions between the BCO units.

Though, of course, these hydrocarbon structures can not be simply related to the conformation of dibromides **3**, they might serve as models of the neutral σ-radicals such as **5** in Scheme 1, which are about to undergo the intramolecular cyclization. Thus, the all-*syn* conformation, which is quite close to the structure of benzene **1**, is the most favorable for trimer **6** (n = 3). However, the conformation containing one *anti* fragment (the *SAS* conformation) is favored for tetramer **6** (n = 4) rather than the all-*syn* conformation, due to the steric repulsion between both terminal BCO units.

Synthesis of Cyclooctatetraene 4. Exactly in the same manner as in the case of synthesis of benzene **1**, the reaction of tetrameric dibromide **3** (n = 4) was carried out with 2–3 equiv of sodium naphthalenide in THF at 0 °C. Separation of the products by chromatography over SiO_2 impregnated with $AgNO_3$ (7 %) afforded the expected COT **4** in 20 % yield. However, the main product of this reaction was the ring-contracted benzene **1** (40 % yield). A control experiment showed that **4** could not be converted to **1** under the present conditions nor at a higher temperature such as 250 °C.

These results could be explained by the reaction pathway shown in Scheme 2. First, the σ-radical **7**, with a conformation probably similar to the most stable conformation of **6** (n = 4), is formed by the dissociative electron transfer. Between the two possible sites of cyclization, carbon *a* and carbon *b*, carbon *a* would be somewhat more favored because of the formation of a less strained six-membered ring, whereas the cyclization at carbon *b* would require the whole

molecule to take a preorganized structure close to a tub-form of COT. Then, the second one-electron reduction of the cyclized radicals followed by ejection of the bromide ion or the 3-bromobicyclo[2.2.2]oct-2-en-2-yl anion affords the hydrocarbon **4** or **1**, respectively.

Scheme 2

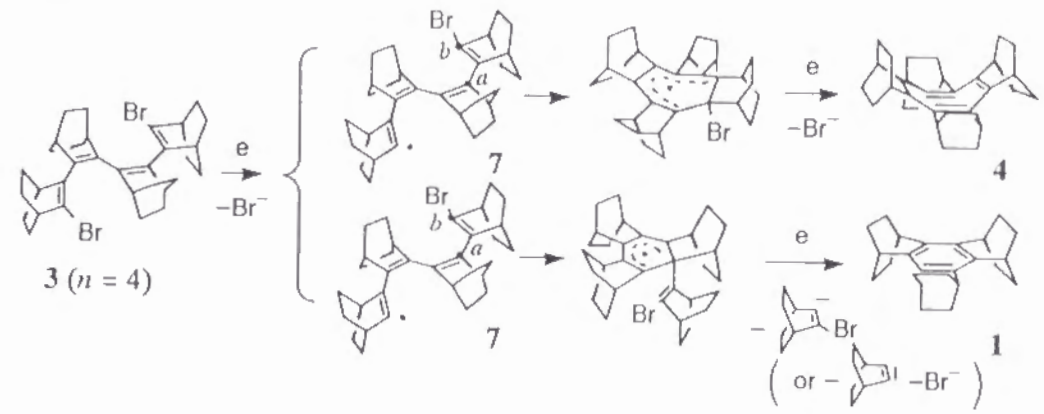

Structure of COT 4. The structure of newly synthesized COT **4** was determined by X-ray crystallography as shown in Figure 3. The bond lengths and angles are given in Tables 1 and 2. The observed external dihedral angle (α) for the tub-shaped COT ring ranges from 41.3° to 44.9°. In a series of COT annelated with cycloalkene unit **8**, the COT ring has been shown to become less puckered as the size of the cycloalkene is reduced.[16] In contrast, reported data of X-ray structure analysis revealed that the octasubstituted COT (C_8R_8, **9**) becomes more puckered as the bulkiness of the substituent (R) increases (α and α', 41.7°

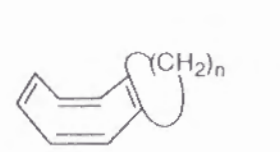

8

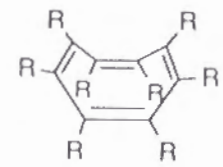

9

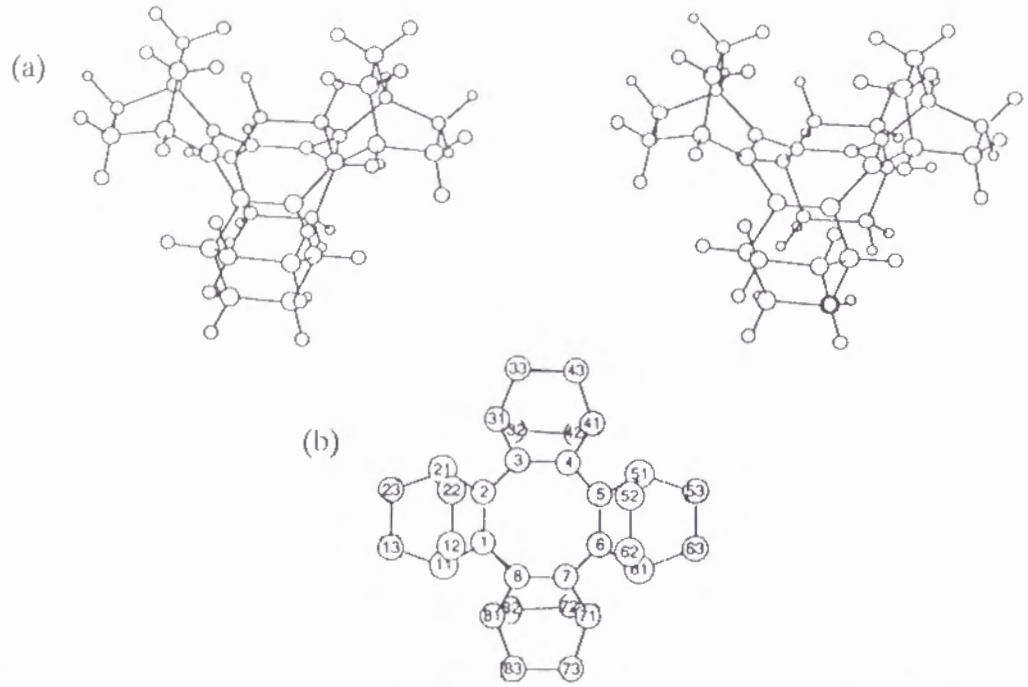

Figure 3. (a) Stereoscopic and (b) top view of the X-ray crystal structure of **4**.

Table 1. Observed Bond Lengths of **4** (ESD of Bond Lengths: 0.003Å)

Bond Length(Å)		Bond Length(Å)	
C1-C2	1.339	C21-C22	1.545
C1-C8	1.475	C21-C23	1.535
C1-C11	1.516	C31-C32	1.541
C2-C3	1.465	C31-C33	1.531
C2-C21	1.522	C32-C42	1.530
C3-C4	1.342	C33-C43	1.537
C3-C31	1.520	C41-C42	1.544
C4-C5	1.469	C41-C43	1.534
C4-C41	1.507	C51-C52	1.530
C5-C6	1.331	C51-C53	1.536
C5-C51	1.514	C52-C62	1.540
C6-C7	1.464	C53-C63	1.528
C6-C61	1.521	C61-C62	1.522
C7-C8	1.336	C61-C63	1.536
C7-C71	1.517	C71-C72	1.542
C8-C1	1.475	C71-C73	1.534
C8-C81	1.515	C72-C82	1.533
C11-C12	1.538	C73-C83	1.531
C11-C13	1.532	C81-C82	1.536
C12-C22	1.538	C81-C83	1.544
C13-C23	1.540		

Table 2. Observed Bond Angles of **4** (ESD of Bond Angles: 0.2 deg)

Bond Angles(deg)		Bond Angles(deg)	
C2-C1-C8	126.57	C12-C22-C21	108.59
C2-C1-C11	113.56	C13-C23-C21	109.27
C8-C1-C11	119.81	C3-C31-C32	107.62
C1-C2-C3	126.24	C3-C31-C33	109.12
C1-C2-C21	113.34	C32-C31-C33	107.96
C3-C2-C21	120.40	C31-C32-C42	109.40
C2-C3-C4	126.15	C31-C33-C43	109.28
C2-C3-C31	121.08	C4-C41-C42	107.42
C4-C3-C31	112.75	C4-C41-C43	108.24
C3-C4-C5	126.64	C42-C41-C43	108.23
C3-C4-C41	114.46	C32-C42-C41	109.40
C5-C4-C41	118.89	C33-C43-C41	109.49
C4-C5-C6	125.89	C5-C51-C52	107.76
C4-C5-C51	120.56	C5-C51-C53	109.04
C6-C5-C51	113.37	C52-C51-C53	108.07
C5-C6-C7	126.45	C51-C52-C62	109.43
C5-C6-C61	113.55	C51-C53-C63	109.01
C7-C6-C61	120.01	C6-C61-C62	107.08
C6-C7-C8	126.51	C6-C61-C63	109.02
C6-C7-C71	119.66	C62-C61-C63	108.90
C8-C7-C71	113.73	C52-C62-C61	108.75
C1-C8-C7	127.05	C53-C63-C61	109.42
C1-C8-C81	119.12	C7-C71-C72	107.38
C7-C8-C81	113.76	C7-C71-C73	108.91
C1-C11-C12	107.63	C72-C71-C73	108.01
C1-C11-C13	108.62	C71-C72-C82	109.39
C12-C11-C13	108.76	C71-C73-C83	109.09
C11-C12-C22	109.64	C8-C81-C82	107.47
C11-C13-C23	109.08	C8-C81-C83	108.17
C2-C21-C22	107.51	C82-C81-C83	108.02
C2-C21-C23	109.16	C72-C82-C81	109.49
C22-C21-C23	108.27	C73-C83-C81	109.86

and 41.0° for R = F;[17] 52.8° and 49.7° for R = CH_3;[4b] 58.0° and 53.3° for R = C_6H_5[18]). These two effects seem to be balanced in the present COT derivative **4** to give the observed values of α (an averaged value 42.4°).

The structure of **4** obtained by molecular mechanics calculation with MM2(87) agreed well with the one determined by X-ray analysis, although the calculated value of α (46.4°) was larger than the observed value 42.4°. The calculated steric energy (69.6 kcal mol^{-1}) was nearly four times that for bicyclo-[2.2.2]octene (18.27 x 4 = 73.1 kcal mol^{-1}), indicating that no additional strain is accumulated in the molecule of COT **4**.

Structural Flexibility of COT 4 and Its Two-electron Reduction. Intuitively the ring inversion of the COT **4** appears to require quite high energy due to the presence of rigid BCO frameworks with sticking-out bridgehead hydrogens. Besides, the bond shifting is not feasible since this will also result in a planar structure **10**.

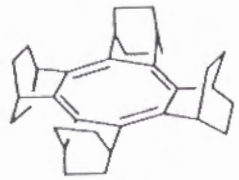

10

The ^{13}C NMR spectrum of COT **4** at room temperature showed signals for one olefinic carbon, one bridgehead carbon and two types of methylene carbon. This indicates that COT **4** is fixed at D_{2d} symmetric tub-structure in an NMR time scale. No line broadening was observed for any of these ^{13}C NMR signals at 22.5 MHz in nitrobenzene-d_5 at the temperature up to 150 °C and, therefore, the barrier for ring inversion is calculated to be larger than 24 kcal mol^{-1} at least. The molecular mechanics calculations (MM2) indicated that the COT **4** with a

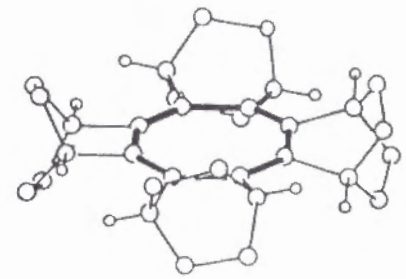

Figure 4. MM2 Calculated structure of **4** with a planar central COT ring. The methylene hydrogens are omitted for clarity.

planar central ring has the steric energy higher than the tub form by 53.9 kcal mol^{-1} and that the surrounding bicyclic units are tilted by *ca*. 17° due to steric repulsion between the bridgehead hydrogens as shown in Figure 4.

In spite of such disadvantage for planarity, COT **4** was smoothly reduced to orange-colored[19] dianion $\mathbf{4}^{2-}$ (λ_{max} (THF) 266, 357 nm) upon treatment with potassium mirror in THF–d_8 in a vacuum-sealed tube (Scheme 3). As shown in Figure 5, the ^{13}C NMR signal for the central ring of $\mathbf{4}^{2-}$ was upfield shifted as had been expected from the Spiesecke–Sneider correlation[20] ($\delta_{C\text{-}13}$ (calc) = 140.0–(2e/8C)x160 = 100.0; obsd, 97.8), while the bridging ethylene carbons exhibited one sharp signal and this signal did not broaden even at −60 °C supporting an essentially planar COT^{2-} structure. In good agreement, the ^1H NMR signal for the bridgehead protons is down-field shifted relative to **4** due to the effect of diamagnetic ring current. The hydrocarbon **4** was quantitatively recovered upon air oxidation of the dianion $\mathbf{4}^{2-}$.

Scheme 3

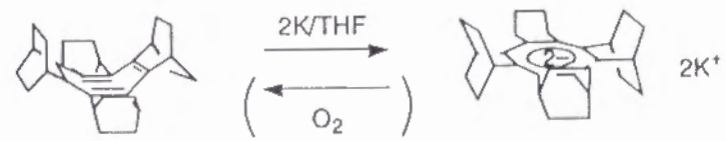

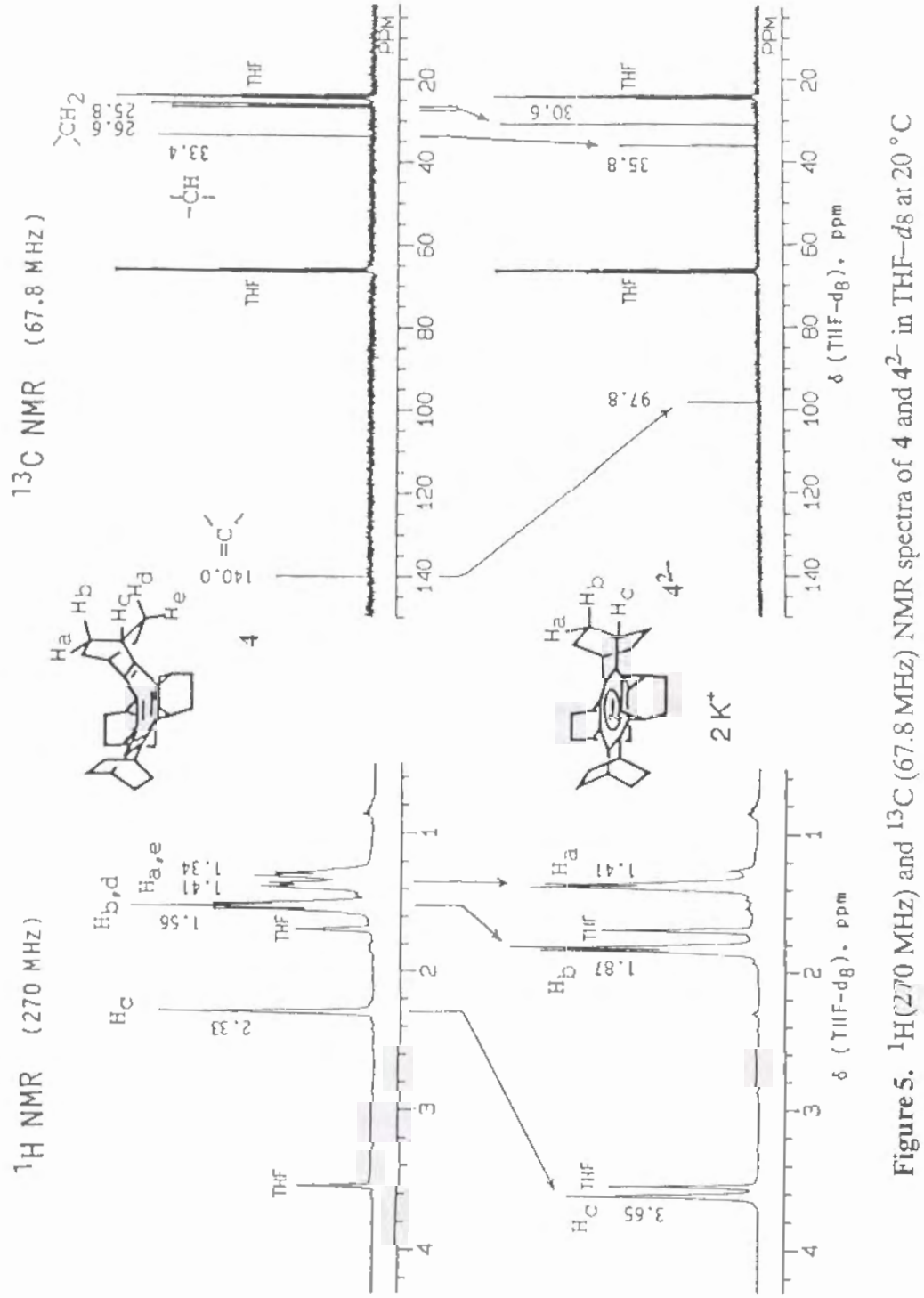

Figure 5. ^{1}H(270 MHz) and ^{13}C (67.8 MHz) NMR spectra of **4** and $\mathbf{4}^{2-}$ in THF–d_8 at 20 °C

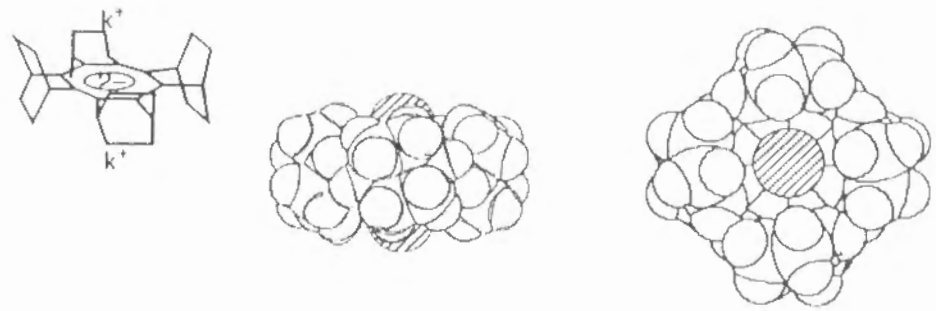

Figure 6. The space filling model for planar dianion $\mathbf{4}^{2-}$ by AM1 calculation. The counter cations ($2K^+$) are placed at the nearly same position as observed previously.[9]

Thus, it is supposed that the gain of 10π aromatic stabilization has overcome the steric disadvantage mentioned above. It would also be possible that the planar structure is more advantageous in ion-pairing with K^+ at the both sides of the ring as shown in Figure 6.

Experimental Section

General Procedures. Melting points were determined on a Yamato MP–21 apparatus and are uncorrected. Elemental analysis was performed by Microanalytical Center, Kyoto University, Kyoto. NMR spectra were recorded on JEOL GSX270 (270 MHz for ^{1}H and 67.8 MHz for ^{13}C NMR) or on JEOL FX90 (90 MHz for ^{1}H and 22.5 MHz for ^{13}C NMR) spectrometers using Me_4Si as an internal standard, unless otherwise noted. IR spectra were taken on Hitachi 215 or Perkin Elmer 1640 spectrometer. UV–vis spectra were taken on Hitachi 200–10 spectrometer. A Sartorius 4503MP6 microbalance was employed for weighing

samples less than 1 mg. MM2 calculations were carried out on a FACOM M780 computer at the Date Processing Center of Kyoto University.

THF was freshly distilled from sodium benzophenone ketyl before use. All reactions where anhydrous conditions were required were conducted under an atmosphere of argon or nitrogen. The dibromide of BCO tetramer, **3** (n = 4), was prepared by the method previously reported.[11b]

MM2 Calculations of Bicyclo[2.2.2]oct-2-ene-2,3-diyl Oligomers 6 (n = 2–5). **(a) Dimer 6 (n = 2).** MM2 calculations were performed on dimer **6** (n = 2) with the dihedral angle θ (∠1234; see Figure 2) varied by increments of 10°. The energy-minimized structures were those with θ of 20° ("*syn*" conformer; steric energy (SE) = 33.4 kcal mol^{-1}) and 160° ("*anti*"; SE = 33.7 kcal mol^{-1}). The SE for the energy-maximum structure with θ = 90° was 36.9 kcal mol^{-1}.

(b) Trimer 6 (n = 3). The calculations were conducted for six conformers made from all possible combinations of the most likely values of θ (taken from the above-mentioned results for **6** (n = 2); θ (*syn*) = 20° and θ (*anti*) = 160°) for the two single bonds connecting the BCO units, and for four extra conformers that appeared possible from inspection of a molecular model. All the input structures converged into three conformers as the energy-minimized structures. The values of θ_1, θ_2, and SE for each of the calculated structures are: conformer *SS* (*syn*, *syn*); θ_1 = 38.4°, θ_2 = 38.4°; SE = 50.6 kcal mol^{-1}: *SA* (*syn*, *anti*); 43.3°, −149.9°; 52.1 kcal mol^{-1}: *AA* (*anti*, *anti*); 149.3°, 152.2°; 55.9 kcal mol^{-1}.

(c) Tetramer 6 (n = 4). Similarly, structure optimizations were performed for all six *syn*/*anti* conformers made from the most suitable values of θ for each of the single bond rotamers obtained from the results for **6** (n = 4), and six extra conformers, to give the following energy-minimized structures: conformer *SAS*; θ_1 = 38.7°, θ_2 = −148.4°, θ_3 = 38.7°; SE = 68.6 kcal mol^{-1}: *ASA*; 151.0°, 54.8°, 151.0°; 69.6 kcal mol^{-1}: *SSA*; 35.8°, 52.8°, −150.8°; 70.1 kcal mol^{-1}: *AAS*; 100.8°, 137.2°, -38.9°; 71.5 kcal mol^{-1}: *SSS*; 28.6°, 58.0°, 24.9°; 71.7 kcal mol^{-1}: *AAA*; 163.1°, 159.0°, 163.6°; 78.6 kcal mol^{-1}.

(d) Pentamer 6 (n = 5). Exactly the same treatment for all the possible conformers of **6** (n = 5) gave the following results: conformer *SSAS*, θ_1 = 30.3°, θ_2 = 54.1°, θ_3 = −155.0°, θ_4 = 34.7°; SE = 86.9 kcal mol^{-1}: *ASAS*; 142.1°, −86.8°, 117.7°, −31.2°; 88.2 kcal mol^{-1}: *SSSS*; 14.3°, −87.5°, −87.5°, 14.4°; 90.5 kcal mol^{-1} : *SAAS*; 37.0°, −156.2°, −157.6°, 37.5°; 90.8 kcal mol^{-1}: *SSAA*; 21.1°, 57.5°, −161.1°, −141.1°; 91.8 kcal mol^{-1}: *AASA*; −147.5°, −163.6°, 59.7°, −163.3°; 93.8 kcal mol^{-1}: *ASSA*; −150.4°, 62.9°, 62.9°, −150.5°; 94.5 kcal mol^{-1}: *SAAA*; −36.3°, 160.4°, 159.4°, 169.8°; 96.1 kcal mol^{-1}: *AAAA*; 160.6°, 165.2°, 164.0°, 163.1°; 100.0 kcal mol^{-1}. No energy-minimum was observed for the structure corresponding to conformer *SSSA*.

Reductive Cyclization of the Tetrameric Dibromide 3 (n = 4). To a stirred solution of the dibromide of BCO tetramer **3** (n = 4) (22.7 mg, 0.0388 mmol) in THF (1.5 mL) at 0 °C was added dropwise a solution of 0.075 M sodium naphthalenide in THF (2.1 mL, 0.16 mmol). Addition of each drop of the naphthalenide solution caused rapid coloration to deep red-purple. After stirring for 15 min the reaction mixture was quenched with water, and extracted with ether. The ethereal solution was evaporated to give 34.4 mg of crude products which apparently contained some naphthalene (the molar ratio of **4** : **1** was 1 : 2 as estimated from ^{1}H NMR). Separation by the use of MPLC afforded 11.2 mg of a mixture containing **4** and 19.3 mg of a mixture containing **1** and naphthalene. The first mixture **4** was chromatographed over SiO_2 impregnated with $AgNO_3$ (7%) and the fraction eluted with hexane–ether (24 : 1) gave **4** (3.2 mg, 0.0076 mmol, 20% yield). The similar experiments were repeated, and then a single crystal of **4** was prepared by very slow recrystallization from hexane. **4**: mp 288.5–289 °C sealed tube (sublimed at > 260 °C); ^{1}H NMR ($CDCl_3$, 270 MHz) δ 2.30 (s, 8H,

CH(bridgehead)), 1.52 (m, 16H, CH_2^{anti}), 1.38 (d, J = 6.6 Hz, 8H, CH_2^{syn}), 1.31 (d, J = 6.6 Hz, 8H, CH_2^{syn}); ^{13}C NMR ($CDCl_3$, 67.8 MHz) δ 140.3(s), 33.7(d), 27.2(d), 26.4(t); IR (KBr) ν 2935, 2855, 1465, 1450, 1150, 1022, 865, 849, 833, 812 cm^{-1}; UV (C_6H_{12}) λ_{max} 218 nm (log e 4.46), 286 (2.91).

Anal. Calcd for $C_{32}H_{40}$: C, 90.51; H, 9.49. Found: C, 90.30; H, 9.59.

X-ray Crystallography of 4. The crystal of **4** belongs to the monoclinic system with unit cell parameters at 297 K: a = 16.158(5) Å, b = 9.691(3) Å, c = 17.122(5) Å, β = 122.55(3) ° and V = 2473.9 Å^3. The space group is $P2_1/c$ with Z = 4. The intensity data were collected on a STOE STADI 4 four cycle diffractometer using monochromic MoKα radiation. The total of 3666 reflections were measured with $3 \leq 2\theta \leq 45°$. The structure was solved by direct methods (SHELXS–86). The total of 2988 reflections with $F \geq 2\alpha$ were used for anisotropic refinement. All hydrogen atoms were positioned geometrically. A final difference-Fourier map was feature-less ρ (min) = 0.13 eÅ^3. Final R = 0.0483 R_w = 0.0692. Crystallographic data, i.e., bond lengths, bond angles, atomic coordinate, and anisotropic displacement parameters are given in Tables 1–4 respectively.

Table 3. Atomic Coordinates and Equivalent Isotropic Temperature Factors for **4**

Atom	X/a	Y/b	Z/c	U(EQ)
C(1)	0.6739(01)	0.1867(02)	0.6502(01)	0.036(01)
C(2)	0.7285(01)	0.2008(02)	0.6084(01)	0.039(01)
C(3)	0.7732(01)	0.0889(02)	0.5822(01)	0.040(01)
C(4)	0.8269(01)	-0.0075(02)	0.6328(01)	0.039(01)
C(5)	0.8527(01)	-0.0201(02)	0.7247(01)	0.040(01)
C(6)	0.7969(01)	-0.0394(02)	0.7642(01)	0.038(01)
C(7)	0.6989(01)	-0.0424(02)	0.7251(01)	0.038(01)
C(8)	0.6458(01)	0.0560(02)	0.6767(01)	0.038(01)
C(11)	0.6364(01)	0.3223(02)	0.6663(01)	0.048(01)
C(12)	0.7161(01)	0.4145(02)	0.7180(01)	0.059(01)
C(13)	0.5848(01)	0.3920(02)	0.5810(01)	0.058(01)
C(21)	0.7401(01)	0.3499(02)	0.5865(01)	0.054(01)
C(22)	0.7793(01)	0.4312(02)	0.6705(01)	0.064(01)
C(23)	0.6479(01)	0.4109(02)	0.5334(01)	0.062(01)
C(31)	0.7634(01)	0.0743(02)	0.4906(01)	0.050(01)
C(32)	0.7239(01)	-0.0697(02)	0.4598(01)	0.066(01)
C(33)	0.8563(01)	0.0812(02)	0.4865(01)	0.065(01)
C(41)	0.8642(01)	-0.1094(02)	0.5883(01)	0.053(01)
C(42)	0.7838(01)	-0.1798(02)	0.5186(01)	0.067(01)
C(43)	0.9171(01)	-0.0290(02)	0.5454(01)	0.064(01)
C(51)	0.9505(01)	-0.0233(02)	0.7835(01)	0.059(01)
C(52)	0.9653(02)	0.0898(03)	0.8499(01)	0.073(01)
C(53)	0.9713(01)	-0.1629(03)	0.8294(01)	0.076(01)
C(61)	0.8444(01)	-0.0603(02)	0.8592(01)	0.051(01)
C(62)	0.8996(01)	0.0690(02)	0.8945(01)	0.064(01)
C(63)	0.9079(01)	-0.1845(02)	0.8755(01)	0.060(01)
C(71)	0.6483(01)	-0.1626(02)	0.7425(01)	0.047(01)
C(72)	0.5870(01)	-0.2227(02)	0.6563(01)	0.057(01)
C(73)	0.5886(01)	-0.1083(02)	0.7871(01)	0.067(01)
C(81)	0.5467(01)	0.0277(02)	0.6521(01)	0.050(01)
C(82)	0.5253(01)	-0.1088(02)	0.6027(01)	0.060(01)
C(83)	0.5292(01)	0.0077(02)	0.7339(01)	0.074(01)
H(111)	0.592(00)	0.306(00)	0.700(00)	0.053(03)
H(121)	0.752(00)	0.367(00)	0.779(00)	0.087(03)
H(122)	0.692(00)	0.515(00)	0.727(00)	0.087(03)
H(131)	0.529(00)	0.328(00)	0.544(00)	0.083(03)
H(132)	0.561(00)	0.491(00)	0.591(00)	0.083(03)
H(211)	0.783(00)	0.356(00)	0.552(00)	0.053(03)
H(221)	0.785(00)	0.539(00)	0.657(00)	0.087(03)
H(222)	0.845(00)	0.391(00)	0.709(00)	0.087(03)
H(231)	0.655(00)	0.519(00)	0.523(00)	0.083(03)
H(232)	0.620(00)	0.358(00)	0.473(00)	0.083(03)
H(311)	0.721(00)	0.155(00)	0.452(00)	0.053(02)
H(321)	0.721(00)	-0.086(00)	0.396(00)	0.087(02)
H(322)	0.657(00)	-0.076(00)	0.460(00)	0.087(02)
H(331)	0.850(00)	0.062(00)	0.422(00)	0.083(02)

(Table 3. Continued)

Atom	X/*a*	Y/*b*	Z/*c*	*U*(EQ)
H(332)	0.885(00)	0.182(00)	0.506(00)	0.083(02)
H(411)	0.907(00)	-0.184(00)	0.632(00)	0.053(02)
H(421)	0.746(00)	-0.237(00)	0.547(00)	0.087(02)
H(422)	0.808(00)	-0.249(00)	0.483(00)	0.087(02)
H(431)	0.974(00)	0.020(00)	0.593(00)	0.083(02)
H(432)	0.940(00)	-0.099(00)	0.509(00)	0.083(02)
H(511)	0.993(00)	-0.008(00)	0.748(00)	0.053(02)
H(521)	1.033(00)	0.084(00)	0.896(00)	0.087(02)
H(522)	0.954(00)	0.190(00)	0.819(00)	0.087(02)
H(531)	1.040(00)	-0.164(00)	0.875(00)	0.083(02)
H(532)	0.962(00)	-0.245(00)	0.784(00)	0.083(02)
H(611)	0.797(00)	-0.078(00)	0.888(00)	0.053(02)
H(621)	0.856(00)	0.157(00)	0.883(00)	0.087(02)
H(622)	0.937(00)	0.057(00)	0.962(00)	0.087(02)
H(631)	0.869(00)	-0.277(00)	0.852(00)	0.083(02)
H(632)	0.946(00)	-0.194(00)	0.943(00)	0.083(02)
H(711)	0.694(00)	-0.239(00)	0.781(00)	0.053(02)
H(721)	0.547(00)	-0.305(00)	0.666(00)	0.087(02)
H(722)	0.627(00)	-0.263(00)	0.624(00)	0.087(02)
H(731)	0.630(00)	-0.069(00)	0.849(00)	0.083(02)
H(732)	0.547(00)	-0.191(00)	0.794(00)	0.083(02)
H(811)	0.506(00)	0.111(00)	0.615(00)	0.053(02)
H(821)	0.536(00)	-0.097(00)	0.544(00)	0.087(02)
H(822)	0.456(00)	-0.136(00)	0.588(00)	0.087(02)
H(831)	0.460(00)	-0.019(00)	0.718(00)	0.083(02)
H(832)	0.544(00)	0.102(00)	0.770(00)	0.083(02)

Table 4. Anisotropic Temperature Factors for **4**

Atom	*U*11	*U*22	*U*33	*U*23	*U*13	*U*12
C(1)	0.034(01)	0.033(01)	0.042(01)	0.001(01)	0.011(01)	0.005(01)
C(2)	0.041(01)	0.036(01)	0.040(01)	0.005(01)	0.011(01)	0.005(01)
C(3)	0.039(01)	0.043(01)	0.037(01)	0.002(01)	0.017(01)	0.001(01)
C(4)	0.035(01)	0.041(01)	0.040(01)	0.005(01)	0.018(01)	0.005(01)
C(5)	0.036(01)	0.042(01)	0.041(01)	0.008(01)	0.014(01)	0.004(01)
C(6)	0.038(01)	0.038(01)	0.038(01)	0.004(01)	0.014(01)	0.003(01)
C(7)	0.037(01)	0.035(01)	0.040(01)	0.000(01)	0.018(01)	0.002(01)
C(8)	0.034(01)	0.036(01)	0.044(01)	-0.002(01)	0.017(01)	0.002(01)
C(11)	0.046(01)	0.038(01)	0.059(01)	-0.003(01)	0.020(01)	0.006(01)
C(12)	0.072(01)	0.044(01)	0.061(01)	-0.010(01)	0.017(01)	-0.001(01)
C(13)	0.057(01)	0.042(01)	0.074(01)	0.004(01)	0.013(01)	0.015(01)
C(21)	0.056(01)	0.043(01)	0.062(01)	0.010(01)	0.024(01)	-0.003(01)
C(22)	0.063(01)	0.046(01)	0.082(01)	-0.006(01)	0.017(01)	-0.012(01)
C(23)	0.073(01)	0.043(01)	0.070(01)	0.015(01)	0.017(01)	0.007(01)
C(31)	0.056(01)	0.058(01)	0.036(01)	0.005(01)	0.019(01)	0.005(01)
C(32)	0.064(01)	0.079(01)	0.056(01)	-0.016(01)	0.022(01)	-0.005(01)
C(33)	0.071(01)	0.074(01)	0.050(01)	0.006(01)	0.036(01)	-0.002(01)
C(41)	0.050(01)	0.049(01)	0.058(01)	0.003(01)	0.032(01)	0.011(01)
C(42)	0.074(01)	0.053(01)	0.075(01)	-0.014(01)	0.041(01)	-0.004(01)
C(43)	0.058(01)	0.073(01)	0.063(01)	-0.000(01)	0.038(01)	0.004(01)
C(51)	0.034(01)	0.087(01)	0.055(01)	0.025(01)	0.015(01)	0.004(01)
C(52)	0.066(01)	0.094(02)	0.059(01)	0.007(01)	-0.004(01)	-0.034(01)
C(53)	0.054(01)	0.099(02)	0.074(01)	0.041(01)	0.025(01)	0.029(01)
C(61)	0.049(01)	0.067(01)	0.038(01)	0.011(01)	0.017(01)	0.004(01)
C(62)	0.070(01)	0.077(01)	0.045(01)	-0.006(01)	0.003(01)	-0.010(01)
C(63)	0.055(01)	0.069(01)	0.055(01)	0.026(01)	0.016(01)	0.009(01)
C(71)	0.045(01)	0.042(01)	0.056(01)	0.007(01)	0.023(01)	-0.003(01)
C(72)	0.054(01)	0.042(01)	0.074(01)	-0.003(01)	0.025(01)	-0.008(01)
C(73)	0.061(01)	0.064(01)	0.077(01)	0.006(01)	0.045(01)	-0.002(01)
C(81)	0.033(01)	0.046(01)	0.070(01)	0.001(01)	0.018(01)	0.003(01)
C(82)	0.051(01)	0.054(01)	0.075(01)	-0.004(01)	0.005(01)	-0.010(01)
C(83)	0.058(01)	0.066(01)	0.099(02)	0.002(01)	0.052(01)	0.006(01)

Preparation and Spectral Observation of the Dianion 4^{2-}. (a) **NMR Measurements.** A 5-mm o.d. NMR tube having a 8-mm o.d. Pyrex grass tube as a side arm at an upper part was used for preparation of an NMR sample. COT **4** (2.8 mg, 6.6 x 10^{-3} mmol) was added in the NMR tube and potassium (0.066g, 1.7 mmol) washed with ligroin was placed in the 8-mm o.d. tube, and then the whole apparatus was evacuated on a vacuum line. Then, THF–*d*8 (1 mL), which had been degassed by repeating the freeze-pump-thaw cycle for three times and dried with sodium–potassium alloy, was transferred into the NMR tube by distillation under vacuum. While the THF solution was frozen by liquid nitrogen, potassium in the 8-mm tube was heated with free flame to make a potassium mirror at the upper part of the NMR tube. The NMR tube was sealed off under vacuum above the potassium mirror. The THF solution of **4** was brought into contact with the potassium mirror for 10 min at room temperature to afford an orange-colored solution of dianion 4^{2-}. The ^{13}C and ^{1}H NMR spectra were measured at room temperature and also at –60 °C. The ^{13}C NMR spectrum at lower temperature did not show any change from one taken at room temperature.

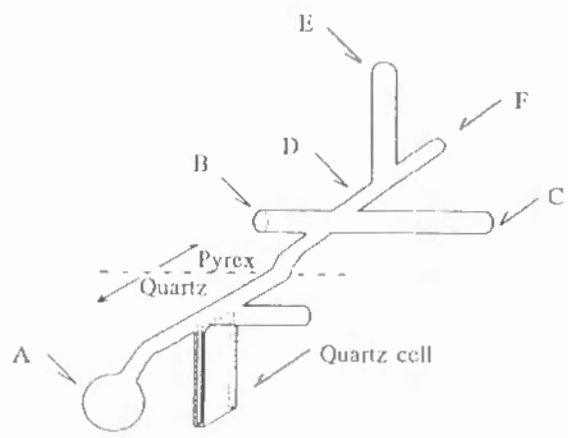

Figure 7. A quartz cell used for the measurement of UV–vis spectrum under vacuum: cell path, 1 mm

(b) UV–vis Measurements. For UV–vis measurements was employed a quartz cell shown in Figure 7. COT **4** (1.271 mg, 2.99 x 10^{-3} mmol) in a tared small grass tube was weighed, and was placed in the chamber C through the inlet B. Then the inlet B was sealed. Potassium (0.077 g, 2.0 mmol) washed with ligroin was placed in the chamber E. After the vessel was evacuated from the tube end F, THF (1 mL), which had been degassed by repeating the freeze-pump-thaw cycle for three times and dried with sodium–potassium alloy, was transferred into the chamber A by distillation under vacuum. While the THF solution was frozen by liquid nitrogen, potassium in the chamber E was heated with free flame to make a potassium mirror at the part D. Then, the tube was sealed off under vacuum above the potassium mirror. The THF solution of **4** was brought into contact with the potassium mirror for 10 min at room temperature to afford an orange-colored solution of dianion 4^{2-}. The UV–vis spectrum was measured at room temperature; λ_{max} (THF) 266 nm (log ε 4.06), 357 (3.42).

References and Notes

(1) Willstätter, R.; Waser, E. *Chem. Ber.* **1911**, *44*, 3423.

(2) (a) Hückel, E. *Physik.* **1931**, *70*, 204. (b) Hückel, E. *Physik.* **1937**, *76*, 204. (c)Hückel, E. *Electrochem.* **1937**, *43*, 752.

(3) (a) Schroeder, G. *Cyclooctatetraene*; Verlag Chemie: Weinheim, 1965. (b) Paquette, L.A. *Tetrahedron* **1975**, *31*, 2855. (c) Fray, G. I.; Saxton, R. G. *The Chemistry of Cyclooctatetraene and Its Derivatives*; Cambridge University Press: New York, 1978.

(4) (a) Person, W. B.; Pimentel, G. C.; Pitzer, K. S. *J. Am. Chem. Soc.* **1952**, *74*, 3437. (b) Bordner, J.; Parker, R. G.; Stanford, R. H., Jr. *Acta Crystallogr.*

1972, *28B*, 1069. (c) Cobbledick, R. E.; Einstein, F. W. B. *Acta Crystallogr.* **1972**, *33B*, 2339.

(5) Paquette, L. A. *Pure Appl. Chem.* **1982**, *54*, 987.

(6) (a) Anet, F. A. L. *J. Am. Cem. Soc.* **1962**, *84*, 671. (b) Anet, F. A. L.; Baurn, A. J. P. *J. Am. Cem. Soc.* **1964**, *86*, 3576. (c) Anet, F. A. L.; Bock, L. A. *J. Am.Cem. Soc.* **1968**, *90*, 7130.

(7) Paquette, L. A. *Acc. Chem. Res.* **1993**, *26*, 57 and references are cited therein.

(8) (a) Katz, T. J. *J. Am. Cem. Soc.* **1968**, *90*, 7130. (b) Streitwieser, A., Jr.*Molecular Orbital Theory for Organic Chemists*; Wiley: New York, 1961.

(9) Goldberg, S. Z.; Raymond, K. N.; Harmon, C. A.; Templeton, D. H. *J. Am. Cem. Soc.* **1974**, *96*, 1348.

(10) Heinz, W.; Langensee, P.; Müllen, K. *J. Chem. Soc., Chem. Commun.* **1986**, 949.

(11) (a) Komatsu, K.; Jinbu, Y.; Gillette, G. R.; West, R. *Chem. Lett.* **1988**, 2029. (b) Komatsu, K.; Aonuma, S.; Jinbu, Y.; Tsuji, R.; Hirosawa,C.; Takeuchi, K. *J. Org. Chem.* **1991**, *56*, 195.

(12) Komatsu, K.; Akamatsu, H.; Jinbu, Y.; Okamoto, K. *J. Am. Chem. Soc.* **1988**, *110*, 633.

(13) Andrieux, C. P.; Merz, A.; Savéant, J. -M. *J. Am. Chem. Soc.* **1985**, *107*, 6097 and the references are cited therein. See also Garst, J. F.; Barbas, J. T. *J. Am. Chem. Soc.* **1974**, *96*, 3239.

(14) The MM2(87) program was obtained from QCPE, Indiana University.

(15) The rotation barrier around the central single bond for the dimer **6** (n = 2) was calculated as 3.5 kcal mol^{-1}: see Experimental section.

(16) Paquette, L. A.; Wang, T-Z.; Cottrell, C. E. *J. Am. Chem. Soc.* **1987**, *109*, 3730.

(17) Laird, B. B.; Davis, R. E. *Acta Crystallogr., Sect. B* **1982**, B38, 678.

(18) Pawley, G. S.; Lipscomb, W. N.; Freedman, H. H. *J. Am. Chem. Soc.* **1964**, *86*, 4725.

(19) UV-vis (THF) λ_{max} 266 nm (log ε 4.06), 357 (3.42).

(20) J. B. Stothers, "Carbon-13 NMR Spectroscopy", Academic Press, New York, 1972, p. 91.

Chapter 3

Properties of the Cation Radical and the Dication of Tetrakis(bicyclo[2.2.2]octeno)cyclooctatetraene

Abstract

Structural and electronic properties of the cation radical and the dication of the cyclooctatetraene (COT) tetra-annelated with a bicyclo[2.2.2]octene framework **1** were investigated. In accord with the results of cyclic voltammetry suggesting the formation of both cation radical $\mathbf{1}^{\cdot+}$ and dication $\mathbf{1}^{2+}$ as stable species under appropriate conditions, these species were chemically generated and directly observed. The electrolytic oxidation of **1** in an ESR cell gave a green solution exhibiting a persisting ESR spectrum composed of nine-lines (a_H = 0.194 mT, g = 2.0023). Chemical one-electron oxidation of **1** with $NO^+SbCl_6^-$ allowed us to isolate and determine the X-ray structure of a salt of a COT cation radical for the first time. The X-ray structure of $\mathbf{1}^{\cdot+}SbCl_6^-$ was in good agreement with the previous theoretical prediction for its structure. Also the electronic spectrum was interpreted successfully by MNDO calculation using the X-ray structure. Further one-electron oxidation of $\mathbf{1}^{\cdot+}SbCl_6^-$ with SbF_5 gave dication $\mathbf{1}^{2+}$ as a single product stable in solution. From low-temperature ^{13}C NMR measurements, $\mathbf{1}^{2+}$ was found to be in a non-planar tub-structure, which was inverting rapidly ($\Delta G^{\ddagger}$ (−35°C), 10.8 ± 0.7 kcal mol^{-1}) despite of its 6π aromatic nature.

Introduction

In contrast to the cyclooctatetraene (COT) dianions and anion radicals which have been extensively studied,[1] experimental studies on the cationic species of COT are quite limited because of its instability under oxidative conditions. For example, the 6π-aromatic dication of the di- or tetra-substituted derivative has been once reported to be generated only under stable-ion conditions at low temperatures (−80 ~ −20°C):[2] the cation radical of the parent COT has been observed by ESR in solution only by the use of rapid-flow technique[3a] or in freon matrix at low temperature (−196 °C);[3b,c] the electronic spectrum has also been taken on the matrix-isolated species.[3b,c] However, like the cationic species of other olefinic hydrocarbons, the COT dication or cation radical is a highly unstable species, whose structures could have only been inferred from NMR spectrum,[2] from ESR coupling constant,[3a] or from theoretical calculations.[4]

In the previous chapter was described the synthesis of the COT derivative (**1**) fully annelated with bicyclo[2.2.2]octene.[5] Such structural modification with bicycloalkene frameworks was proved to be remarkably effective in stabilization of the tropylium ion and benzene cation radical such as **2** [6] and **3**.[7] The present chapter describes the first X-ray structure of a COT cation radical, i.e., the hexachloroantimonate salt of cation radical $\mathbf{1}^{\cdot+}$, and also an NMR observation of a stable COT dication with a non-planar structure, i.e., dication $\mathbf{1}^{2+}$.

1

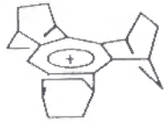

2

3

Results and Discussion

Electrochemical Oxidation. Cyclic voltammetry (CV) of COT **1** in acetonitrile–dichloromethane (3:1) (with 0.1M $Bu_4N^+ClO_4^-$ as an electrolyte) at room temperature under argon exhibited a well-defined reversible one-electron oxidation wave at $E_{1/2}$ = +0.48 V vs Ag/Ag^+ together with an irreversible oxidation wave at +0.99 V as shown in Figure 1a. This result implies that **1** provides a stable cation radical even at room temperature and a less stable dication upon further oxidation. In fact, the electrolytic oxidation in an ESR cell at the electrode potential of +0.5 V vs Ag/Ag^+ in dichloromethane under the similar conditions as above gave a green solution, which exhibited an ESR spectrum composed of nine-lines with the relative intensities proportional to the coefficients in the binomial expansion (a_H = 0.194 mT, g = 2.0023) as shown in Figure 2a. This signal was persistent at room temperature for several hours even after cutting off the anodic current.

In contrast, the CV in dichloromethane–trifluoroacetic acid–trifluoroacetic anhydride (20:1:1)[8] (with 0.1M $Bu_4N^+BF_4^-$ as an electrolyte) conducted in a vacuum-sealed cell at −78 °C exhibited two well-defined reversible oxidation waves at $E_{1/2}$ +0.39 and +1.14 V vs Ag/Ag^+ as shown in Figure 1b. This is the first electrochemical detection of both the radical cation and dication of a COT derivative as stable species, and suggests that even the dication could be observed under appropriate conditions.

Chemical One-electron Oxidation. As shown in Scheme 1, chemical one-electron oxidation of **1** by the use of 1 equiv of $NO^+SbCl_6^-$ [9] instantly occurred in dichloromethane at room temperature to give a dark green solution. After reprecipitation with benzene and filtration there was obtained 76% yield of crude $\mathbf{1}^{\cdot+}SbCl_6^-$ as a dark green solid. The single crystal of $\mathbf{1}^{\cdot+}SbCl_6^-$, obtained

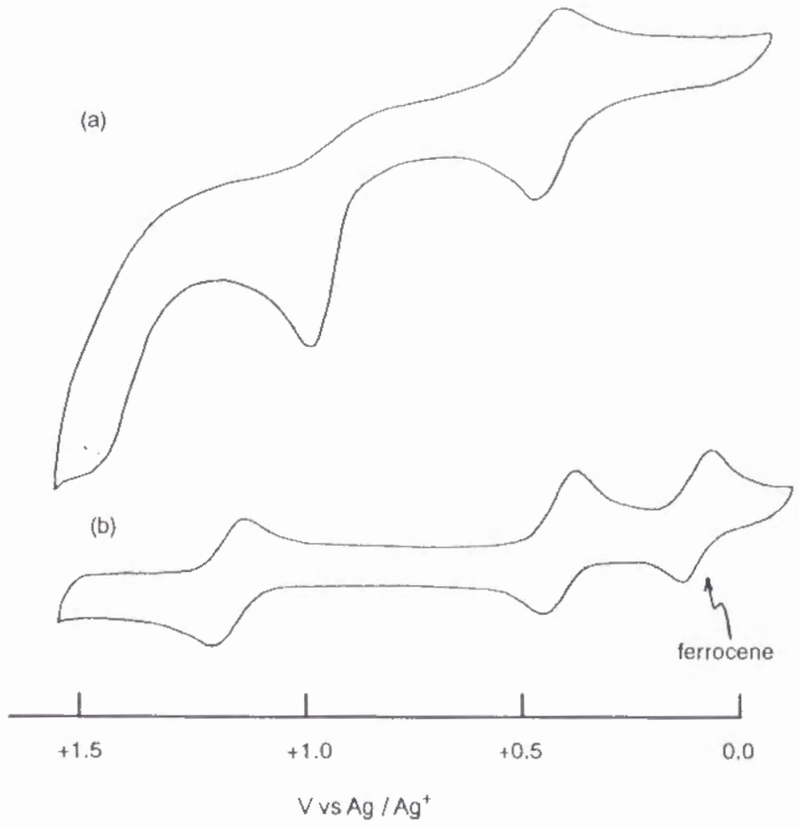

Figure 1. Cyclic voltammograms of **1** (0.5 mM) in (a) acetonitrile–dichloromethane (3:1) at room temperature (supporting electrolyte, $Bu_4N^+ClO_4^-$ (0.1 M)) and (b) dichloromethane–trifluoroacetic acid–trifluoroacetic anhydride (20:1:1) at −78 °C (supporting electrolyte, $Bu_4N^+BF_4^-$ (0.1 M)); scan rate, 0.1 V s^{-1}.

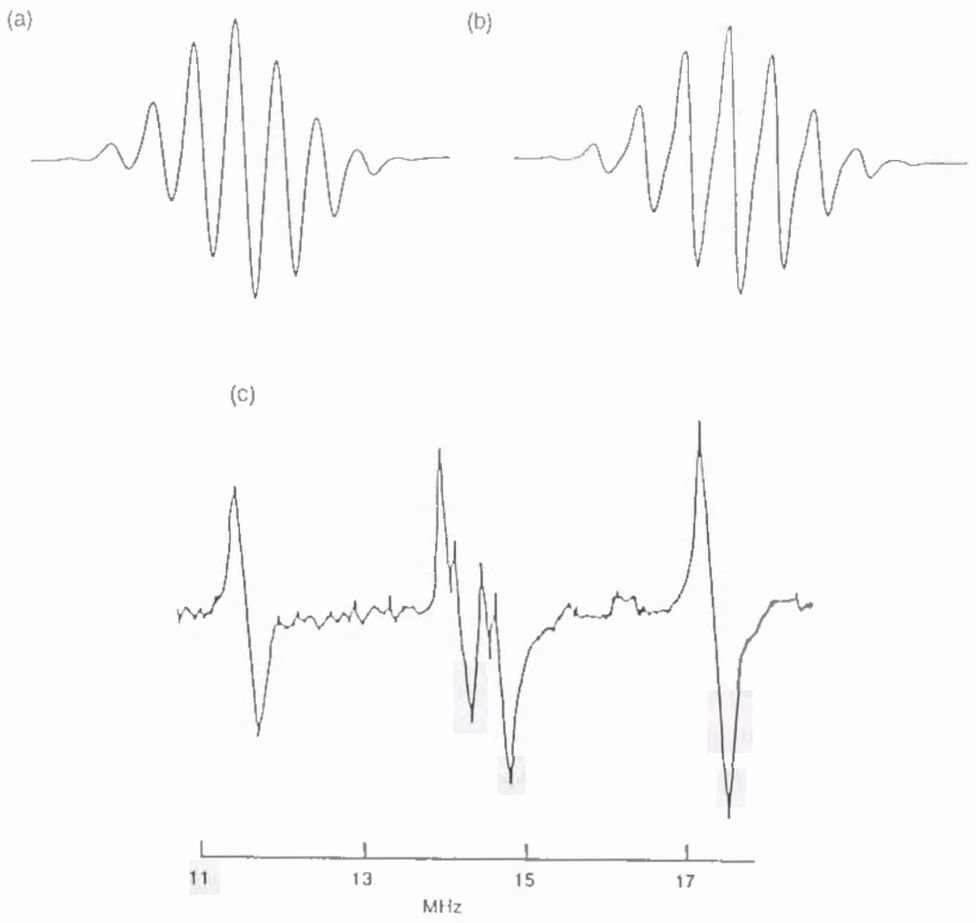

Figure 2. (a) ESR spectrum of $\mathbf{1}^{\cdot+}$ electrolytically generated in dichloromethane containing $Bu_4N^+ClO_4^-$, (b) simulated ESR spectrum using the coupling constants obtained from ENDOR measurement, (c) ENDOR spectrum of $\mathbf{1}^{\cdot+}SbCl_6^-$ in nitromethane at −80 °C.

Scheme 1

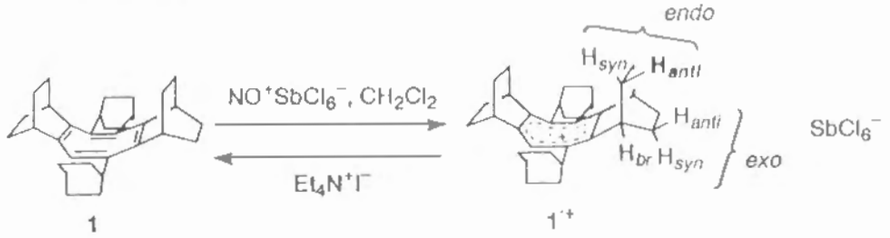

as described below in 20% yield, was stable at room temperature under air for several hours and can be stored in a refrigerator under argon for more than six months without any decomposition.

Upon dissolution in dichloromethane, this salt gave the same ESR signal as the one obtained by electrolytic oxidation and was reduced back to the starting COT **1** by iodide ion in acetonitrile. Apparently, a structure with the planar COT ring can not explain the nine-line ESR signal. On the other hand, if we assume the COT ring to take a tub form, the nine-line ESR signal could be assigned as due to the coupling with the eight *anti*-protons of the *endo*-site ethano-bridge, since these protons are at the geometry nearly in the W-shaped conformation involving the 2p orbital. Actually, the highest spin density (0.0022) was found on this proton by INDO calculation. The smaller spin densities residing on other protons (0.0013 on $H_{bridgehead}$, −0.0008 on *exo*-H_{anti}, −0.0005 on *endo*-H_{syn}, and −0.0004 on *exo*-H_{syn}) seem to be the cause of broadening of the ESR signal. In fact, ENDOR spectrum indicated presence of smaller couplings 0.019 mT, 0.09 mT as shown in Figure 2c, which could not be observed in ESR measurements. A simulated ESR spectrum using the coupling constants obtained from ENDOR measurement well reproduced the observed one as shown in Figure 2b.

X-ray Structure of $\mathbf{1}^{\cdot+}SbCl_6^-$. In order to clarify the structure of the cation radical, X-ray structure determination on the single crystal was most

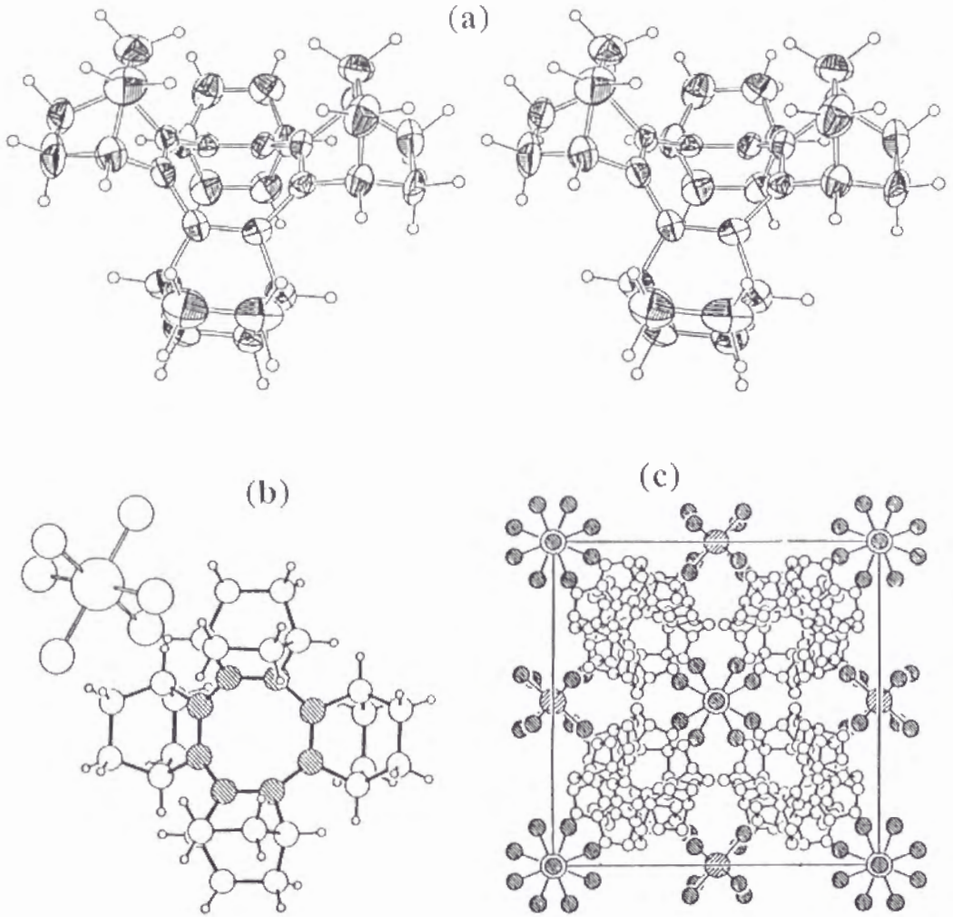

Figure 3. X-ray crystal structures of $\mathbf{1}^{\cdot+}$ $SbCl_6^-$: (a) an ORTEP stereoview; (b) a top view; (c) a view of a unit cell.

Table 1. Comparison of Calculated and Observed Structural Parameters for the Neutral and Cationic COTs.

Species	Method	Bond lengths Å			C-C-C angle degree
COT [a]	MINDO/2	1.355	:	1.473	125.3
$COT^{\cdot+}$ [a]	MINDO/2	1.379	:	1.442	129.9
1 [b]	X-ray cryst[c]	1.339(1)	:	1.465(1)	126.6
$\mathbf{1}^{\cdot+}$ [d]	X-ray cryst[c]	1.365(5)	:	1.448(5)	125.8
$\mathbf{1}^{\cdot+}$ [d]	AM1	1.382	:	1.425	128.0
$\mathbf{1}^{\cdot+}$ [d]	MNDO	1.410	:	1.450	126.6

[a] Ref. 4. [b] Ref. 5. [c] ESD's of mean values in parentheses. [d] This work.

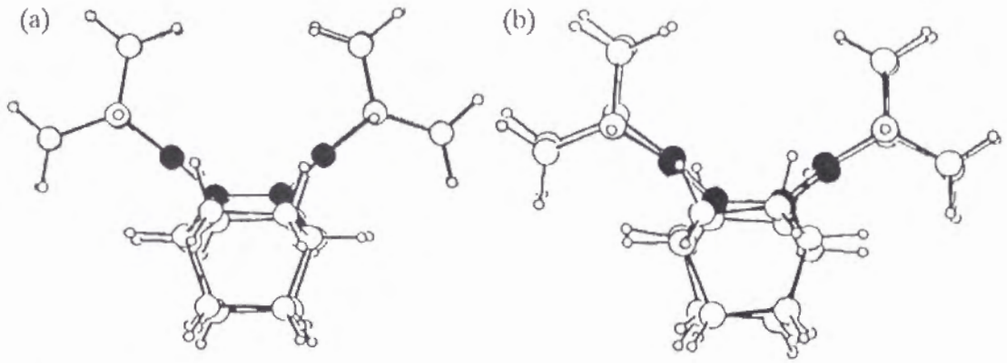

Figure 4. Side views of X-ray crystal structures of (a) **1** and (b) $\mathbf{1}^{\cdot+}$ $SbCl_6^-$.

required. The single crystal of the salt of COT cation radical $\mathbf{1}^{\cdot+}SbCl_6^-$ was grown by slow diffusion of benzene into a saturated solution of $\mathbf{1}^{\cdot+}SbCl_6^-$ in dichloromethane. The X-ray crystallography revealed that cation radical $\mathbf{1}^{\cdot+}$ actually is in the tub form as shown in Figure 3. The averaged values for bond lengths and angles of the central COT ring are given in Table 1 together with some calculated values for unsubstituted COT, $COT^{\cdot+}$ and $\mathbf{1}^{\cdot+}$ prepared in the present work. For all the bond lengths and angles, see Tables 5 and 6 in p.58–59.

The results of X-ray crystallography indicate that the central eight-membered ring of $\mathbf{1}^{\cdot+}$ is in a tub form similar to the structure of the neutral **1** as shown in Figure 4, which is different only in bond lengths from that in **1**.[5]

As to the cation radical of the parent COT, earlier theoretical calculations by MINDO/2 predicted that the extent of bond-length alternation would be reduced as compared with neutral COT and the eight-membered ring somewhat flattened (see Table 1) so that the more effective π-conjugation would result.[4] In good agreement, the X-ray structure of $\mathbf{1}^{\cdot+}SbCl_6^-$ reveals elongation of the original double bond in **1** by 0.026 Å and shortening of the single bond by 0.017 Å; the difference in shorter and longer bonds in $\mathbf{1}^{\cdot+}$ is only about 0.08 Å. The bond angle of $\mathbf{1}^{\cdot+}$, however, is not so much changed or even slightly reduced from that of **1**, presumably due to the non-bonded interaction between the bridgehead hydrogens of surrounding bicycloalkene frameworks, which would prevent the central ring from flattening. These results were qualitatively reproduced also by AM1 and MNDO calculations as shown in Table 1.

Electronic Spectrum of $\mathbf{1}^{\cdot+}SbCl_6^-$. As shown in Figure 5, the dark green salt of $\mathbf{1}^{\cdot+}SbCl_6^-$ exhibits an essentially the same electronic spectrum in solid state (λ_{max} (KBr pellet) 745 nm and 475 nm) and in solution (λ_{max} (CH_2Cl_2) 745 nm (log ε 3.66) and 438 nm (3.10)), indicating that there is no substantial difference in the structure of $\mathbf{1}^{\cdot+}$ between these two phases. Previously, the cation radical of the parent COT in freon matrix at −196 °C was reported to have a red color absorbing at 507 nm.[3b,c] In order to elucidate the cause of the considerable bathochromic shift in $\mathbf{1}^{\cdot+}$ as compared with $COT^{\cdot+}$, the MNDO calculations of Koopmans energies were conducted for the neutral molecule at the cation geometry obtained by X-ray analysis.[10] The energy gap between the a_1 orbital (HOMO, which is SOMO in cation radical) and degenerate e orbital (the second HOMO) and that

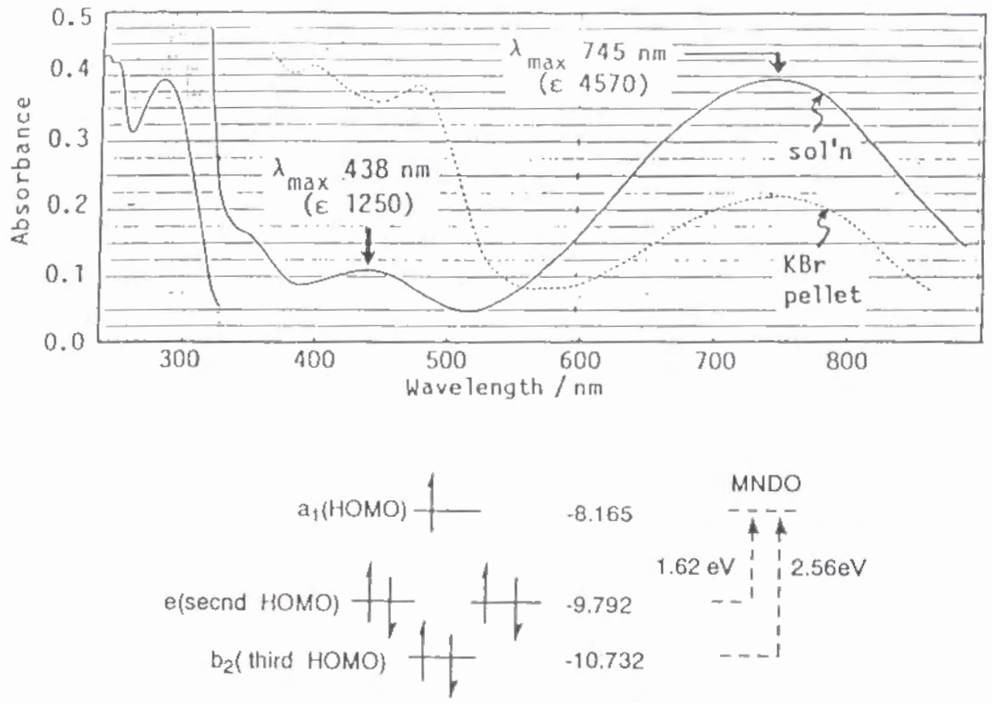

Figure 5. Electronic spectrum of $\mathbf{1}^{\cdot+}SbCl_6^-$ in dichloromethane and the calculated energy level of **1** using the structure of the X-ray structure of $\mathbf{1}^{\cdot+}$.

between the a_1 and b_2 (the third HOMO) orbitals were found to be 1.62 eV (763 nm) and 2.56 eV (484 nm),[11] respectively, in good agreement with the observed absorptions. This narrowing of energy gaps could be qualitatively interpreted by relative destabilization of lower orbitals (e and b_2) in $\mathbf{1}^{\cdot+}$,[3c] in which flattening of the COT ring is prohibited by steric reason, as compared with the parent $COT^{\cdot+}$ which is predicted to be more flattened.

Preparation of the Dication of 1. In spite of the Hückel aromatic stability expected for the cyclic 6π/8C π-electron system, surprisingly little is known for the COT dications. Thus, there has been virtually only one report describing the NMR observation of 1,4-di- and 1,3,5,7-tetrasubstituted COT

Scheme 2

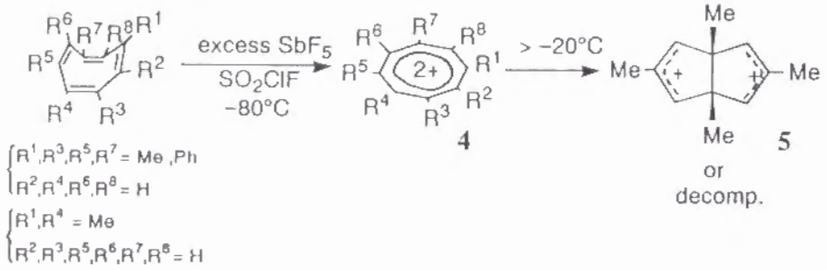

dication generated under stable conditions, i.e., by oxidation of the neutral COT with SbF_5 in SO_2ClF at low temperatures (scheme 2).[2]

All these dications are unstable at higher temperatures. The 1,3,5,7-tetramethyl derivative rearranges to the bicyclic bis-allylic dication **5** at the temperature higher than −20°C.[2] Based on these reported results, we first attempted a direct two-electron reduction of COT **1** by the use of a large excess (*ca.* 100 equiv) of SbF_5 at −78°C in SO_2ClF under vacuum. The resultant dark colored solution exhibited ^{13}C NMR signals for sp^2 carbons at δ 239.8, 239.5, 177.9, and 157.2, a signal for a tertiary carbon at δ 93.8, and fifteen signals for methine and methylene carbons at δ 47.5–18.5. From comparison of these data with those reported by Olah and Paquette for the planar and ring-closed dications **4** and **5**, it can be assumed that a mixture of dications with the similar structures **6** and **7** was formed, but there was no further supporting evidence. Next, we tried the one-electron oxidation of the $SbCl_6^-$ salt of the cation radical $\mathbf{1}^{\cdot+}$, which had already been isolated and purified.

When a green solution of $\mathbf{1}^{\cdot+}SbCl_6^-$ in dichloromethane (or dichloromethane-*d*2) was mixed with a large excess (*ca.* 100 equiv) of SbF_5 at −78 °C in a vacuum-scaled tube, a red solution immediately resulted, which was stable at room temperature and exhibited only three ^{13}C NMR signals at δ 177.9, 41.0, and 23.9 ppm. The ^{13}C and ^1H NMR spectra are shown in Figure 6. By comparison

Scheme 3

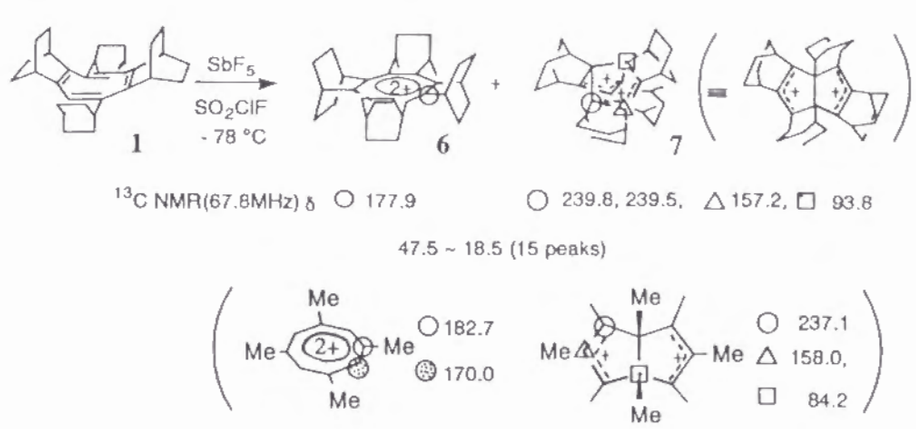

of the NMR data with those of **1** and dianion $\mathbf{1}^{2-}$ shown in Table 2, the newly formed red species is assigned as dication $\mathbf{1}^{2+}$. According to the Spiesecke-Schneider relationship,[12] an average of 40-ppm downfield shift of the ^{13}C signal for the COT ring carbon is in good agreement with the consecutive decrease of 1/4 unit charge per carbon in the sequence, $\mathbf{1}^{2-}$, **1**, and $\mathbf{1}^{2+}$. Deshielding of the bridgehead proton of $\mathbf{1}^{2+}$ as compared with **1** ($\Delta\delta_H$ 1.86 ppm) is comparable to that reported for the methyl proton in the 1,3,5,7-tetramethyl COT dication **4** ($\Delta\delta_H$ 1.87 ppm) recorded at low temperature,[2] suggesting that both of these dications are subjected to ring current effects to a similar extent.

Structure of Dication $\mathbf{1}^{2+}$. All these findings in NMR spectra of dication $\mathbf{1}^{2+}$ appeared to be in accord with the structure **A** (Scheme 4) having a planar COT ring. However, upon lowering the temperature down to −80 °C, the original singlet peak for the methylene carbon in the bicyclic framework at δ 23.9 was found to split into two peaks of equal intensity at δ 24.8 and 20.5. This is ascribed to the presence of lower-energy structure with two non-identical ethano-

Table 2. NMR data for 1^{2-}, **1**, and 1^{2+}

			δ_C /ppm			δ_H /ppm	
Compd	Solvent	Temp/°C	C(sp^2)	CH	CH_2	CH	CH_2
1^{2-} [a]	THF-d_8	25	97.8	35.8	30.6	3.65	1.87 1.41
1 [b]	THF-d_8	25	140.0	33.4	26.6 25.8	2.33	1.56 1.38
1^{2+} [c]	CD_2Cl_2	25	177.9	41.0	23.9	4.19	2.40 1.65
1^{2+} [c]	CD_2Cl_2	-80	176.6	39.5	24.8 20.4	4.09	2.6 - 1.5

[a] Ref. 5. No spectral change was observed when the temperature was lowered to –60 °C. [b] Ref. 5. No spectral change was observed when the temperature was raised to 150 °C in nitrobenzene-d_5. [c] The chemical shifts were read using the CD_2Cl_2 signal (δ 53.1) as a reference.

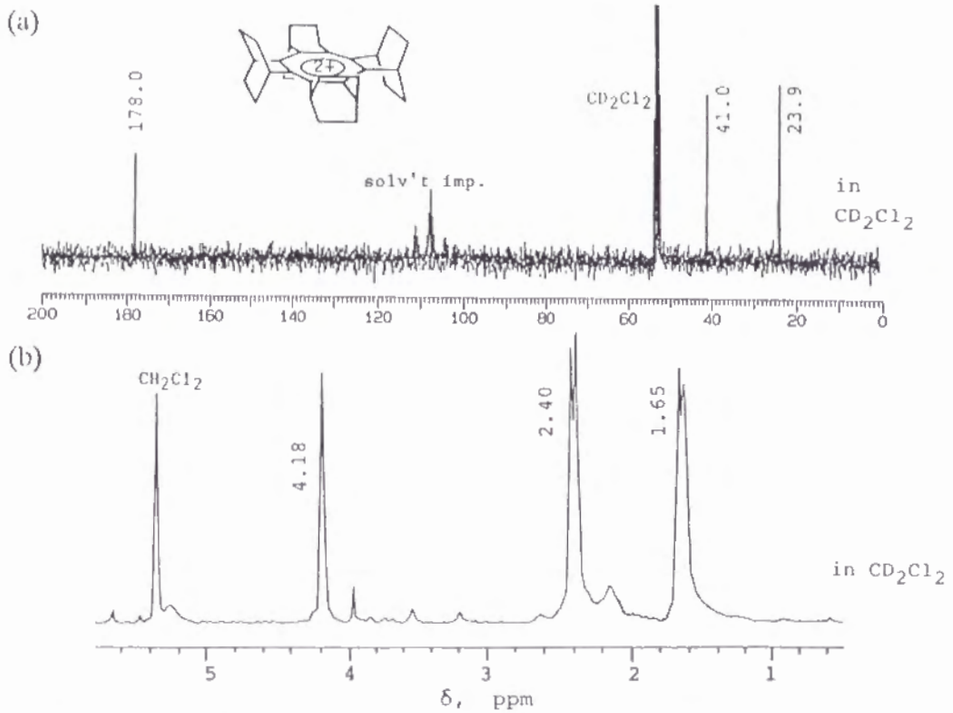

Figure 6. (a) ^{13}C (67.5MHz) and (b) ^1H (270 MHz) NMR spectra of 1^{2+} at room temperature.

Scheme 4

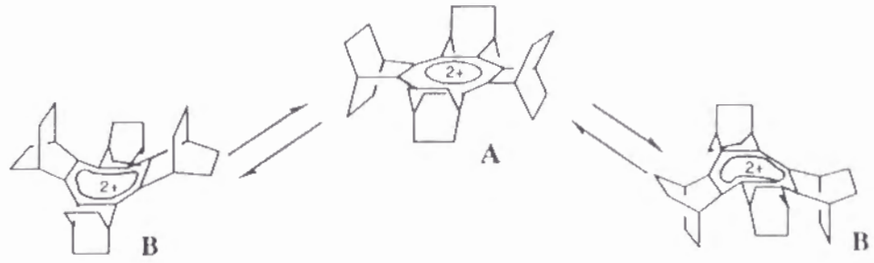

bridges, i.e., the tub-shaped dication **B**, which undergoes rapid ring inversion at room temperature as shown in Scheme 4. This spectral change in ^{13}C NMR spectrum is shown in Figure 7. The energy barrier for this process ($\Delta G^{\ddagger}$) was estimated to be 10.8 ± 0.7 kcal mol^{-1} from the observed coalescence temperature of –35 ± 15 °C.

In order to rationalize these results, semiempirical MO calculations were conducted by the use of PM3 method for the structure **A** with the COT ring enforced to a planar geometry, the structure **A'** with a non-planar COT ring obtained by energy minimization of the structure **A**, and the structure **B** with a tub COT ring. The energy-minimized structures thus obtained are shown in Figure 8 together with the values of heat of formation (ΔH_f) for each structure. The ΔH_f for the tub structure **B** was found to be lower than those for the structures **A** and **A'** by 30.7 and 22.3 kcal mol^{-1} respectively, supporting the experimental observation that the tub form is the most stable. From the observed $\Delta G^{\ddagger}$ value, conceivably the transition-state for the ring inversion would involve a structure more stable than **A'**, and/or the ion-pairing effect would be exerting more stabilization to the transition-state structure which has apparently a more planar COT ring.

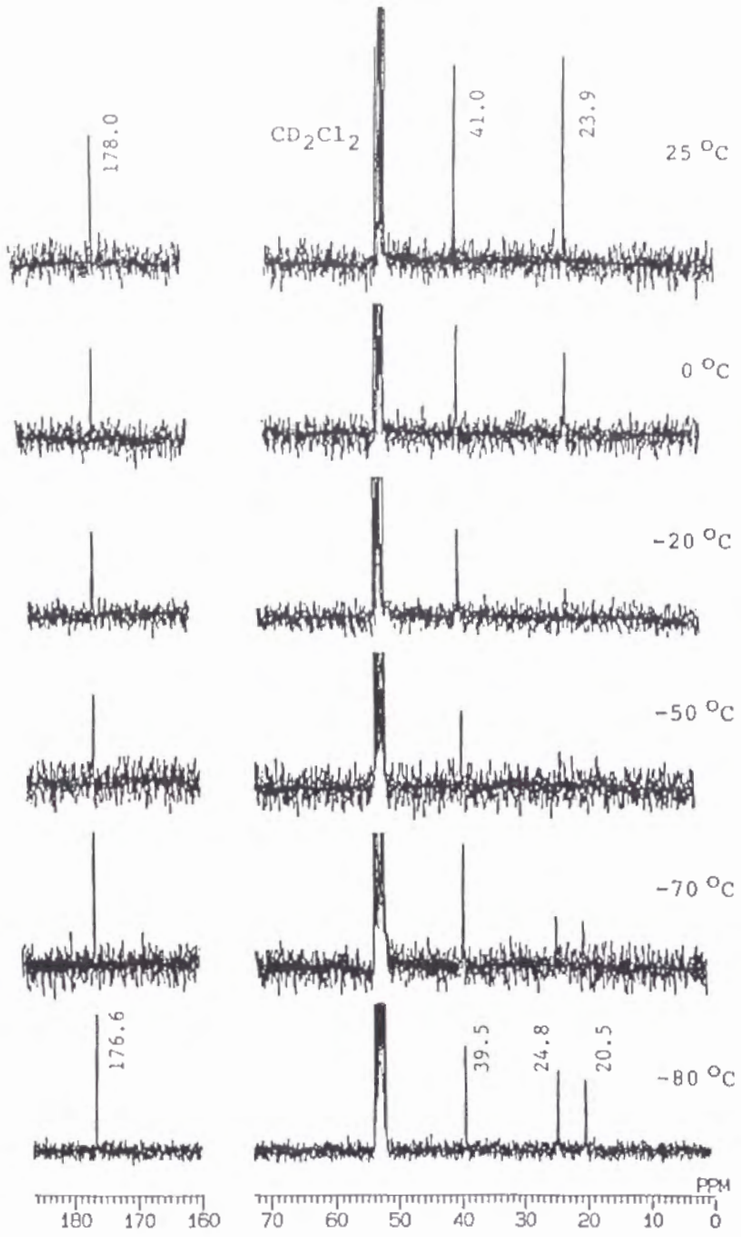

Figure 7. The ^{13}C NMR (67.5 MHz) spectrum of $\mathbf{1}^{2+}$ in dichloromethane-d_2 at various temperatures.

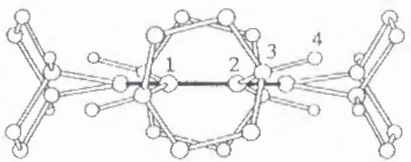

A, ΔH_f = 478.7 kcal mol^{-1}

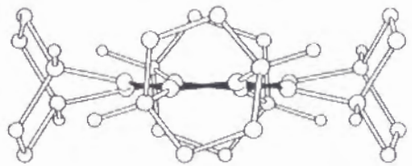

A', ΔH_f = 470.3 kcal mol^{-1}

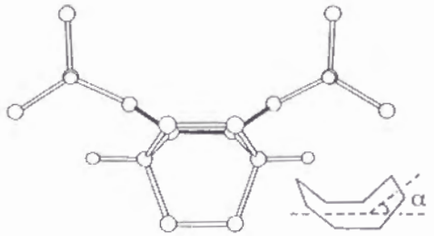

B, ΔH_f = 448.0 kcal mol^{-1}

Figure 8. The PM3 calculated structures (side views) for the dication $\mathbf{1}^{2+}$; with a COT ring enforced to be planar (the dihedral angle ∠ 1-2-3-4 = 16.2°) (A) ; with a COT ring energy-minimized starting from the structure A (the central ring has a shallow crown shape with the bond angle of 133.6° and the dihedral angle 27.1°) (A') ; with a tub-shaped COT ring (bent angle α = 34.5°) (B). Methylene hydrogens are omitted for clarity.

Electronic Spectrum of Dication 1^{2+}. The electronic spectrum of 1^{2+} in dichloromethane measured in a vacuum-sealed cell exhibited an absorption at much longer wavelength (λ_{max} 532 (log ε 3.8)) than those of other planar 6π aromatic systems which are fully annelated with BCO frameworks (i.e., the benzene, 260 nm;[6b] the tropylium ion, 308 nm,[6a] both in acetonitrile). This bathochromic shift also reflects the non-planar structure of the COT ring in 1^{2+} from the following reasoning. As the COT ring of the dication undergoes the transformation from planar to tub structures, the HOMO-LUMO gap gradually decreases due to both the splitting of the originally degenerate LUMOs of the dication and the concomitant rising of the HOMO. In fact, the CNDO/S calculations for the unsubstituted COT dication predicted a 0.85 eV decrease in transition energy (the HOMO-LUMO gap) upon going from the planar structure to the tub structure (with the bent angle (α) of 34.5°) which corresponds to the calculated value for the structure **B**.

In conclusion, we have succeeded in the first isolation and X-ray structure determination of the cation radical salt of a COT derivative $1^{\cdot+}$, and have experimentally proved the previous theoretical prediction for the structure of COT cation radical. The remarkable stability of $1^{\cdot+}$ is ascribed to the full annelation of the COT ring with a rigid bicycloalkene framework. Further one-electron oxidation of this cation radical $1^{\cdot+}$ successfully led to the formation of dication 1^{2+}. Dication 1^{2+} was found to be stable at room temperature in solution, and to take a tub conformation rather than a planar structure. It seems that the aromatic stability in the planar 6π COT dication is delicately balanced with destabilization caused by the angle strain.[13] Apparently, the annelation with rigid bicyclic systems in the present dication 1^{2+} induces considerable angle strain as well as the non-bonded interaction between bridgehead hydrogens, in the planar form **A**. Nevertheless, a gain of aromatic stabilization has made the planar (or nearly planar) structure stable enough, so that the ring inversion can occur quite readily

in contrast to the case of neutral COT **1** in which no such inversion was observed in an NMR time-scale even by heating at 150 °C (the lower limit of the inversion barrier, 24 kcal mol^{-1}).[5]

Experimental Section

General Procedures. The melting point was determined on a Yamato MP–21 apparatus and is uncorrected. Elemental analysis was performed by Microanalytical Center, Kyoto University, Kyoto. NMR spectra were recorded on JEOL GSX270 (270 MHz for ^1H and 67.8 MHz for ^{13}C NMR) spectrometer or a JEOL FX 90 (90 MHz for ^1H and 22.5 MHz for ^{13}C NMR) using Me_4Si as an internal standard unless otherwise noted. IR spectra were taken on Perkin Elmer 1640 spectrometer. UV–vis spectra were taken on Hitachi 200–10 spectrometer. Cyclic Voltammograms were obtained by the use of a Hokuto–Denko Model HA 104 potensiostat, a Hokuto–Denko Model HB 107A function generator and a Hitachi 057 X–Y recorder. ESR spectra were recorded on a JEOR PE–2X spectrometer. Theoretical calculations were performed on a FACOM VP–400E computer of Kyoto University Data Processing Center or on a CRAY Y–MP2E/264 computer of Supercomputer Laboratory, Institute for Chemical Research, Kyoto University.

$NO^+SbCl_6^-$ was prepared according to the literature procedure.[9] THF was freshly distilled from sodium benzophenone ketyl before use. All reactions where anhydrous conditions were required were conducted under an atmosphere of argon or nitrogen. Dichloromethane was distilled over CaH_2 under nitrogen atmosphere

Electrochemical Oxidation. **(a) CV Measurement under Argon atmosphere.** A three-electrode cell was used, consisting of Pt-wire counter and working electrodes, and a Ag/ $AgNO_3$ (0.01 M in acetonitrile) as a reference electrode. The reference electrode was connected to the sample solution by a salt bridge made up with a $Bu_4N^+ClO_4^-$ solution in acetonitrile (0.1M). The sample solution was prepared with **1** (1.4 mg, 3.3 x 10^{-3} mmol), and $Bu_4N^+ClO_4^-$ (0.1M) in dichloromethane (2 mL) and acetonitrile (6 mL). After bubbling the solution with argon gas, the measurement was carried out with a 0.1 V sec^{-1} scan rate. The observed potential was corrected with reference to ferrocene ($E_{1/2}$ = 0.083 V vs Ag/Ag^+) which was added as an internal standard after each measurement.

(b) CV Measurement under Vacuum. An originally made three-electrode cell equipped with Pt wire working and counter electrodes and a Ag wire as a reference electrode was used. It was ascertained that this cell could keep the vacuum (~10^{-4} mmHg). The sample of COT **1** (2.6 mg; 6.1 x 10^{-3} mmol) and $Bu_4N^+BF_4^-$ (273 mg; 8.29 x 10^{-1} mmol) as a supporting electrolyte were placed in the cell, which was then connected to a vacuum line. Dichloromethane (8 mL), trifluoroacetic acid (0.4 mL) and trifluoroacetic anhydride (0.4 mL) which had been degassed by three freeze-pump-thaw cycles were directly transferred by vacuum-distillation into the cell, which was then sealed under vacuum, and subjected to the measurement. The observed potential was corrected with reference to ferrocene ($E_{1/2}$ = 0.083 V vs Ag/Ag^+).

(c) ESR Measurement. An originally made electrolytic cell was used. The cell consisted of a 5–mm o.d. Pyrex grass tube (length, 65 mm) which was connected to a 3–mm o.d. tube (length 40 mm) at the bottom and a 20–mm o.d. tube (length, 40 mm) at the top (Figure 9). A platinum wire (diameter, 0.5 mm) reaching the bottom, which was shielded with a polyethylene tube except the bottom part, served as a working electrode and a gold helical wire was used as a

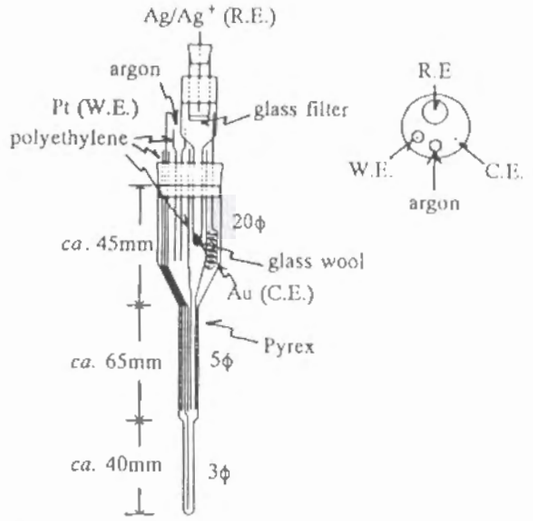

Figure 9. ESR cell for electrolytic oxidation.

counter electrode. A reference electrode ($Ag/AgNO_3$) was also inserted into an upper part together with a capillary polyethylene tube for the purpose of introducing an argon gas.

A solution of **1** (1 mg, 2.4 x 10^{-3} mmol) in 5 mL of 0.1 M solution of $Bu_4N^+ClO_4^-$ in acetonitrile was placed in the cell. After bubbling with argon for a few minutes, the solution was electrolyzed at +0.5 V vs Ag/Ag^+ at room temperature. The ESR signal composed of nine-line signals (see text) appeared 1–2 min after initiation of electrolysis and lasted for 5–10 min after cutting off the anodic current.

Preparation of Cation Radical salt $1^{\cdot+}SbCl_6^-$. A 27.9 mg amount (7.65 x 10^{-2} mmol) of $NO^+SbCl_6^-$ and 25.1 mg of COT **1** (5.91 x 10^{-2} mmol) were weighed into a dried 10 mm–o.d. test-tube under argon atmosphere, and there was added 3 mL of dichloromethane under argon. Immediately a dark-green solution was formed. Reprecipitation with benzene gave $1^{\cdot+}SbCl_6^-$ (34.2 mg; 76 %) as a

dark green solid. A single crystal of $\mathbf{1}^{\cdot+}SbCl_6^-$ was grown by slow diffusion of benzene into the saturated solution in dichloromethane. $\mathbf{1}^{\cdot+}SbCl_6^-$; dark green-black plates; mp. 134–135°C (dec.). IR (KBr) ν 2935, 2860, 1653, 1487, 1452, 1147, 1024, and 668 cm^{-1}. For the electronic and ESR spectra, see text.

Anal. Calcd for $C_{32}H_{40}Cl_6Sb$: C, 50.63; H, 5.31; Cl, 28.02. Found: C, 50.28; H, 5.31; Cl, 27.93.

One-Electron Reduction of $\mathbf{1}^{\cdot+}SbCl_6^-$. Into a saturated acetonitrile solution of $Bu_4N^+I^-$ (10 mL) was added 13.2 mg of $\mathbf{1}^{\cdot+}SbCl_6^-$. The reaction mixture was treated with 10 mL ether and 10 mL 10 % HCl*aq* for the removal of the ammonium salt. The organic layer was dried with $MgSO_4$ and evaporated to give a pale green solid. This solid was confirmed as neutral COT **1** by NMR measurements.

X-ray Analysis of $\mathbf{1}^{\cdot+}SbCl_6^-$. Crystal data for $\mathbf{1}^{\cdot+}SbCl_6^-$ at 20°C : tetragonal, space group $P4_{cc}$, a = 18.525 (3) Å, c = 19.261 (4) Å, V = 6610 (8) $Å^3$, Z = 8, d_{calc} = 1.526 g cm^{-3}, μ(MoKα) = 134 mm^{-1}. A total of 4348 with 2238 independent reflections was collected on a STOE STADI 4 four cycle diffractometer using graphite monochromated MoKα radiation. The structure was solved by direct methods (SHELXS86) and refined by full matrix least squares (SHELXL93) R(F) = 0.029 based on 1662 reflections with $|F| \geq 4\ \sigma F$, wR^2 = 0.069. Crystallographic data, i.e., atomic coordinate, anisotropic displacement parameters, bond lengths, and bond angles are given in Tables 3–6 respectively. The atom numbering of $\mathbf{1}^{\cdot+}SbCl_6^-$ was given in Figure 10.

Table 3. Atomic Coordinates and Equivalent Isotropic Temperature Factors for $\mathbf{1}^{\cdot+}SbCl_6^-$

Atom	X/*a*	Y/*b*	Z/*c*	*U*(EQ)
Sb1	0.0000	0.0000	0.0001(1)	0.052(1)
Sb2	0.0000	0.5000	0.1770(1)	0.043(1)
Sb3	0.5000	0.5000	0.5061(1)	0.053(1)
Cl1	0.0000	0.0000	0.1241(3)	0.098(2)
Cl2	0.0000	0.0000	-0.1202(4)	0.109(2)
Cl3	-0.0472(1)	0.1184(1)	0.0019(2)	0.103(1)
Cl4	0.0586(1)	0.4325(1)	0.2662(2)	0.071(1)
Cl5	-0.0584(1)	0.5680(1)	0.0911(2)	0.080(1)
Cl6	0.0963(1)	0.5839(1)	0.1779(2)	0.078(1)
Cl7	0.5000	0.5000	0.6296(5)	0.210(5)
Cl8	0.5000	0.5000	0.3882(4)	0.143(3)
Cl9	0.5609(1)	0.6111(1)	0.5078(3)	0.129(2)
C1	0.7386(4)	0.1876(4)	0.2588(4)	0.041(2)
C2	0.8023(4)	0.1973(4)	0.2957(4)	0.042(2)
C3	0.8151(3)	0.2487(4)	0.3505(4)	0.038(2)
C4	0.7776(4)	0.2553(4)	0.4106(4)	0.040(2)
C5	0.7110(4)	0.2196(4)	0.4289(4)	0.039(2)
C6	0.6481(4)	0.2178(4)	0.3907(4)	0.046(2)
C7	0.6371(4)	0.2493(4)	0.3223(5)	0.045(2)
C8	0.6754(4)	0.2345(4)	0.2651(4)	0.041(2)
C9	0.7460(4)	0.1342(4)	0.1995(5)	0.058(2)
C10	0.8634(4)	0.1517(4)	0.2668(5)	0.053(2)
C11	0.8854(4)	0.2925(4)	0.3495(5)	0.051(2)
C12	0.8166(5)	0.3022(4)	0.4626(5)	0.054(2)
C13	0.7017(4)	0.1892(4)	0.5017(5)	0.049(2)
C14	0.5857(4)	0.1868(4)	0.4312(4)	0.052(2)
C15	0.5726(4)	0.2963(4)	0.3093(5)	0.058(2)
C16	0.6450(4)	0.2683(4)	0.1988(4)	0.053(2)
C17	0.7693(4)	0.0631(4)	0.2325(6)	0.076(3)
C18	0.8059(5)	0.1585(5)	0.1516(5)	0.079(3)
C19	0.8398(4)	0.0727(4)	0.2721(6)	0.070(2)
C20	0.8747(5)	0.1717(5)	0.1899(5)	0.067(2)
C21	0.8630(5)	0.3717(4)	0.3619(5)	0.068(3)
C22	0.9337(4)	0.2679(5)	0.4086(5)	0.072(3)
C23	0.8237(5)	0.3767(5)	0.4318(5)	0.068(3)
C24	0.8917(5)	0.2711(5)	0.4765(5)	0.064(3)
C25	0.6766(5)	0.1121(4)	0.4946(5)	0.060(2)
C26	0.6436(5)	0.2322(4)	0.5406(5)	0.069(3)
C27	0.6066(4)	0.1089(4)	0.4531(5)	0.059(2)
C28	0.5748(5)	0.2297(5)	0.4975(5)	0.078(3)
C29	0.6011(5)	0.3665(5)	0.2783(6)	0.077(3)
C30	0.5237(5)	0.2586(5)	0.2557(6)	0.083(4)
C31	0.6464(5)	0.3500(4)	0.2133(6)	0.069(3)
C32	0.5660(4)	0.2447(4)	0.1890(6)	0.074(3)

(Table 3. Continued)

Atom	X/*a*	Y/*b*	Z/*c*	*U*(EQ)
H9	0.7004(4)	0.1287(4)	0.1743(5)	0.069
H10	0.9078(4)	0.1597(4)	0.2933(5)	0.064
H11	0.9100(4)	0.2873(4)	0.3048(5)	0.061
H12	0.7890(5)	0.3045(4)	0.5060(5)	0.065
H13	0.7476(4)	0.1911(4)	0.5270(5)	0.059
H14	0.5316(4)	0.1866(4)	0.4031(4)	0.062
H15	0.5463(4)	0.3056(4)	0.3525(5)	0.070
H16	0.6744(4)	0.2559(4)	0.1583(4)	0.063
H171	0.7755(4)	0.0269(4)	0.1967(6)	0.091
H172	0.7320(4)	0.0465(4)	0.2640(6)	0.091
H181	0.7913(5)	0.2026(5)	0.1282(5)	0.069
H182	0.8138(5)	0.1219(5)	0.1164(5)	0.069
H191	0.8331(4)	0.0596(4)	0.3204(6)	0.084
H192	0.8767(4)	0.0417(4)	0.2525(6)	0.084
H201	0.9130(5)	0.1426(5)	0.1702(5)	0.080
H202	0.8883(5)	0.2221(5)	0.1860(5)	0.080
H211	0.9054(5)	0.4023(4)	0.3624(5)	0.082
H212	0.8314(5)	0.3878(4)	0.3249(5)	0.082
H221	0.9500(4)	0.2190(5)	0.4001(5)	0.087
H222	0.9757(4)	0.2990(5)	0.4114(5)	0.087
H231	0.7762(5)	0.3976(5)	0.4251(5)	0.069
H232	0.8506(5)	0.4076(5)	0.4632(5)	0.082
H241	0.9171(5)	0.3012(5)	0.5096(5)	0.076
H242	0.8874(5)	0.2230(5)	0.4960(5)	0.076
H251	0.7135(5)	0.0839(4)	0.4613(5)	0.072
H252	0.6689(5)	0.0916(4)	0.5403(5)	0.072
H261	0.6951(5)	0.2818(4)	0.5469(5)	0.083
H262	0.6352(5)	0.2112(4)	0.5860(5)	0.083
H271	0.5685(4)	0.0880(4)	0.4812(5)	0.070
H272	0.6131(4)	0.0790(4)	0.4123(5)	0.070
H281	0.5601(5)	0.2785(5)	0.4859(5)	0.094
H282	0.5365(5)	0.2078(5)	0.5247(5)	0.094
H291	0.6306(5)	0.3914(4)	0.3123(6)	0.093
H292	0.5610(5)	0.3976(4)	0.2661(6)	0.093
H301	0.4822(5)	0.2889(5)	0.2457(6)	0.099
H302	0.5063(5)	0.2132(5)	0.2744(6)	0.099
H311	0.6269(5)	0.3760(4)	0.1738(6)	0.083
H312	0.6957(5)	0.3658(4)	0.2205(6)	0.083
H321	0.5641(4)	0.1937(4)	0.1775(6)	0.089
H322	0.5445(4)	0.2715(4)	0.1510(6)	0.089

Table 4. Anisotropic Temperature Factors for $1^{\cdot+}SbCl_6^-$

Atom	*U*11	*U*22	*U*33	*U*23	*U*13	*U*12
Sb1	0.047(1)	0.047(1)	0.063(1)	0.0000	0.0000	0.0000
Sb2	0.051(1)	0.046(1)	0.033(1)	0.0000	0.0000	0.010(1)
Sb3	0.046(1)	0.046(1)	0.066(1)	0.0000	0.0000	0.0000
Cl1	0.115(3)	0.115(3)	0.066(4)	0.0000	0.0000	0.0000
Cl2	0.125(3)	0.125(3)	0.075(4)	0.0000	0.0000	0.0000
Cl3	0.105(2)	0.059(1)	0.147(3)	0.018(2)	0.046(2)	0.023(1)
Cl4	0.078(2)	0.080(2)	0.056(2)	0.026(1)	-0.009(1)	0.016(1)
Cl5	0.091(2)	0.089(2)	0.060(2)	0.017(2)	-0.011(2)	0.028(1)
Cl6	0.080(1)	0.083(1)	0.070(1)	0.011(2)	0.002(2)	-0.022(1)
Cl7	0.276(7)	0.276(7)	0.080(5)	0.0000	0.0000	0.0000
Cl8	0.176(4)	0.176(4)	0.076(5)	0.0000	0.0000	0.0000
Cl9	0.073(2)	0.056(1)	0.258(5)	-0.014(2)	-0.037(2)	-0.012(1)
C1	0.040(4)	0.038(4)	0.045(5)	0.005(4)	0.001(4)	0.001(3)
C2	0.033(4)	0.048(4)	0.043(5)	0.004(4)	0.001(4)	-0.003(3)
C3	0.036(4)	0.041(4)	0.035(5)	-0.001(4)	-0.012(4)	0.001(3)
C4	0.048(4)	0.048(5)	0.023(5)	0.004(3)	-0.001(4)	0.000(4)
C5	0.048(5)	0.039(4)	0.032(4)	-0.004(4)	0.003(4)	0.003(4)
C6	0.038(4)	0.047(4)	0.053(6)	-0.009(4)	0.001(4)	-0.002(4)
C7	0.034(4)	0.039(4)	0.063(6)	-0.002(4)	-0.003(4)	-0.006(3)
C8	0.037(4)	0.039(4)	0.045(5)	-0.008(4)	-0.013(4)	-0.002(3)
C9	0.054(5)	0.064(5)	0.054(6)	-0.015(4)	-0.010(4)	0.004(4)
C10	0.038(4)	0.070(5)	0.053(5)	-0.012(5)	-0.007(4)	0.007(4)
C11	0.038(4)	0.062(5)	0.054(5)	0.000(4)	-0.004(4)	-0.006(3)
C12	0.064(5)	0.057(5)	0.043(5)	-0.007(4)	-0.010(4)	-0.007(4)
C13	0.046(4)	0.055(5)	0.046(5)	-0.010(4)	0.001(4)	-0.002(4)
C14	0.049(5)	0.061(5)	0.045(5)	-0.006(4)	0.016(4)	0.007(4)
C15	0.046(5)	0.059(5)	0.070(6)	0.007(5)	0.005(5)	0.007(4)
C16	0.063(5)	0.050(4)	0.045(5)	0.005(4)	-0.014(4)	0.013(4)
C17	0.062(6)	0.047(5)	0.118(9)	0.002(5)	-0.007(6)	0.006(4)
C18	0.086(7)	0.095(7)	0.056(6)	-0.011(6)	-0.001(6)	0.014(6)
C19	0.071(6)	0.057(5)	0.083(7)	0.000(6)	-0.006(6)	0.017(4)
C20	0.072(6)	0.077(6)	0.052(6)	-0.007(5)	0.010(5)	0.000(4)
C21	0.084(7)	0.058(6)	0.061(7)	0.007(5)	-0.009(5)	-0.021(5)
C22	0.039(5)	0.091(7)	0.087(7)	0.005(6)	-0.018(5)	-0.001(4)
C23	0.067(6)	0.058(6)	0.080(7)	-0.005(5)	-0.012(6)	0.003(4)
C24	0.073(6)	0.071(6)	0.047(6)	-0.002(5)	-0.034(5)	-0.021(5)
C25	0.072(6)	0.052(5)	0.057(6)	0.006(5)	0.001(5)	-0.007(4)
C26	0.103(7)	0.055(5)	0.051(6)	-0.015(5)	0.014(6)	-0.014(5)
C27	0.062(5)	0.047(5)	0.068(6)	-0.004(4)	0.012(5)	-0.016(4)
C28	0.079(7)	0.077(6)	0.078(7)	-0.006(6)	0.029(6)	0.001(5)
C29	0.087(6)	0.050(5)	0.095(8)	-0.010(6)	-0.008(7)	0.018(4)
C30	0.037(5)	0.080(6)	0.131(12)	-0.003(6)	-0.030(6)	0.012(4)
C31	0.085(6)	0.039(5)	0.084(7)	0.006(5)	-0.019(6)	-0.008(4)
C32	0.050(5)	0.061(5)	0.111(9)	0.025(6)	-0.034(6)	-0.002(4)

Table 5. Observed Bond Lengths of $1^{\cdot+}SbCl_6^-$

Bond length(Å)		Bond length(Å)	
Sb1-Cl1	2.390(6)	C9-C17	1.524(12)
Sb1-Cl2	2.317(7)	C9-C18	1.511(12)
Sb1-Cl3	2.361(2)	C10-C19	1.530(11)
C1-C2	1.389(10)	C10-C20	1.542(12)
C1-C8	1.464(10)	C11-C21	1.543(10)
C1-C9	1.517(11)	C11-C22	1.516(11)
C2-C1	1.389(10)	C12-C23	1.507(11)
C2-C3	1.440(10)	C12-C24	1.529(11)
C2-C10	1.518(9)	C13-C25	1.507(10)
C3-C2	1.440(10)	C13-C26	1.535(10)
C3-C4	1.356(10)	C14-C27	1.552(10)
C3-C11	1.535(9)	C14-C28	1.520(11)
C4-C3	1.356(10)	C15-C29	1.524(11)
C4-C5	1.444(11)	C15-C30	1.542(12)
C4-C12	1.511(11)	C16-C31	1.540(10)
C5-C4	1.444(11)	C16-C32	1.539(10)
C5-C6	1.377(10)	C17-C19	1.523(12)
C5-C13	1.521(11)	C18-C20	1.493(11)
C6-C5	1.377(10)	C21-C23	1.532(13)
C6-C7	1.455(11)	C22-C24	1.523(13)
C6-C14	1.508(10)	C25-C27	1.525(12)
C7-C6	1.455(11)	C26-C28	1.522(13)
C7-C8	1.338(11)	C29-C31	1.537(13)
C7-C15	1.500(9)	C30-C32	1.526(14)
C8-C16	1.529(10)		

Table 6. Observed Bond Angles of $1^{\cdot+}SbCl_6^-$

Bond angle(deg)		Bond angle(deg)	
Cl1-Sb1-Cl2	180.00	C3-C11-C22	109.5(7)
Cl1-Sb1-Cl3	89.15(11)	C21-C11-C22	109.1(7)
Cl2-Sb1-Cl3	90.85(11)	C4-C12-C23	107.9(7)
C2-C1-C8	124.1(7)	C4-C12-C24	109.5(6)
C2-C1-C9	113.2(6)	C23-C12-C24	109.6(7)
C8-C1-C9	121.4(7)	C5-C13-C25	107.6(7)
C1-C2-C3	126.9(6)	C5-C13-C26	109.7(6)
C1-C2-C10	111.9(7)	C25-C13-C26	108.7(7)
C3-C2-C10	120.9(6)	C6-C14-C27	107.7(6)
C2-C3-C4	126.9(6)	C6-C14-C28	109.7(7)
C2-C3-C11	118.7(7)	C27-C14-C28	106.9(7)
C4-C3-C11	113.4(7)	C7-C15-C29	106.6(7)

(Table 6. Continued)

Bond angle(deg)		Bond angle(deg)	
C3-C4-C5	127.3(7)	C7-C15-C30	108.5(7)
C3-C4-C12	111.9(7)	C29-C15-C30	109.1(8)
C5-C4-C12	120.7(7)	C8-C16-C31	104.2(6)
C4-C5-C6	127.1(7)	C8-C16-C32	109.7(7)
C4-C5-C13	119.4(7)	C31-C16-C32	108.5(6)
C6-C5-C13	112.8(7)	C9-C17-C19	110.5(7)
C5-C6-C7	126.3(7)	C9-C18-C20	111.9(8)
C5-C6-C14	112.4(7)	C10-C19-C17	108.9(7)
C7-C6-C14	120.9(7)	C10-C20-C18	108.7(7)
C6-C7-C8	126.1(7)	C11-C21-C23	108.8(7)
C6-C7-C15	119.7(8)	C11-C22-C24	109.3(6)
C8-C7-C15	113.8(8)	C12-C23-C21	109.4(7)
C1-C8-C7	127.9(7)	C12-C24-C22	109.2(7)
C1-C8-C16	117.9(7)	C13-C25-C27	110.3(7)
C7-C8-C16	114.1(6)	C13-C26-C28	107.8(7)
C1-C9-C17	105.9(7)	C14-C27-C25	108.6(7)
C1-C9-C18	109.4(7)	C14-C28-C26	111.3(7)
C17-C9-C18	107.8(7)	C15-C29-C31	109.8(7)
C2-C10-C19	107.2(6)	C15-C30-C32	109.8(7)
C2-C10-C20	108.7(7)	C16-C31-C29	109.5(7)
C19-C10-C20	109.4(8)	C16-C32-C30	109.7(8)
C3-C11-C21	105.8(6)		

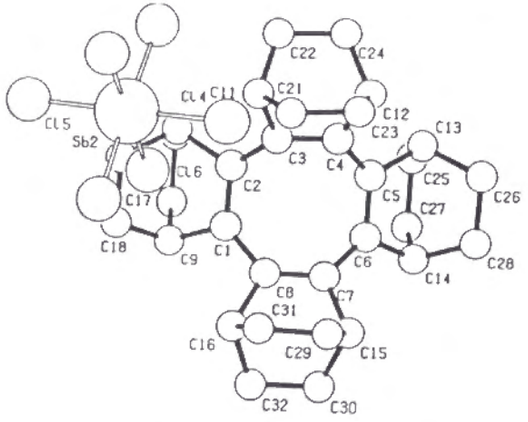

Figure 10. Crystal structure and the atom numbering of $1^{\cdot+}SbCl_6^-$

ESR or ENDOR Measurement of $1^{\cdot+}SbCl_6^-$. A 9-mm o.d. Pyrex glass tube having a 5-mm o.d. ESR sample tube (length, 300 mm) as a side arm was used, which was connectable to a vacuum line. In the 9-mm tube was placed $1^{\cdot+}SbCl_6^-$ (*ca.* 3 mg) and the tube was evacuated to 10^{-4} mmHg. A solvent (1.0 mL) placed in a flask connected to a vacuum line was degassed and dried by repeating the freeze-pump-thaw cycle for three times over CaH_2, and then transferred to the 9-mm tube by vacuum distillation. After sealing off the 9-mm tube, $1^{\cdot+}SbCl_6^-$ was dissolved in the solvent and the ESR spectrum was recorded immediately.

Generation and Observation of 1^{2+}. (a) NMR Measurements. A 5-mm o.d. NMR sample tube having a 9-mm o.d. Pyrex glass tube at the upper part as a side arm was used, which was connectable to a vacuum line. In the 5-mm tube and in the 9-mm o.d. side arm were placed $1^{\cdot+}SbCl_6^-$ (6.4 mg, 8.4 x 10^{-3} mmol) and SbF_5 (0.1 mL, *ca.* 100 equiv) respectively and the tube was evacuated to 10^{-4} mmHg. Dichloromethane-d_2 (1.0 mL) placed in a flask connected to a vacuum line was dried over CaH_2 and degassed by repeating the freeze-pump-thaw cycle for three times, and finally transferred to the 5-mm NMR tube by vacuum distillation. While freezing the sample in the 5-mm NMR tube with liquid nitrogen, SbF_5 was heated by a heat gun to be vacuum-distilled into the 5-mm NMR tube. After sealing off the 5-mm NMR tube, the tube was warmed to *ca.* −78 °C, and $1^{\cdot+}SbCl_6^-$ was dissolved into the solvent. Upon dissolution and mixing, the original green color of the solution turned to red, and the ^1H and ^{13}C NMR spectra recorded at −80, −70, −50, −20, 0, and 25 °C gave the results shown in the text. The chemical shifts were read using the CD_2Cl_2 signal (δ 5.35 for ^1H and δ 53.1 for ^{13}C NMR) as a reference.

(b) UV–vis Measurements. The same quartz cell as the one described in Experimental section of Chapter 2 (Figure 7; p.30) was used. The cation radical salt $1^{\cdot+}SbCl_6^-$ (0.40 mg, 5.3 x 10^{-4} mmol) in a tared small grass tube was weighed, and was placed in the chamber C. Then the inlet B was sealed. SbF_5 (0.1 mL, *ca.* 100 equiv) was placed in the chamber E. After the vessel was evacuated at the tube end, dichloromethane (1 mL), which had been dried over CaH_2 and degassed by repeating the freeze-pump-thaw cycle for three times, was transferred into the chamber A by distillation under vacuum. While the solution was frozen by liquid nitrogen, SbF_5 was heated with a heat gun to be transferred into the frozen dichloromethane. Then, the tube was sealed off under vacuum at the part D. The frozen mixture was melted and mixed well to give a red solution of dication 1^{2+}. The UV–vis spectrum was measured at room temperature; λ_{max} (CH_2Cl_2) 533 nm (log ε 3.8).

CNDO/S Calculation of Parent $COT^{\cdot 2+}$. First, the AM1 calculations were conducted for optimization of each of the two structures of unsubstituted COT dication, i.e., a planar structure **C** with the dihedral angle 1-2-3-4, 2-3-4-5, 3-4-5-6, 4-5-6-7, and 5-6-7-8 fixed at 0 ° and a tub structure **D** with the dihedral angle 2-3-4-5 and 4-5-6-7 fixed at 0 ° and 1-2-3-4, 3-4-5-6, and 5-6-7-8 at 50 ° (nearly the same angle as the one in the optimized structure for 1^{2+}). Then, CNDO/S calculations were performed in order to estimate the transition energy for each of the AM1 optimized structure: the lowest transition energy was calculated to be 4.53 eV and 3.68 eV for the structures of **C** and **D**, respectively.

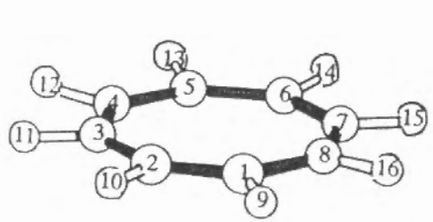

C

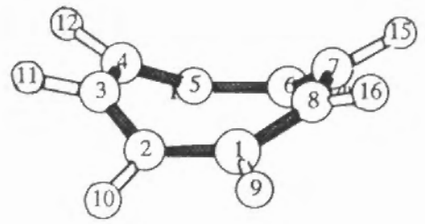

D

References and Notes

(1) (a) Katz, T. J.;Strauss, H. L. *J. Chem. Phys*. **1960**, *32*, 1873-1875. (b) Katz, T. J. *J. Am. Chem. Soc.* **1960**, *82*, 3784-3786. (c) Katz, T. J.; Reinmuth, W. H.; Smith, D. E. *J. Am. Chem. Soc.* **1962**, *84*, 802-808. (d) Strauss, H. L; Katz, T. J.; Frankel, G. K. *J. Am. Chem. Soc.* **1963**, *85*, 2360-2364. (e) Paquette, L. A.; Ley, S. V.; Meisinger, R. H.; Russell, R. K.; Oku, M. *J. Am. Chem. Soc.* **1974**, *96*, 5806-5815. (f) Paquette, L. A.; Trova, M. P.; Luo, J.; Clough, A. E.; Anderson, L. B. *J. Am. Chem. Soc.* **1990**, *112*, 228-239, and the references cited therein.

(2) Olah, G. A.; Staral, J. S.; Liang, G.; Paquette, L. A.; Melega, W. P.; Carmody, M. J. *J. Am. Chem. Soc.* **1977**, *99*, 3349-3355.

(3) (a) Desseau, R. M. *J. Am. Chem. Soc.* **1970**, *92*, 6356-6358. (b) Shida, T.; Iwata, S. *J. Am. Chem. Soc.* **1973**, *95*, 3473-3483. (c) Dai, S.; Wang, J. T.; Williams, F. *J. Am. Chem. Soc.* **1990**, *112*, 2837-2839.

(4) Dewar, M. J. S.; Harget, A.; Haselbach, E. *J. Am. Chem. Soc.* **1969**, *91*, 7521-7523.

(5) Komatsu, K.; Nishinaga, T.; Aonuma, S.; Hirosawa, C.; Takeuchi, K.; Lindner, H. J.; Richter, J. *Tetrahedron Lett.* **1991**, *32*, 6767-6770.

(6) (a) Komatsu, K.; Akamatsu, H.; Jinbu, Y.; Okamoto, K. *J. Am. Chem. Soc.* **1988**, *110*, 633-634. (b) Komatsu, K.; Akamatsu, H.; Aonuma, S.; Jinbu, Y.; Mackawa, N.; Takeuchi, K. *Tetrahedron* **1991**, *47*, 6951-6966.

(7) Komatsu, K.; Aonuma, S.; Jinbu, Y.; Tsuji, R.; Hirosawa, C.; Takeuchi, K. *J. Org. Chem.* **1991**, *56*, 195-203.

(8) O. Hammerich and V. D. Parker, *Electrochimica Acta*, 1973, **18**, 537.

(9) Kim, E. K.; Kochi, J. K. *J. Am. Chem. Soc*. **1991**, *113*, 4962-4974.

(10) Clark, T.; Teasley, M. F.; Nelsen, S. F.; Wynberg, H. *J. Am. Chem. Soc.* **1987**, *109*, 5719-5724.

(11) The MNDO calculation of neutral molecule at the AM1 optimized cation geometry gave 1.77 and 2.66 eV (701 and 465nm), while that for the MNDO optimized geometry afforded 1.47 and 2.22 eV (845 and 465nm).

(12) J. B. Stothers, "Carbon-13 NMR Spectroscopy", Academic Press, New York, 1972, p. 91.

(13) For the similar results obtained by AM1 calculations, see N. S. Mills, *J. Org. Chem*., 1992, **57**, 1899.

Chapter 4

A Polycyclic Pentamer of Bicyclo[2.2.2]octene. A Hydrocarbon Molecule with a Long C-C Single Bond Connecting Two Cofacially Disposed Cyclopentadiene Rings

Abstract

Intramolecular reductive cyclization was examined for the α,ω-dibromide of the bicyclo[2.2.2]oct-2-ene-2,3-diyl pentamer, **1** (n = 5). Reduction of **1** (n = 5) with an excessive amount of sodium naphthalenide in THF at −78 °C afforded hydrocarbon **5** in 61% yield. The structure of **5** was determined by X-ray crystallography to be a bicyclo[2.2.2]octane having two bis(bicyclo[2.2.2]octeno)-cyclopentadiene rings spiro-connected at the vicinal carbons. The X-ray structure disclosed remarkable elongation (1.627(4) Å) of the σ-bond connecting the two cyclopentadiene rings. Theoretical considerations based on both molecular mechanics and molecular orbital calculations on compound **5** and on the related model compounds imply that the major contributing factor for this bond elongation is the σ-π interaction (C-C hyperconjugation) between the σ-bond and the dienyl π-systems in the cyclopentadiene rings. The elongated σ-bond was readily cleaved by potassium metal to give a cyclohexane substituted by two cyclopentadienide anions at the 1,4-positions.

Introduction

The use of a certain molecular unit as a building block to construct highly ordered molecules with well-defined structures is an attractive methodology in modern synthetic and structural organic chemistry.[1] In the previous work in this laboratory, the bicyclo[2.2.2]oct-2-ene (BCO) unit was utilized as such a molecular building block.[2] Thus, linear combination of a dibromo-BCO monomer to oligomeric dibromides **1** followed by reductive cyclization at the two ends of **1** (n = 3 and 4) has successfully led to the formation of benzene **2** [2a] and cyclooctatetraene (COT) **3**[2b] fully annelated with bicyclic σ-frameworks (Scheme 1).

Scheme 1

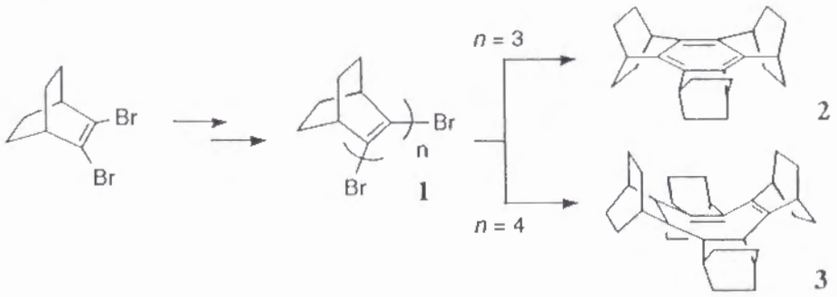

Although the central π-systems in **2** and **3** are simply the classically known aromatic and polyolefinic rings, they demonstrated unusual properties such as remarkable stabilization at the one- or two-electron oxidized states due to steric and electronic effects of the rigid σ-frameworks surrounding the π-systems.[2a, 3, 4] In the present chapter is described the two-electron reduction of BCO-pentamer **1** (n = 5) and the novel structure and properties of a polycyclic hydrocarbon which was produced.

Results and Discussion

Two-Electron Reduction of the Pentameric Dibromide 1(n = 5). The dibromide of BCO-pentamer, **1** (n = 5), was isolated from a mixture of oligomers **1** (n = 2–5), obtained via generation of bicyclo[2.2.2]octyne by lithiation of monomeric dibromide **1** (n = 1) followed by LiBr elimination, as has been reported.[2a] In contrast to the two-electron reduction of dibromides **1** (n = 3, 4), which gave the cyclized hydrocarbons smoothly at room temperature,[2] the reduction of pentamer **1** (n = 5) required cooling to −78 °C in order to effect a "clean" reaction to give a hydrocarbon product in substantial yield.

The hydrocarbon isolated as a major product in 61% yield exhibited ^{13}C NMR signals for two types of sp^2 carbons, three types of methine-, five types of methylene-, and one quaternary carbon by DEPT experiment, and ^1H NMR signals for methine singlets and complex methylene signals. The compound also showed an electronic absorption at 274 nm (log ε 3.62). From these spectral data, the product can not be considered to be a ten-membered ring hydrocarbon such as **4**, which might have been formed if the two ends of **1** (n = 5) were simply connected by a single bond. Neither were ring-contracted products such as COT **3** nor benzene **2** formed.

The structure of this product was determined by X-ray crystallography to be hydrocarbon **5**, that is, a bicyclo[2.2.2]octane having two spiro-connected cyclopentadiene rings at the vicinal carbons, as shown in Figure 1. The data of bond lengths and angles are shown in Tables 1 and 2, respectively.

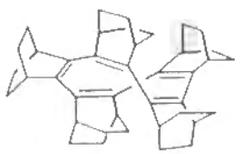

4

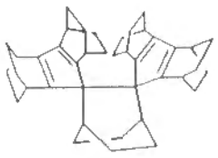

5

(a)

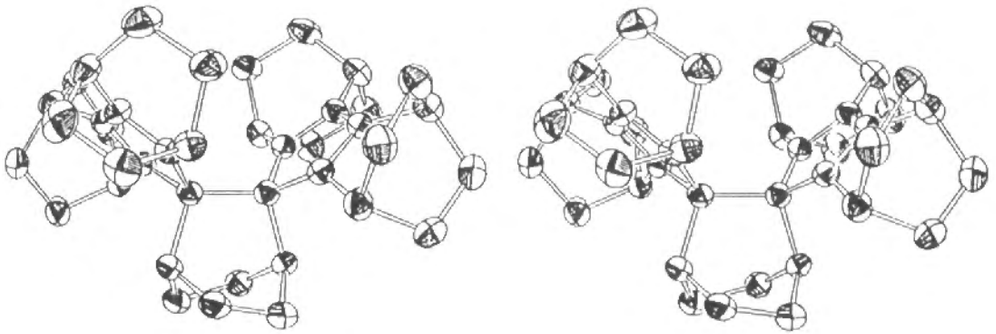

(b)

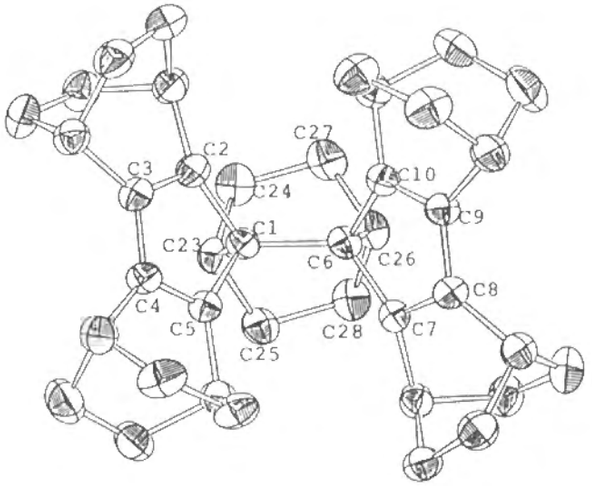

Figure 1. ORTEP drawings of the X-ray structure of **5**: (a) a stereoview of the side view; (b) a top view. Hydrogens are omitted for clarity. Some selected bond lengths (Å) and angles (deg) are: C1-C2, 1.567(5); C2-C3, 1.356(4); C3-C4, 1.447(5); C4-C5, 1.341(5); C5-C1, 1.536(4); C1-C6, 1.627(4); C6-C7, 1.572(5); C7-C8, 1.353(4); C8-C9, 1.439(5); C9-C10, 1.340(5); C10-C6, 1.539(4); C1-C23, 1.581(3); C23-C24, 1.531(5); C24-C27, 1.549(4); C27-C26, 1.526(5); C26-C6, 1.579(3); C1-C2-C3, 109.3(3); C2-C3-C4, 109.9(3); C3-C4-C5, 110.1(3); C4-C5-C1, 110.9(3); C5-C1-C6, 113.6(2); C2-C1-C6, 120.6(2); C1-C6-C10, 113.2(2); C1-C6-C7, 120.0(2); C5-C1-C2, 99.6(2); C7-C6-C10, 99.6(2); C6-C1-C23, 106.6(2); C1-C23-C24, 112.5(2); C1-C23-C25, 110.1(2).

Table 1. Observed Bond Lengths of **5**

Bond	Length(Å)	Bond	Length(Å)
C1-C2	1.567(5)	C14-C16	1.538(5)
C1-C5	1.536(4)	C17-C18	1.540(5)
C1-C6	1.627(4)	C17-C19	1.529(4)
C1-C23	1.581(3)	C18-C21	1.542(4)
C2-C3	1.356(4)	C19-C22	1.536(5)
C2-C11	1.519(5)	C20-C21	1.547(5)
C3-C4	1.447(5)	C20-C22	1.549(4)
C3-C14	1.498(5)	C23-C24	1.531(5)
C4-C5	1.341(5)	C23-C25	1.526(5)
C4-C17	1.500(5)	C24-C27	1.549(4)
C5-C20	1.497(4)	C25-C28	1.543(5)
C6-C7	1.572(5)	C26-C27	1.526(5)
C6-C10	1.539(4)	C26-C28	1.544(5)
C6-C26	1.579(3)	C29-C30	1.560(4)
C7-C8	1.353(4)	C29-C31	1.539(5)
C7-C29	1.524(3)	C30-C33	1.536(5)
C8-C9	1.439(5)	C31-C34	1.551(5)
C8-C32	1.503(3)	C32-C33	1.546(5)
C9-C10	1.340(5)	C32-C34	1.524(5)
C9-C35	1.500(3)	C35-C36	1.537(5)
C10-C38	1.495(3)	C35-C37	1.529(5)
C11-C12	1.535(5)	C36-C39	1.546(5)
C11-C13	1.558(4)	C37-C40	1.540(5)
C12-C15	1.541(4)	C38-C39	1.548(4)
C13-C16	1.543(5)	C38-C40	1.557(4)
C14-C15	1.532(5)		

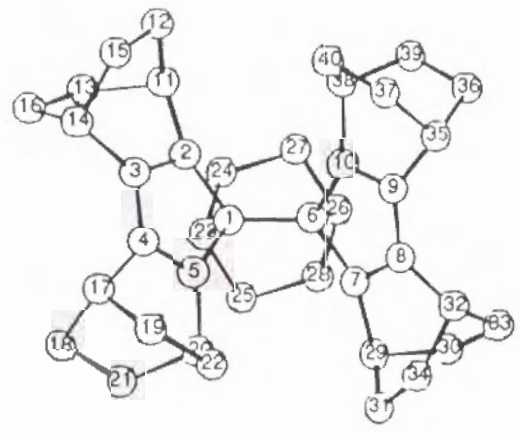

Table 2. Observed Bond Angles of **5**

Bond	Angle(deg)	Bond	Angle(deg)
C2-C1-C5	99.6(2)	C15-C14-C16	108.0(3)
C2-C1-C6	120.41	C12-C15-C14	108.3(3)
C5-C1-C6	115.6(2)	C13-C16-C14	109.4(3)
C2-C1-C23	105.8(2)	C4-C17-C18	106.2(3)
C5-C1-C23	110.2(2)	C4-C17-C19	108.4(2)
C6-C1-C23	106.6(2)	C18-C17-C19	106.9(3)
C1-C2-C3	109.3(3)	C17-C18-C21	109.4(3)
C1-C2-C11	137.0(2)	C17-C19-C22	110.2(2)
C3-C2-C11	110.0(3)	C5-C20-C21	107.8(2)
C2-C3-C4	109.9(3)	C5-C20-C22	108.1(2)
C2-C3-C14	117.5(3)	C21-C20-C22	107.0(3)
C4-C3-C14	131.5(3)	C18-C21-C20	110.1(2)
C3-C4-C5	110.1(3)	C19-C22-C20	109.5(3)
C3-C4-C17	133.0(3)	C1-C23-C24	112.5(2)
C5-C4-C17	116.7(3)	C1-C23-C25	110.1(2)
C1-C5-C4	110.9(3)	C24-C23-C25	105.7(3)
C1-C5-C20	136.6(2)	C23-C24-C27	109.1(3)
C4-C5-C20	112.4(2)	C23-C25-C28	108.2(3)
C1-C6-C7	120.0(2)	C6-C26-C27	110.3(2)
C1-C6-C10	113.2(2)	C6-C26-C28	112.1(2)
C7-C6-C10	99.6(2)	C27-C26-C28	106.5(3)
C1-C6-C26	106.7(2)	C24-C27-C26	107.2(3)
C7-C6-C26	106.6(2)	C25-C28-C26	108.3(3)
C10-C6-C26	110.5(2)	C7-C29-C30	106.8(2)
C6-C7-C8	108.9(3)	C7-C29-C31	111.1(2)
C6-C7-C29	137.0(2)	C30-C29-C31	105.1(3)
C8-C7-C29	110.3(3)	C29-C30-C33	109.9(3)
C7-C8-C9	110.5(3)	C29-C31-C34	110.4(3)
C7-C8-C32	117.6(3)	C8-C32-C33	106.3(2)
C9-C8-C32	131.1(3)	C8-C32-C34	107.7(2)
C8-C9-C10	110.2(3)	C33-C32-C34	108.8(3)
C8-C9-C35	133.5(3)	C30-C33-C32	109.4(3)
C10-C9-C35	116.3(3)	C31-C34-C32	108.4(3)
C6-C10-C9	110.7(3)	C9-C35-C36	106.8(2)
C6-C10-C38	136.4(2)	C9-C35-C37	108.1(2)
C9-C10-C38	112.9(2)	C36-C35-C37	107.4(3)
C2-C11-C12	111.7(2)	C35-C36-C39	109.3(3)
C2-C11-C13	107.3(3)	C35-C37-C40	109.8(3)
C12-C11-C13	104.7(3)	C10-C38-C39	108.5(2)
C11-C12-C15	110.7(3)	C10-C38-C40	107.1(2)
C11-C13-C16	109.4(2)	C39-C38-C40	106.8(3)
C3-C14-C15	108.3(3)	C36-C39-C38	110.0(3)
C3-C14-C16	106.9(3)	C37-C40-C38	109.7(3)

Supposing that the cyclization took place through a σ-radical with the structure similar to the most stable conformation of hydrocarbon analog calculated by MM2[5] as shown in Figure 1 (p. 14) of Chapter 2, the direct ring closure between remote terminal carbons would have been sterically difficult. The formation of **5** most probably proceeded as shown in Scheme 2 by way of tandem double cyclization initiated by the σ-radical formed at one end of the BCO pentamer. This first cyclization can be viewed as an example of radical cyclization of the "5-exo-trig" type according to the classification by Baldwin.[6] The newly formed radical center can then attack the other end of the double bond to furnish two spiro-connected cyclopentadiene rings after further reduction. The second cyclization can alternatively be considered as a disrotatory electrocyclization of the pentadienyl radical.

Scheme 2

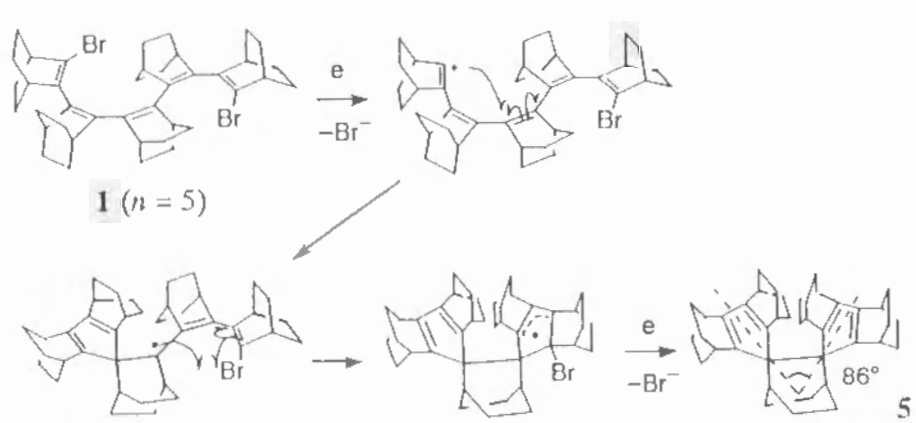

Structure of the BCO Pentamer 5. As shown in Figure 1, hydrocarbon **5** has a highly congested structure with the two BCO-annelated cyclopentadiene rings fixed in close proximity. In order to reduce the congestion, the two cyclopentadiene rings are skewed with each other, and splayed out with the dihedral

angle of 86 ° between the mean planes of cyclopentadiene rings. For a much simpler model **6** having no BCO-annelation, the MM2 calculations indicated no such skewing for the five-membered rings and indicated the splaying angle to be reduced (74.0 °).

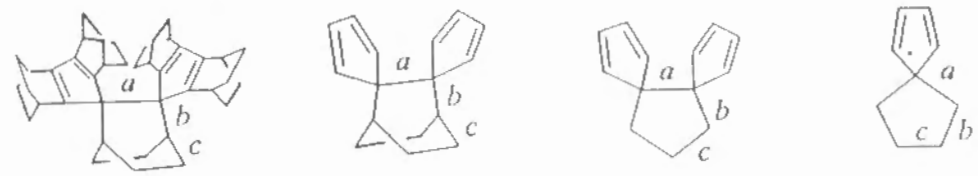

5 **6** **7** **8**

The most remarkable feature in the structure of **5** is a significant elongation (1.627(4) Å) of the central single bond *a* connecting the two cyclopentadiene rings. This bond is much longer than the generally known value of 1.54 Å for single bonds between sp^3-hybridized carbons, and is actually one of the longest C-C single bonds so far reported for cyclophanes,[7] photodimers of polynuclear aromatics,[8] and various other compounds with characteristic structural features.[9,10] The possible factors for the cause of this elongation will be discussed in detail below.

At first sight, the most obvious factor for this bond elongation may seem to be the steric one,[11] that is, the release of severe steric congestion between the two cyclopentadiene moieties with such bulky and rigid frameworks. Whether this is the sole effect for such elongation could be judged from the results of molecular mechanics (MM2) calculations. The calculated structure fairly well reproduced the experimentally observed one *except* that the central σ-bond was calculated to be only 1.570 Å, which is 0.057 Å shorter than the observed value (see Table 3). This difference between the calculated value (by MM2) and the observed value is most probably attributed to an electronic effect which was not fully taken into consideration in the MM2 calculations.[9,10,12]

Table 3. Comparison of Bond Lengths and Splaying Angles for Various Spiro-Cyclopentadienyl Compounds

compd	method	bond length (Å)			Cp - Cp (deg)[a]
		a	*b*	*c*	
5	X-ray	1.627(4)	1.580(3)	1.531(5)	85.9
	MNDO	1.632	1.601	1.563	89.4
	PM3	1.578	1.572	1.533	85.4
	MM2	1.570	1.561	1.549	76.7
6	MNDO	1.591	1.580	1.556	76.9
	STO-3G	1.596	1.569	1.549	76.2
	PM3	1.555	1.548	1.532	76.2
	MM2	1.545	1.545	1.542	74.0
7	MNDO	1.580	1.562	1.540	77.2
	PM3	1.549	1.534	1.522	76.4
	MM2	1.531	1.533	1.541	72.4
8	MNDO	1.560	1.542	1.539	—
	PM3	1.529	1.527	1.526	—
	MM2	1.531	1.538	1.542	—

[a] The splaying-out angle between two spiro-cyclopentadiene rings (dihedral angle between the planes formed by C1, C2, and C5 of the two cyclopenta-2,4-dien-1-yl rings.)

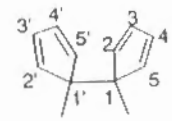

Actually, the results of semiempirical molecular orbital calculations using MNDO[13] for hydrocarbon **5** gave a value of 1.632 Å for this central σ-bond, which is quite close to the observed one. In contrast, calculations by PM3[13b,14] resulted in only a modestly long bond distance of 1.578 Å, and a similar trend was observed for a series of related compounds as summarized in Table 3. For the simpler model **6**, this central bond length was calculated by the MNDO method to be 1.591 Å, which is still considerably long in spite of the absence of any steric congestion. Ab initio molecular orbital calculations (STO-3G)[15] on **6** resulted in a value of 1.596 Å for the same bond, thus supporting the validity of the MNDO

result. These values are to be compared with the length of 1.545 Å calculated for the same bond in **6** by MM2, which is nearly 0.05 Å shorter. (See Table 3.)

From these results, it is tempting to assume that a through-bond coupling[10,12] is operating between the two cofacial cyclopentadiene systems to weaken the central bond. However, when we examine the X-ray structure of **5** more carefully, it is noted that the bonds next to the central bond are also elongated (bond *b*, 1.581(3); bond *b'*, 1.579(3) Å), whereas other single bonds are in the normal range of the C-C single bond length (see Table 1). This suggests that the bond elongation is originating from a σ-π interaction (C-C hyperconjugation) between the diene systems of the cyclopentadiene rings and the single bond connecting them.

As shown in Table 3, in the case of the more simplified model **7**, i.e., a cyclopentane having spiro-cyclopentadiene rings at the vicinal positions, the central bond was calculated by the MNDO method as 1.580 Å while the next bond was calculated as 1.562 Å. Even in the simpler model **8**, i.e., a cyclopentane with only one spiro-cyclopentadiene, the MNDO calculations showed that the cyclopentane's single bond from the spiro-carbon is 1.560 Å, which is nearly 0.02 Å elongated compared with the rest of the single bonds in the same ring (Table 3). Again, there was observed no such bond-elongation in the results of MM2 calculations for compounds **7** and **8**.

From these results, a σ-bond which is in a geometry nearly parallel to the 2p orbitals of a cyclopentadiene ring appears to be elongated due to C-C hyperconjugation with the 2p orbitals. This is in accord with a prediction from a simple frontier orbital model (**9**) that the major interaction between HOMO of the σ-bonds and LUMO of diene would make the σ-bonds longer. A typical example for such interaction is seen in spiro[2.4]hepta-4,6-diene (**10**) which displays marked elongation and shortening of the σ-bonds in the cyclopropane ring.[16] Then it would be quite reasonable to suppose that the central single bond in **5**, **6**

and **7** is further elongated due to doubly enhanced hyperconjugation effects caused by the two adjacent cyclopentadiene rings.[17]

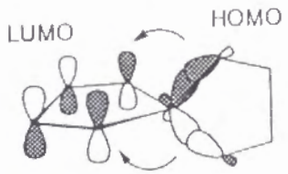

9

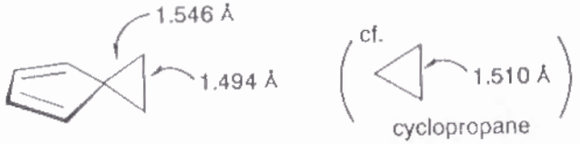

10

Reactions of the BCO Pentamer 5. Reflecting such a strained structure with an elongated central bond, the hydrocarbon **5** was found to be thermally unstable, decomposing into a mixture of unidentified products by heating in xylene at 150 °C in an ampoule sealed under vacuum.

Hydrocarbon **5** exhibited a nearly reversible oxidation wave at a very low potential such as +0.31 V vs Ag/Ag^+ [18] upon cyclic voltammetry carried out in dichloromethane. It is hypothesized that the weak central σ-bond is oxidatively cleaved. The electrolyzed solution exhibited a broad 5-line signal by ESR spectroscopy,. but its life time was too short to allow detailed examination. Hydrocarbon **5** also readily reacted with oxidizing agents such as antimony pentachloride, silver nitrate, and nitrosonium tetrafluoroborate, but did not afford a product with a well-defined structure.

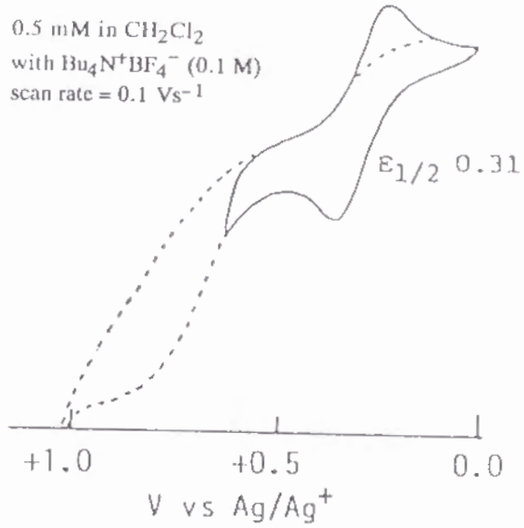

Figure 2. Cyclic Voltammogram of hydrocarbon **5** in dichloromethane.

In contrast, reduction of **5** with potassium metal in THF-d_8 in a vacuum-sealed tube smoothly afforded a solution which exhibited ^1H and ^{13}C NMR spectra that are assignable to 1,4-cyclohexylenebis(cyclopentadienide) dianion **11** (Scheme 3), thus chemically confirming the weakness of the elongated central bond.

Scheme 3

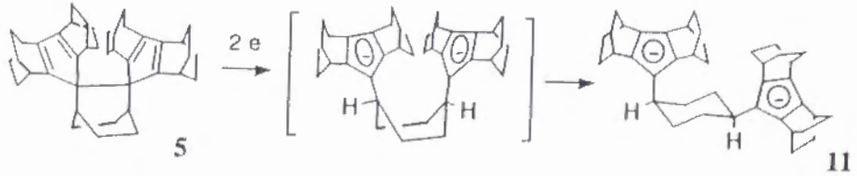

5 **11**

In summary, it was found that two-electron reduction of the α,ω-dibromide of bicyclo[2.2.2]oct-2-en-2,3-diyl pentamer (**1** (n = 5)) results in the formation of a highly congested hydrocarbon, **5**. The most probable reaction pathway is an intramolecular, tandem radical-cyclization forming two cyclopentadiene rings consecutively. Exceedingly high reactivity of the intermediate radical species would possibly be the primary cause for formation of such an overcrowded molecule. The most characteristic feature of this molecule is elongation of the central σ-bond connecting the two cyclopentadiene rings. This is ascribed not simply to steric congestion but more importantly to the σ-π conjugation (C-C hyperconjugation) of this σ-bond with the two dienyl π-systems. The weakness of this σ-bond is experimentally proven by ready cleavage upon reduction. This study presented a rare example in which even a σ-bond in a non-strained medium-sized ring can effectively interact with π-conjugated systems when both moieties are rigidly disposed with each other at an appropriate arrangement for such electronic interaction.

Experimental Section

General Procedures. The melting point was determined on a Yamato MP-21 apparatus and is uncorrected. Elemental analysis was performed by Microanalytical Center, Kyoto University, Kyoto. NMR spectra were recorded on JEOL GSX270 (270 MHz for ^{1}H and 67.8 MHz for ^{13}C NMR) spectrometer using Me_4Si as an internal standard unless otherwise noted. IR spectra were taken on Perkin Elmer 1640 spectrometer. UV-vis spectra were taken on Hitachi 200-10 spectrometer. Mass spectra were taken on a JEOL JMS-SG spectrometer.

THF was freshly distilled from sodium benzophenone ketyl before use. All reactions where anhydrous conditions were required were conducted under an atmosphere of argon or nitrogen. Commercial tetrabutylammonium perchlorate was recrystallized from n-hexane and ethyl acetate. The pentameric dibromide **1** (n = 5) was prepared following the literature procedure.[2a]

Reduction of the Pentameric Dibromide 1 (n = 5). To a stirred solution of **1** (n = 5) (215 mg, 0.311 mmol) in THF (25 mL) at −78 °C was added dropwise a solution of about 0.6 M sodium naphthalenide in THF (1.7 mL, 1.0 mmol). Addition of each drop of the naphthalenide solution caused a rapid coloration to deep red-purple. After stirring for 15 min at −78 °C the reaction mixture was quenched with methanol (20 mL) and allowed to warm to room temperature. The white solid that separated was collected by filtration and identified as hydrocarbon **5** (100.5 mg, 61%). Hydrocarbon **5** is unstable under acidic conditions, and decomposed on a silica gel column during attempted chromatography. A single crystal of **5** was prepared by very slow recrystallization from benzene: mp 247–248 °C (dec); ^{1}H NMR (C_6D_6, 270 MHz) δ 3.23 (s, 4 H, CH), 2.81 (s, 4 H, CH), 2.26 (br d, J = 8.1 Hz, 4 H, CH_2), 1.60–0.89 (m, 38 H, CH and CH_2); ^{13}C NMR (C_6D_6, 67.8 MHz)[19] δ 151.2 (>C=), 143.9 (>C=), 67.4 (>C<), 37.3 (CH), 35.5 (CH), 29.2 (CH_2), 28.6 (CH), 27.5 (CH_2), 27.3 (CH_2), 26.4 (CH_2), 25.8 (CH_2); IR (KBr) 3010, 2990, 2960, 2930, 2855, 1485, 1465, 1450, 1355, 1340, 1320, 1180, 1155, 1140, 990, 860, 875, 870, 810, 760 cm^{-1}; UV (THF) λ_{max} 274 (log ε 3.62); HRMS Calcd for $C_{40}H_{50}$: 530.3910. Found, 530.3918.

Anal. Calcd for $C_{40}H_{50}$: C, 90.51; H, 9.49. Found: C, 88.85, 88.87; H, 9.39, 9.53.[20]

Potassium Metal Reduction of 5. A 10 mm diameter Pyrex glass tube, which was connectable to a vacuum line and equipped with a 5-mm diameter NMR tube as a side arm, was prepared. Into the side-arm NMR tube was placed hydrocarbon **5** (3.5 mg, 0.0066 mmol), and potassium metal (70 mg, 1.8 mmol)

was added to the Pyrex glass tube, which was then evacuated by a vacuum line. The potassium was sublimed under vacuum by external heating to form a mirror at the upper part of the NMR tube. Then, THF–d_8 (1 mL), which had been dried over sodium-potassium alloy under vacuum, was transferred into the side-arm NMR tube under vacuum, and the NMR tube was sealed off just above the potassium mirror. The THF–d_8 solution of **5** was allowed to react with the potassium mirror in a ultrasonic bath for 1 h. A resulting pale-yellow solution exhibited the following spectra: ^{1}H NMR (THF–d_8 , 270 MHz; OCH_2 signal (3.60 ppm) of THF as an internal standard) δ 3.18 (s, bridgehead CH), 2.91 (s, bridgehead CH), 1.75 - 0.89 (m, CH and CH_2); ^{13}C NMR (THF–d_8, 67.8 MHz; CH_2 signal (24.05 ppm) of THF–d_8 as an internal standard) δ 115.3, 112.4, 108.9, 35.3, 34.1, 30.2, 29.5, 29.4, 29.1.

X-ray Structure Determination of 5. A rhombic plate of **5** was mounted on a glass capillary. All measurements were done on a STOE STADI4 diffractometer using graphite monochromated Mo Kα radiation. Cell dimensions and the orientation matrix were obtained from a least squares refinement of 54 reflections in the range of $35° < 2\theta < 42°$, measured using the ± ω scan technique. The lattice constants were a = 28.374(3) Å, b = 11.248(2) Å, c = 19.456(3) Å and β = 111.394(7)°. A data set of 5151 reflections was collected at 20 °C using a $\omega/2\theta$ scan in the range of $-29 \le h \le 30$, $0 \le k \le 12$ and $-20 \le l \le 3$. The space group determined for the monoclinic crystal system was C 2/c (No.15). For Z = 8, the formula weight 530.90, and a volume of 5782(2) Å^3, a density of 1.220 g/cm^3 was calculated. After solving the structure using the program SHELXS-86[21] the crystal was identified as a twin. The twinning law for this crystal was $h' = h$, $k' = k$, $l' = -(l+h/2)$. The intensities for each part were calculated using $I(h) = a/(2a-1)I'(h) + (a-1)/(2a-1)I'(h')$ and $I(h') = (a-1)/(2a-1)I'(h) + a/(2a-1)I'(h')$ with a = 0.75 for all reflections with $h = 2n$. The resulting data set contains 2740 independent reflections out of 3444. The structure model was refined with the program SHELXL-93 [22] using 2727 reflections with $I > 2\sigma(I)$. The hydrogen atoms were positioned geometrically with a fixed U_{eq} that was given by the U_{eq} of the atom connected to the hydrogen atom multiplied by 1.2. All other atoms were refined anisotropically. The final R-values were R_1=0.0668, wR_2=0.1668 for 361 variable parameters. The largest electron density peak/hole resulting from the difference fourier calculation were 0.373 and –0.190 e/Å^3, respectively. Crystallographic data, i.e., atomic coordinate and anisotropic displacement parameters are given in Tables 4 and 5 respectively.

Table 4. Atomic Coordinates and Equivalent Isotropic Temperature Factors for **5**

Atom	X/a	Y/b	Z/c	U(EQ)
C(1)	0.1552(01)	0.2661(02)	0.2413(02)	0.029(01)
C(2)	0.1179(01)	0.2273(03)	0.1630(02)	0.029(01)
C(3)	0.0873(01)	0.1395(03)	0.1704(02)	0.031(01)
C(4)	0.0974(01)	0.1181(03)	0.2479(02)	0.032(02)
C(5)	0.1351(01)	0.1885(03)	0.2896(02)	0.030(01)
C(6)	0.1613(01)	0.4057(03)	0.2650(02)	0.029(01)
C(7)	0.1617(01)	0.4442(03)	0.3429(02)	0.031(01)
C(8)	0.1275(01)	0.5323(03)	0.3338(02)	0.034(02)
C(9)	0.1003(01)	0.5544(03)	0.2565(02)	0.033(02)
C(10)	0.1175(01)	0.4836(03)	0.2155(02)	0.030(01)
C(11)	0.1169(01)	0.2297(03)	0.0844(02)	0.034(01)
C(12)	0.0630(01)	0.2457(03)	0.0279(02)	0.041(01)
C(13)	0.1334(01)	0.1042(03)	0.0677(02)	0.041(01)
C(14)	0.0575(01)	0.0702(03)	0.1027(02)	0.036(01)
C(15)	0.0263(01)	0.1579(03)	0.0433(02)	0.044(02)
C(16)	0.0960(01)	0.0102(03)	0.0752(02)	0.048(01)
C(17)	0.0771(01)	0.0300(03)	0.2879(02)	0.041(01)
C(18)	0.1225(01)	-0.0458(03)	0.3352(03)	0.055(01)
C(19)	0.0585(01)	0.0978(04)	0.3413(02)	0.052(01)
C(20)	0.1481(01)	0.1678(03)	0.3704(02)	0.036(01)
C(21)	0.1640(01)	0.0361(03)	0.3867(02)	0.046(01)

(Table 4. Continued)

Atom	X/*a*	Y/*b*	Z/*c*	*U*(EQ)
C(22)	0.0994(01)	0.1851(03)	0.3877(02)	0.048(01)
C(23)	0.2093(01)	0.2215(03)	0.2469(02)	0.035(01)
C(24)	0.2268(01)	0.2792(03)	0.1891(02)	0.041(01)
C(25)	0.2488(01)	0.2556(03)	0.3217(02)	0.042(01)
C(26)	0.2132(01)	0.4487(03)	0.2609(02)	0.032(01)
C(27)	0.2162(01)	0.4146(03)	0.1867(02)	0.038(01)
C(28)	0.2591(01)	0.3902(03)	0.3209(02)	0.042(02)
C(29)	0.1990(01)	0.4415(03)	0.4224(02)	0.036(01)
C(30)	0.2232(01)	0.5678(03)	0.4397(02)	0.043(01)
C(31)	0.1715(01)	0.4243(03)	0.4767(02)	0.045(01)
C(32)	0.1294(01)	0.6003(03)	0.4012(02)	0.038(01)
C(33)	0.1819(01)	0.6608(03)	0.4317(02)	0.046(01)
C(34)	0.1259(01)	0.5106(03)	0.4579(02)	0.047(01)
C(35)	0.0598(01)	0.6414(03)	0.2151(02)	0.042(01)
C(36)	0.0813(02)	0.7165(03)	0.1673(03)	0.059(01)
C(37)	0.0148(01)	0.5714(03)	0.1628(02)	0.048(01)
C(38)	0.0907(01)	0.5021(03)	0.1344(02)	0.036(01)
C(39)	0.0972(01)	0.6336(03)	0.1162(02)	0.045(01)
C(40)	0.0332(01)	0.4828(03)	0.1176(02)	0.045(01)
H(111)	0.1395(01)	0.2914(03)	0.0786(02)	0.041
H(121)	0.0628(01)	0.2324(03)	-0.0214(00)	0.049
H(122)	0.0517(01)	0.3265(03)	0.0304(02)	0.049
H(131)	0.1338(01)	0.1026(03)	0.181(02)	0.050
H(132)	0.1673(01)	0.0867(03)	0.1020(02)	0.050
H(141)	0.0357(01)	0.0113(03)	0.1135(02)	0.043
H(151)	0.0028(01)	0.2006(03)	0.0601(02)	0.053
H(152)	0.0069(01)	0.1153(03)	-0.0015(02)	0.053
H(161)	0.0785(00)	-0.0272(03)	0.0278(02)	0.057
H(162)	0.1144(01)	-0.0509(03)	0.1098(02)	0.057
H(171)	0.0502(01)	-0.0191(03)	0.2536(02)	0.049
H(181)	0.1118(01)	-0.1022(03)	0.3643(03)	0.066
H(182)	0.1358(00)	-0.0901(03)	0.3035(03)	0.066
H(191)	0.0506(01)	0.0420(04)	0.3736(02)	0.062
H(192)	0.0279(01)	0.1411(04)	0.3137(02)	0.062
H(201)	0.1751(01)	0.2214(03)	0.4001(02)	0.043
H(211)	0.1955(01)	0.0225(03)	0.3792(02)	0.055
H(212)	0.1693(01)	0.0179(03)	0.4377(02)	0.055

(Table 4. Continued)

Atom	X/*a*	Y/*b*	Z/*c*	*U*(EQ)
H(221)	0.1067(01)	0.1711(03)	0.4398(02)	0.057
H(222)	0.0873(01)	0.2660(03)	0.3764(02)	0.057
H(231)	0.2087(01)	0.1349(03)	0.2412(02)	0.042
H(241)	0.2088(01)	0.2444(03)	0.1410(02)	0.049
H(242)	0.2627(01)	0.2653(03)	0.2017(02)	0.049
H(251)	0.2798(01)	0.2112(03)	0.3305(02)	0.050
H(252)	0.2364(01)	0.2371(03)	0.3680(02)	0.050
H(261)	0.2158(01)	0.5353(03)	0.2666(02)	0.039
H(271)	0.2432(01)	0.4582(03)	0.1786(02)	0.046
H(272)	0.1846(01)	0.4330(03)	0.1469(02)	0.046
H(281)	0.2641(01)	0.4246(03)	0.3687(02)	0.051
H(282)	0.2895(01)	0.4036(03)	0.3101(02)	0.051
H(291)	0.2250(01)	0.3803(03)	0.4293(02)	0.043
H(301)	0.2481(01)	0.5697(03)	0.4895(02)	0.051
H(302)	0.2402(01)	0.5863(03)	0.4058(02)	0.051
H(311)	0.1948(01)	0.4390(03)	0.5276(02)	0.054
H(312)	0.1596(01)	0.3429(03)	0.4741(02)	0.054
H(321)	0.1020(01)	0.6590(03)	0.3892(02)	0.046
H(331)	0.1836(01)	0.7234(03)	0.3984(02)	0.055
H(332)	0.1871(01)	0.6963(03)	0.4794(02)	0.055
H(341)	0.0944(01)	0.4666(03)	0.4379(02)	0.056
H(342)	0.1266(01)	0.5515(03)	0.5021(02)	0.056
H(351)	0.0498(01)	0.6913(03)	0.2488(02)	0.050
H(361)	0.1103(02)	0.7615(03)	0.1987(03)	0.070
H(362)	0.0558(02)	0.7723(03)	0.1379(03)	0.070
H(371)	-0.0096(01)	0.6257(03)	0.1298(02)	0.058
H(372)	-0.0017(01)	0.5286(03)	0.1910(02)	0.058
H(381)	0.1033(01)	0.4478(03)	0.1056(02)	0.043
H(391)	0.1323(01)	0.6485(03)	0.1229(02)	0.054
H(392)	0.0766(01)	0.6499(03)	0.0651(02)	0.054
H(401)	0.0143(01)	0.4946(03)	0.0653(02)	0.054
H(402)	0.0274(01)	0.4021(03)	0.1302(02)	0.054

Table 5. Anisotropic Temperature Factors for **5**

Atom	*U*11	*U*22	*U*33	*U*23	*U*13	*U*12
C(1)	0.028(02)	0.027(02)	0.034(02)	0.001(01)	0.015(02)	-0.001(01)
C(2)	0.029(02)	0.027(02)	0.033(02)	0.000(02)	0.014(01)	0.000(01)
C(3)	0.029(02)	0.034(02)	0.032(02)	0.001(02)	0.012(02)	0.000(01)
C(4)	0.029(02)	0.031(02)	0.036(02)	0.000(02)	0.013(02)	-0.005(01)
C(5)	0.029(02)	0.030(02)	0.034(02)	0.002(02)	0.013(02)	0.004(01)
C(6)	0.027(01)	0.029(02)	0.030(02)	0.000(01)	0.010(01)	0.001(01)
C(7)	0.028(02)	0.033(02)	0.032(02)	-0.002(02)	0.012(02)	-0.002(01)
C(8)	0.031(02)	0.039(02)	0.033(02)	-0.003(02)	0.015(02)	0.000(01)
C(9)	0.029(02)	0.036(02)	0.033(02)	0.001(02)	0.010(02)	0.005(01)
C(10)	0.030(02)	0.029(02)	0.031(02)	-0.001(02)	0.013(01)	-0.001(01)
C(11)	0.037(02)	0.032(02)	0.036(02)	-0.001(02)	0.016(02)	-0.004(01)
C(12)	0.046(02)	0.040(02)	0.032(02)	-0.001(02)	0.011(02)	-0.001(01)
C(13)	0.049(02)	0.040(02)	0.042(02)	-0.005(02)	0.024(02)	-0.002(02)
C(14)	0.036(02)	0.037(02)	0.036(02)	-0.001(02)	0.015(02)	-0.009(01)
C(15)	0.038(02)	0.048(02)	0.041(02)	-0.003(02)	0.007(02)	-0.003(01)
C(16)	0.055(02)	0.035(02)	0.055(03)	-0.010(02)	0.023(02)	-0.003(02)
C(17)	0.042(02)	0.040(02)	0.042(02)	0.002(02)	0.018(02)	-0.010(02)
C(18)	0.061(02)	0.038(02)	0.064(03)	0.012(02)	0.019(02)	-0.003(02)
C(19)	0.044(02)	0.070(02)	0.048(02)	0.000(02)	0.024(02)	-0.012(02)
C(20)	0.035(02)	0.039(02)	0.036(02)	0.003(02)	0.014(02)	-0.004(01)
C(21)	0.048(02)	0.045(02)	0.045(02)	0.013(02)	0.016(02)	0.008(02)
C(22)	0.045(02)	0.057(02)	0.047(03)	-0.005(02)	0.024(02)	-0.006(02)
C(23)	0.029(02)	0.030(02)	0.048(02)	-0.001(02)	0.016(02)	0.003(01)
C(24)	0.032(02)	0.041(02)	0.054(03)	-0.005(02)	0.021(02)	0.000(01)
C(25)	0.030(02)	0.043(02)	0.052(03)	0.004(02)	0.015(02)	0.007(01)
C(26)	0.029(02)	0.030(02)	0.042(02)	-0.002(02)	0.017(02)	-0.006(01)
C(27)	0.036(02)	0.038(02)	0.046(02)	0.004(02)	0.020(02)	-0.004(01)
C(28)	0.031(02)	0.046(02)	0.052(03)	-0.006(02)	0.017(02)	-0.003(01)
C(29)	0.036(02)	0.036(02)	0.034(02)	-0.002(02)	0.011(02)	0.003(01)
C(30)	0.035(02)	0.046(02)	0.040(02)	-0.008(02)	0.006(02)	-0.006(01)
C(31)	0.058(02)	0.046(02)	0.029(02)	-0.003(02)	0.013(02)	-0.001(02)
C(32)	0.038(02)	0.041(02)	0.036(02)	-0.004(02)	0.014(02)	0.006(01)
C(33)	0.050(02)	0.04002)	0.048(03)	-0.012(02)	0.017(02)	-0.005(02)
C(34)	0.055(02)	0.054(02)	0.036(02)	-0.006(02)	0.022(02)	0.000(02)
C(35)	0.044(02)	0.040(02)	0.042(03)	0.002(02)	0.017(02)	0.013(02)
C(36)	0.075(03)	0.040(02)	0.065(03)	0.009(02)	0.030(02)	0.012(02)
C(37)	0.035(02)	0.068(02)	0.040(02)	0.000(02)	0.011(02)	0.015(02)
C(38)	0.040(02)	0.035(02)	0.033(02)	0.002(02)	0.015(02)	0.005(01)
C(39)	0.053(02)	0.041(02)	0.046(02)	0.009(02)	0.021(02)	0.004(02)
C(40)	0.034(02)	0.060(02)	0.037(02)	-0.003(02)	0.008(02)	0.004(02)

References and Notes

(1) Mathias, J. P.; Stoddart, J. F. *Chem. Soc. Rev.* **1992**, 215-225. Mekelburger, H.-B.; Jaworek, W.; Vögtle, F. *Angew. Chem., Int. Ed. Engl.* **1992**, *31*, 1571-1576. Wu, Z.; Lee, S.; Moore, J. S. *J. Am. Chem. Soc.* **1992**, *114*, 8730-8732. McKinley, A. J.; Ibrahim, P. N.; Balaji, V.; Michl, J. *J. Am. Chem. Soc.* **1992**, *114*, 10631-10637. Rubin, Y.; Kahr, M.; Knobler, C. B.; Diederich, F.; Wilkins, C. L. *J. Am. Chem. Soc.* **1991**, *113*, 495-500. Schmidt-Radde, R. H.; Vollhardt, K. P. C. *J. Am. Chem. Soc.* **1992**, *114*, 9713-9715. Miller, T. M.; Neenan, T. X.; Zayas, R.; Bair, H. E. *J. Am. Chem. Soc.* **1992**, *114*, 1018-1025. Rajca, A.; Utamapanya, S.; Thayumanavan, S. *J. Am. Chem. Soc.* **1992**, *114*, 1884-1885

(2) (a) Komatsu, K.; Aonuma, S.; Jinbu, Y.; Tsuji, R.; Hirosawa, C.; Takeuchi, K. *J. Org. Chem.* **1991**, *56*, 195-203. (b) Komatsu, K.; Nishinaga, T.; Aonuma, S.; Hirosawa, C.; Takeuchi, K.; Lindner, H. J.; Richter, J. *Tetrahedron Lett.* **1991**, *32*, 6767-6770.

(3) Nishinaga, T.; Komatsu, K.; Sugita, N.; Lindner, H. J.; Richter, J. *J. Am. Chem. Soc.* **1993**, *115*, 11642-11643.

(4) For the case of the tropylium analogue, see Komatsu, K.; Akamatsu, H.; Jinbu, Y.; Okamoto, K. *J. Am. Chem. Soc.* **1988**, *110*, 633-634. Komatsu, K.; Akamatsu, H.; Aonuma, S.; Jinbu, Y.; Maekawa, N.; Takeuchi, K. *Tetrahedron* **1991**, *47*, 6951-6966.

(5) The MM2(87) program was obtained from QCPE, Indiana University.

(6) Baldwin, J. E. *J. Chem. Soc., Chem. Commun.* **1976**, 734-736

(7) Gleiter, R.; Eckert-Maksic, M.; Schäfer, W.; Truesdale, E. A. *Chem. Ber.* **1982**, *115*, 2009-2011. Kovac, B.; Allan, M.; Heilbronner, E. *Helv. Chim. Acta* **1981**, *64*, 430-448, and references cited therein. Hanson, A. W. *Acta*

Crystallogr. **1977**, *B33*, 2003-2007. Zhou, X.; Liu, R.; Allinger, N. L. *J. Am. Chem. Soc.*, **1993**, *115*, 7525-7526.

(8) For example, Anderson, B. F.; Ferguson, J.; Morita, M.; Robertson, G. B. *J. Am. Chem. Soc.*, **1979**, *101*, 1832-1840. Ehrenberg, M. *Acta Crystallogr.* **1966**, *20*, 182-186. Choi, C. S.; Marinkas, P. L. *Acta Crystallogr.* **1980**, *B36*, 2491-2493. Dougherty, D. A.; Choi, C. S.; Kaupp, G.; Buda, A. B.; Rudzinski, J. M.; Osawa, E. *J. Chem. Soc., Perkin Trans. 2*, **1986**, 1063-1070.

(9) Osawa, E.; Kanematsu, K. In *Molecular Structure and Energetics. Vol. 3. Studies of Organic Molecules;* Liebman, J. F., Greenberg, A., Eds.; VCH: New York, 1986; pp 329-369.

(10) Anstead, G. M.; Srinivasan, R.; Peterson, C. S.; Wilson, S. R.; Katzenellenbogen, J. A. *J. Am. Chem. Soc.* **1991**, *113*, 1378-1385, and references cited therein.

(11) For examples of bond elongation solely due to steric repulsion, see Beckhaus, H.-D.; Kratt, G.; Lay, K.; Geiselmann, J.; Rüchardt, C.; Kitschke, B.; Lindner, H. J. *Chem. Ber.* **1980**, *113*, 3441-3455. Winiker, R.; Beckhaus, H.-D.; Rüchardt, C. *Chem. Ber.* **1980**, *113*, 3456-3476. Beckhaus, H.-D.; Hellmann, G.; Rüchardt, C. *Chem. Ber.* **1978**, *111*, 3764-3779.

(12) Hoffmann, R. *Acc. Chem. Res.* **1971**. *4*, 1-9. Dougherty, D. A.; Schlegel, H. B.; Mislow, K. *Tetrahedron* **1978**, *34*, 1441-1447.

(13) (a) Dewar, M. J. S.; Thiel, W. *J. Am. Chem. Soc.* **1977**, *99*, 4899-4907. (b) The calculations were conducted using the standard method implemented in the MOPAC 6.0 semiempirical orbital package.

(14) Stewart, J. J. P. *J. Comput. Chem.* **1989**, *10*, 221-264. The results with AM1 calculations showed a similar tendency.

(15) Frisch, M. J.; Trucks, G. W.; Head-Gordon, M.; Gill, P. M. W.; Wong, M. W.; Foresman, J. B.; Johnson, B. G.; Schlegel, H. B.; Robb, M. A.; Replogle, E. S.; Gomperts, R.; Andres, J. L.; Raghavachari, K.; Binkley, J. S.; Gonzalez, C.; Martin, R. L.; Fox, D. J.; Defrees, D. J.; Baker, J.; Stewart, J. J. P.; Pople, J. A.; *GAUSSIAN 92, Revision C*; Gaussian, Inc., Pittsburgh, PA, 1992.

(16) Staley, S. W.; Howard, A. E.; Harmony, M. D.; Mathur, S. N.; Kattija-Ari, M.; Choe, J-I.; Lind, G. *J. Am. Chem. Soc.* **1980**, *102*, 3639-3640. Harmony, M. D.; Mathur, S. N.; Choe, J-I.; Kattija-Ari, M.; Howard, A. E.; Staley, S. W. *J. Am. Chem. Soc.* **1981**, *103*, 2961-2966. We are indebted to Professor L. T. Scott for calling our attention to this work.

(17) The through-bond coupling (ref. 14) between the 2p orbitals of the two cyclopentadiene rings in **7**, if present, would not be significant since the two π-systems are opened up with an angle of 86 °, which seems too large to cause the effective interaction.

(18) This potential is even lower than the oxidation potential (+0.48 V vs Ag/Ag^+) found for COT **3** to give a stable cation radical $\mathbf{3}^{\cdot+}$ in acetonitrile-CH_2Cl_2 (3:1): ref. 3.

(19) The signal assignment was made based on DEPT measurements.

(20) Repeated analyses on carefully recrystallized samples from different lots did not give satisfactory analytical data, presumably due to ready air oxidation.

(21) Sheldrick, G. M. *Acta Crystallogr.* **1990**, *A46*, 467-473.

(22) Sheldrick, G. M. *J. Appl. Cryst.* **1993**, in preparation.

Chapter 5

1,1-Dimethylsila-, -germa-, and -stannacycloheptatrienes Fully Annelated with Bicyclo[2.2.2]octene: Syntheses, Structures, and Properties

Abstract

A series of 1,1-dimethyl-2,3:4,5:6,7-tris(bicyclo[2.2.2]octeno)metallacycloheptatrienes (metallepins) containing silicon (**2a**), germanium (**2b**) and tin (**2c**), were synthesized by dilithiation of the terminal dibromide of the linear trimer of bicyclo[2.2.2]octene (**3**) followed by the reaction with $(CH_3)_2MCl_2$ (M = Si, Ge, Sn). The X-ray structure determination was conducted for the first time for these metallepins containing Group 14 elements, and indicated that the central seven-membered ring is in a boat-form for all of **2a–c**. As the effective size of the Group 14 metal atom increases, the dihedral angle between the base plane and the stern part of the boat form was found to increase, i.e., the boat structure becomes more deeply folded, for release of the inner angle strain. Variable-temperature NMR measurements indicated that the metallepin ring of **2** is rapidly inverting in solution, and the line-shape analyses gave the activation parameters for ring-inversion at 25 °C as follows: **2a**, E_a = 13.9 ± 1.3 kcal mol^{-1}, $\Delta S^{\ddagger}$ = 3 ± 5 cal K^{-1} mol^{-1}, $\Delta G^{\ddagger}$ = 12.4 ± 0.2 kcal mol^{-1} ; **2b**, E_a = 16.6 ± 1.8 kcal mol^{-1}, $\Delta S^{\ddagger}$ = 7 ± 6 cal K^{-1} mol^{-1}, $\Delta G^{\ddagger}$ = 14.0 ± 0.1 kcal mol^{-1} ; **2c**, E_a = 21.9 ± 3.0 kcal mol^{-1}, $\Delta S^{\ddagger}$ = 10 ± 9 cal K^{-1} mol^{-1}, $\Delta G^{\ddagger}$ = 18.4 ± 0.5 kcal mol^{-1}. Thus, the energy barrier for ring inversion increases as the carbon–metal bond is elongated, reflecting the increasing instability of the planar transition-state structure due to the inner-angle strain. The observed larger E_a value of **2a** than that of the corresponding cycloheptatriene **6** implies that the cyclic (p–d)π delocalization would not be operating in a planar transition-state structure or negligibly small if present. The UV absorption of **2a**, **2b**, and **2c** (λ_{max} in *n*-hexane 275, 274, and 266 nm, respectively) did not show much difference from that of the C-unsubstituted metallepins **1a**, **1b**, and **1c** in spite of annelation with three bicyclo[2.2.2]octene units, probably because of the more folded boat structure of the central seven-membered ring and less π-conjugation in **2a–c** than in **1a–c** having no substituents.

Introduction

The fully unsaturated seven-membered heterocycles containing Group 14 elements, metallepins **1**, are of interest from various points of view.[1–6] Thus, silepins[1–4] were studied, in search for a possibility of cyclic (p–d)π conjugation,[3] for examination of molecular flexibility,[2b] and also as a possible precursor of a yet unknown silatropylium ion.[3b,c,7] On the other hand, stannepins[5] have attracted interest as a precursor of borepins.[8] If the six π-electrons can delocalize over the whole seven-membered ring, the tropylium-ion like stabilization could be expected.

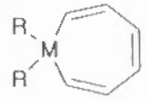

1a, M = Si, R = CH_3
1b, M = Ge, R = CH_3
1c, M = Sn, R = C_3H_7

Recently a series of C-unsubstituted metallepins containing Group 14 elements **1a–c** were reported by Nakadaira et al.[4] These compounds were considered to have a boat-conformation as judged from the NMR coupling

constants of the olefinic ring protons. However, there has been no X-ray structural data reported for any of these or C-substituted metallepins containing Group 14 elements:[9] the X-ray crystallographic data have so far been limited only to the lattice parameters of a tribenzosilepin derivative.[2] The energy barrier for ring inversion of silepin is of particular interest with respect to the degree of the possible stabilization by the (p–d)π cyclic conjugation. However, such a data has not been measured yet in spite of several attempts.[2b,3,4a] The barrier of the tribenzo-derivative was too large[2b] and that for other derivatives was too small[3,4a] to be observed by NMR. It is therefore highly desirable to determine the X-ray structures for a series of metallepins with the completely same substituents and also to examine their dynamic behavior such as ring inversion.

In previous studies, we prepared a series of cyclic π-conjugated system annelated with a rigid bicyclic σ-framework, bicyclo[2.2.2]octene, and demonstrated the presence of effective σ–π conjugation between the 2p orbital and the rigidly held σ-bonds.[10] In particular, the full annelation with bicyclo[2.2.2]octene was found to cause remarkable stabilization of the tropylium ion.[10a] Such a structural modification was also found to be advantageous in growth of single crystals owing to the presence of highly symmetrical structural units.[11] We now synthesized a series of 1,1-dimethylmetallacycloheptatrienes (1,1-dimethylmetallepins) fully annelated with bicyclo[2.2.2]octene, containing silicon (**2a**), germanium (**2b**), and tin (**2c**), and investigated their structure and properties.

2a, M = Si
2b, M = Ge
2c, M = Sn

Results and Discussion

Synthesis. Previously, the terminal dibromide of bicyclo[2.2.2]octene trimer (**3**) was synthesized by linear trimerization of the bicyclic units initiated by monolithiation of 2,3-dibromobicyclo[2.2.2]octene with *n*-BuLi in THF at −78 °C, which involved repeated formation of bicyclo[2.2.2]octyne, its insertion into the precursor's C–Li bond, and Li/Br exchange.[10b] Further reaction of dibromide **3** with 2 equiv of *n*-BuLi in THF at room temperature resulted in cyclization to benzene derivative **4**. This reaction was supposed to proceed via a σ-radical formed by dissociative electron-transfer.[12] In contrast, treatment of **3** with 4–5 equiv of *t*-BuLi in THF at −78 °C resulted in the formation of dilithiated compound **5**, which was then allowed to react with dichlorodimethylsilane, -germane, and -stannane to give the desired metallepins **2a**, **2b**, and **2c** as shown in Scheme 1.[13]

Scheme 1

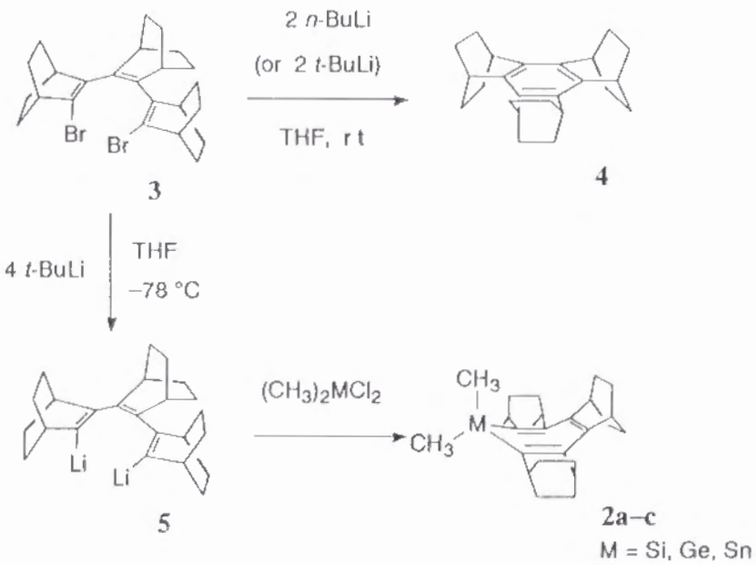

The same reaction, when carried out at room temperature, resulted in cyclization to benzene **4**. Purification of **2a**, **2b**, and **2c** was attained only by recrystallization after removal of most of byproducts by passing through a column of alumina. The isolated yield of the purified product was 44% for **2a**, 28% for **2b** and 17% for **2c**.

These metallepins **2a–c** were stable in solid state but readily decomposed under even slightly acidic conditions, for example, in chloroform solutions or during elution in a silica-gel column. The relatively low yield of **2c** is apparently due to its instability reflecting the weakest carbon-metal bond among the three. In fact, stannepin **2c** decomposed to benzene **4** when it was heated in nitrobenzene–d_5 at 110°C ($t_{1/2}$ = 41 min.),[14] whereas no such structural change was observed for **2b** and **2c** under the same conditions.

X-ray Structures. The X-ray crystallographic analyses were performed for the single crystals of the metallepins **2a-c**, which were grown by slow diffusion of acetonitrile into the solution in benzene. As shown by the ORTEP views in Figure 1, all of these compounds have a quite similar structure with the central seven-membered ring in a boat form. The selected X-ray structural parameters of these compounds are summarized in Table 1 . Apparently, the most notable difference in their structures is the M–C_1 bond length. As the atomic radii of the Group 14 elements increases, the M–C_1 bond is elongated while the lengths of the rest of the triene-part of the seven-membered ring remain essentially the same.

As to the bond angles in the central seven-membered ring, no significant difference was observed except for the angle C_1–M–C_6. On the other hand, appreciable difference was observed for the bent angles in the boat structure, i.e., the angle α between the base plane (C_1–C_2–C_5–C_6) and the bow (C_1–M–C_6) and the

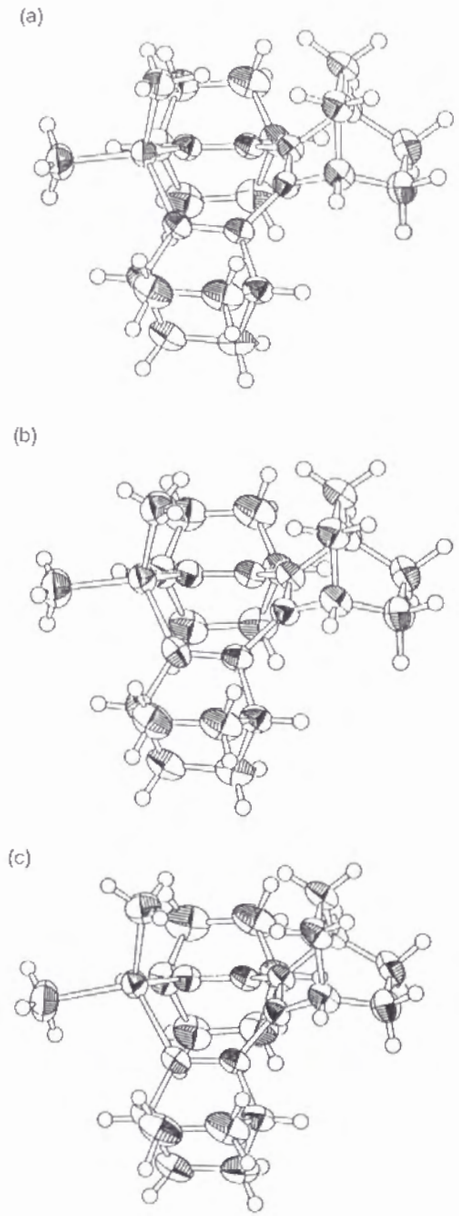

Figure 1. ORTEP views of the X-ray crystal structures of (a) **2a**, (b) **2b** and (c) **2c** (50% probability).

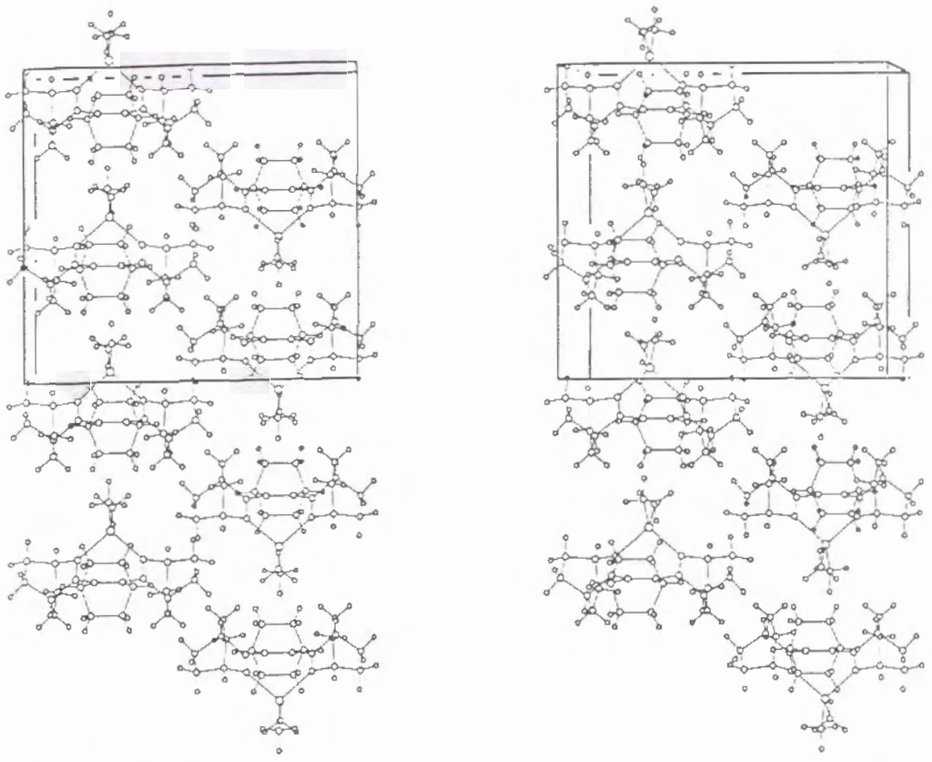

Figure 2. Stereoview of the crystal packing of **2c**. The *a*-axis points vertically downward, *b* from left to right and *c* toward the reader.

Table 1. The Observed and Calculated Bond Lengths, Bond Angles and Bent Angles of the Central Ring in **2a–c**.

compd	bond length, Å						bond angle, deg				bent angle, deg[a]	
	M–Me[1]	M–Me[2]	M–C$_1$	C$_1$–C$_2$	C$_2$–C$_3$	C$_3$–C$_4$	C$_1$–M–C$_6$	M–C$_1$–C$_2$	C$_1$–C$_2$–C$_3$	C$_2$–C$_3$–C$_4$	α	β
2a obs.	1.875(4)	1.869(4)	1.857(2)	1.350(3)	1.461(3)	1.363(4)	103.2(1)	120.6(2)	126.6(2)	128.3(1)	45.7	32.7
calc.[b]	1.900	1.899	1.831	1.351	1.442	1.356	104.3	122.8	126.9	127.9	40.3	33.4
2b obs.	1.942(6)	1.933(6)	1.926(3)	1.346(4)	1.469(4)	1.360(6)	102.0(2)	120.3(2)	127.1(3)	128.7(2)	44.8	33.5
calc.[b]	1.976	1.972	1.901	1.344	1.451	1.356	96.6	122.5	126.8	128.2	40.4	35.6
2c obs.	2.135(9)	2.145(9)	2.129(9)	1.32(1)	1.464(10)	1.36(1)	97.5(4)	119.3(6)	127.6(7)	129.6(4)	43.1	36.7
calc.[b]	2.119	2.114	2.092	1.347	1.456	1.354	93.4	121.0	125.9	128.5	41.3	40.6

[a] Defined in the text. [b] PM3 calculations.

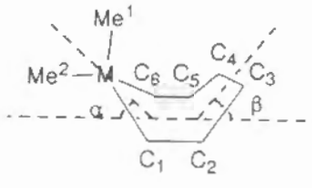

M = **2a** Si, **2b** Ge, **2c** Sn

angle β between the base plane and the stern (C_2–C_3–C_4–C_5). With the increase in the M–C_1 bond length, the angle C_1–M–C_6 decreases and the boat form becomes more folded as is shown by the increase in the angle β. The results of PM3 semiempirical molecular orbital calculations[15] showed the same tendency as the observed values for the angles C_1–M–C_6 and β, as shown in Table 1. These results are ascribable to the release of the inner angle strain in the central seven-membered ring. On the other hand, the observed α value, which should also be correlated with the β value in principle, exhibited relatively small change in the reverse direction; also the change in α value obtained from PM3 calculations is quite small. This discrepancy may be attributed to the crystal packing effect.

The unit cells of the crystals **2a**, **2b**, and **2c** are all orthorhombic (the space group P_{nma}). The mode of crystal packing of all three compounds is the same as exemplified by the packing of **2c** shown in Figure 2. The most notable difference in the lattice constants was observed in the length of *a*–axis (see the Experimental Section). Since the C_1–M–C_6 plane and the CH_3–M–CH_3 plane are placed nearly parallel to the *ab*-plane and *ac*-plane, respectively, a gradual increase in C–M bond length is reflected in lengthening of the *a*-axis most pronouncedly.

Dynamic Behaviors. Although the structures of **2a–c** were found to be similar in the solid state, their behavior in solution was quite different with each other. In the ^{1}H NMR spectra (270 MHz) taken at room temperature, the signal of methyl protons of **2a** exhibited a sharp singlet peak as shown in Figure 3a. However, the signal of the methyl protons of **2b** showed a broad single peak (Figure 3b) and that of **2c** was split into two separate peaks of equal intensity (Figure 3c). These results clearly demonstrate that the boat structure of **2a** is inverting rapidly but that of **2c** is fixed at room temperature in an NMR time-scale. The line shape analyses of the two-site exchange provided the activation parameters at 25 °C as summarized in Table 2.[16] For the purpose of comparison,

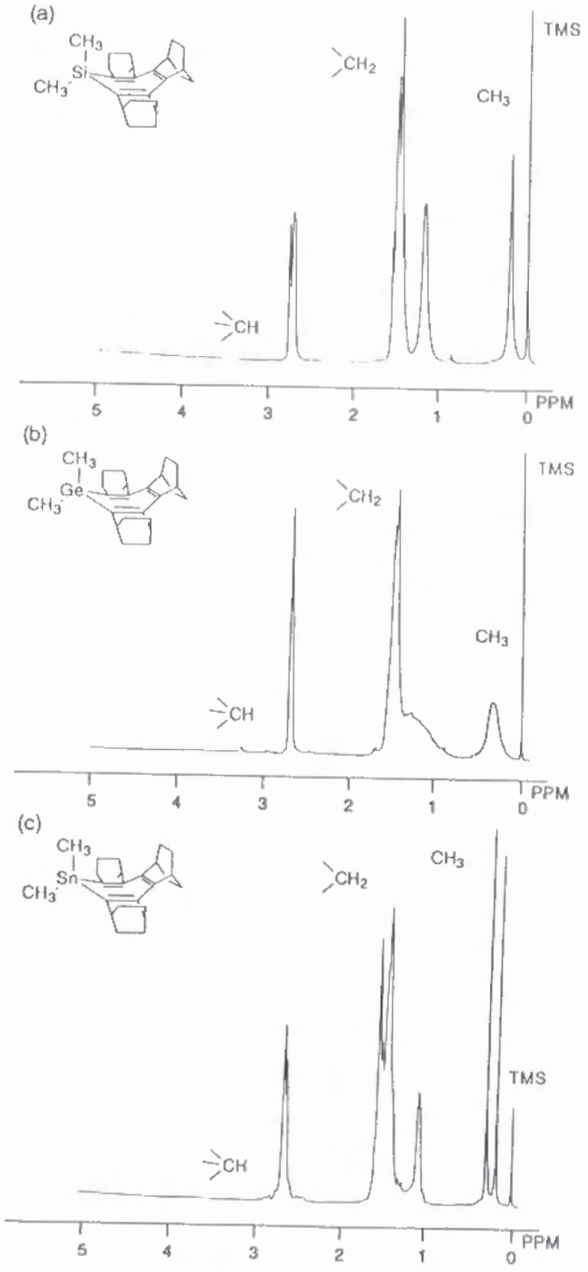

Figure 3. ^{1}H NMR spectra (270 MHz; C_6D_6) of (a) **2a**, (b) **2b** and (c) **2c** at room temperature.

Table 2. The Activation Parameters (25 °C) for the Ring Inversion and Calculated $\Delta\Delta H_f$ of **2a–c** and **6**

compd	E_a/kcal mol^{-1}	$\Delta S^{\ddagger}$/cal K^{-1} mol^{-1}	$\Delta G^{\ddagger}$/kcal mol^{-1}	$\Delta\Delta H_f$[a]/kcal mol^{-1}
6	8.5 ± 0.5	−11 ± 3	11.3 ± 0.2	6.0
2a	13.9 ± 1.3	3 ± 5	12.4 ± 0.2	10.0
2b	16.6 ± 1.8	7 ± 6	14.0 ± 0.1	10.1
2c	21.9 ± 3.0	10 ± 9	18.4 ± 0.5	17.0

[a] ΔH_f(planar) – ΔH_f(boat). PM3 calculation.

the data of the cycloheptatriene fully annelated with bicyclo[2.2.2]octene (**6**)[17] are also included.

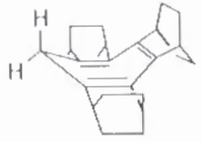

6

The ring inversion of the seven-membered ring of the boat form would proceed most probably via a planar structure B in the transition state as shown in Scheme 2. This was supported for the case of unsubstituted cycloheptatriene by ab initio molecular orbital calculations[18] and also for the tris(bicyclo[2.2.2]-octeno) derivative **6** by molecular mechanics calculations.[17] Then, the PM3 calculations were carried out to obtain the heat of formation (ΔH_f) for both the boat structure and the structure with the seven-membered ring fixed at a planar geometry for **2a–c** and **6**, and their difference ($\Delta\Delta H_f$) was examined. The values of $\Delta\Delta H_f$ of **2a–c** and **6** were in fair agreement with the observed E_a values as shown in Table 2, thus supporting the planarity of the seven-membered ring at the transition state of the ring inversion of **2a–c**.

Scheme 2

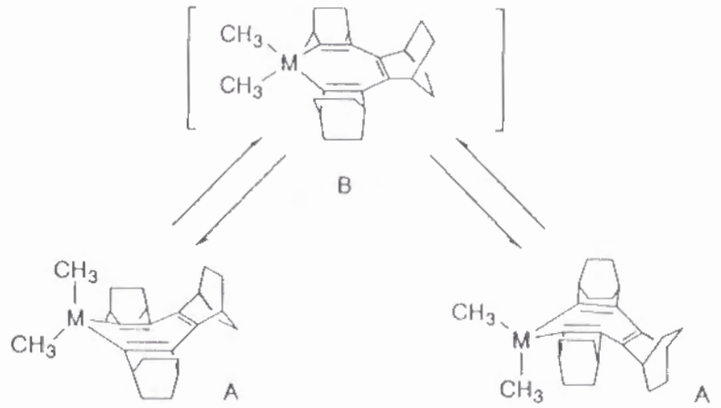

As shown by the E_a data in Table 2, the barrier for ring inversion increases upon going from cycloheptatriene **6** to metallepins **2a–c** and also as the atomic size of the Group 14 element of metallepins increases. This is primarily attributed to the increase in strain in the planar structure at the transition state: the larger strain is generated by elongation of the C_1–M bond that demands widening of inner angles in the planar seven-membered ring. The possibility of cyclic (p–d)π delocalization in silepins has once attracted some interest.[3] If such electronic state is actually contributing to the planar form of **2a**, the inversion barrier should be appreciably lowered. The observed larger E_a value of **2a** than that of **6** by 5.4 kcal mol^{-1} as shown in Table 2 implies that such effect would not be operating or negligibly small if present.

Electronic Spectrum. For the case of C-unsubstituted metallepins **1a, 1b** and **1c**, the longest-wavelength UV absorption corresponding to the π–π^* transition was reported as 281, 279 and 279 nm, respectively, in *n*-hexane. The bathochromic shift of the absorption of silepin **1a** as compared with that of unsubstituted cycloheptatriene **7** (261 nm) was ascribed to the possible cyclic σ–π

conjugation involving the Si–C_{methyl} σ-bonds,[4] and not to the cyclic (p–d) π delocalization mentioned above.[3]

On the other hand, the metallepins in the present work, **2a**, **2b**, and **2c**, were found to absorb at 276, 275, and 268 nm, respectively, in *n*-hexane. The absorption of silepin **2a** in ethanol is identical to that in *n*-hexane, and, in sharp contrast to the case of silepin **1a** (see above), **2a** did not show any bathochromic shift as compared with the absorption of corresponding cycloheptatriene **6** (λ_{max} 276 nm in ethanol).[17] The absorption of **6** is considered to be bathochromically shifted as compared with the parent cycloheptatriene **7** due to the annelation with three bicyclo[2.2.2]octene units, which raise the HOMO of the π-system by inductive and σ-π conjugative effects and thereby lower the π–π* transition energy. Then, the similar effects may be expected to cause some bathochromic shift for the metallepins **2a–c** as compared with absorptions of **1a–c**. However, no such shift was experimentally observed at all as described above. The most conceivable reason for the absence of such shift is the less effective π-conjugation in the triene part of the seven-membered ring due to the more folded structure in **2a–c** than in **1a–c**: the observed value for β of the seven-membered ring in **2a–c** is 32.7 – 36.7 ° (Table 1), while the β value for **1a**, **1b**, and **1c** was estimated as 25 °, 26 °, and 27 °, respectively, from the ^{1}H NMR coupling constants.[4] This interpretation is supported by slight hypsochromic shift observed upon going from **2a** to **2c** (see above) with the boat structure becoming more deeply folded. The effect of the cyclic σ–π conjugation involving the Si-C_{methyl} σ–bonds in **2a** seems to be counterbalanced by the less effective π-conjugation in the triene part in comparison with **6**.

In summary, a previously reported technique of cyclization of the bicyclo-[2.2.2]octene trimer was modified and applied for the syntheses of a series of metallepins fully annelated with bicyclo[2.2.2]octene units, **2a–c**. The X-ray structure determination was conducted for these metallepins for the first time, and

revealed that their structure is a boat form with the seven-membered ring folded deeper with an increase in the size of the metal atom. Dynamic NMR studies on metallepins **2a–c** quantitatively substantiated the notable effect of the carbon–metal bond length upon the relative stability of a planar transition-state structure for the ring inversion. Metallepins **2a–c** are considered to have the deeply folded structure also in solution, similar to that determined by X-ray crystallography, as judged from the electronic spectra. The present study clearly demonstrated that the structural modification such as annelation with bicyclo[2.2.2]octene units is quite advantageous in the structural analysis of the conjugated cyclic π-system both in solid state and in solution.

Experimental Section

General Procedures. Melting points were determined on a Yamato MP–21 apparatus and are uncorrected. Elemental analyses were performed by Micro-analytical Center, Kyoto University, Kyoto. NMR spectra were recorded on varian XL–300 (300 MHz for ^{1}H and 75.4 MHz for ^{13}C NMR), on JEOL GSX270 (270 MHz for ^{1}H and 67.8 MHz for ^{13}C NMR), or on JEOL FX90 (90 MHz for ^{1}H and 22.5 MHz for ^{13}C NMR) spectrometers using Me_4Si as an internal standard unless otherwise noted. IR spectra were taken on Perkin Elmer 1640 spectrometer. UV–vis spectra were taken on Shimadzu UV–2100PC spectrometer. The PM3 calculations were conducted using the standard methods as implemented in the MOPAC 6.0 semiempirical molecular orbital package on a CRAY Y–MP2E/264 machine.

THF was freshly distilled from sodium benzophenone ketyl before use. A pentane solution of *t*-BuLi was titrated using a THF solution of N-pivaloyl-*o*-

toluidine.[19] The dibromide of bicyclo[2.2.2]octene trimer **3** was prepared as reported previously.[10b]

1,1-Dimethyl-2,3:4,5:6,7-tris(bicyclo[2.2.2]octeno)silacycloheptatriene (2a). To a stirred solution of dibromide **3** (53.1 mg, 0.111 mmol) in THF (5 mL) at −78 °C was added dropwise a solution of 1.5 N *t*-BuLi in pentane (0.37 mL, 0.55 mmol). Addition of each drop of *t*-BuLi solution caused yellow coloration indicative of formation of dilithiated compound **5**. After stirring for 15 min at −78 °C, dichlorodimethylsilane (0.13 mL, 142 mg, 1.1 mmol) was added dropwise to the reaction mixture, which gradually turned colorless. After being stirred for 30 min at −78 °C, the mixture was warmed to room temperature over 10 min. The solvent was then removed by evaporation, and the crude product was purified by chromatography over alumina eluted with hexane to give **2a** (18.3 mg, yield 43.8%) as a white solid. A single crystal for X-ray analysis was grown by slow diffusion of acetonitrile into a benzene solution: mp 187–188 °C (dec) ; ^{1}H NMR (270 MHz, C_6D_6, 25 °C) δ 2.77 (br s, 6H), 1.59 (br m, 16H), 1.20 (br s, 8H), 0.20 (s, 6H; this signal split into two peaks at δ 0.41 (3H) and –0.20 (3H) when measured in THF-d_8 at −70 °C with the frequency of 90 MHz[20]); ^{13}C NMR (67.8 MHz, C_6D_6, 25 °C) δ 150.2, 141.2, 140.8, 33.8, 33.0, 32.9, 26.7, 26.5, 25.7, −3.5 (at −80 °C in THF-d_8 with 22.5 MHz frequency, this signal split into two signals at δ −2.8 and −4.5[21]); IR (KBr) 2945, 2855, 1531, 1453, 1251, 1239, 1160, 1076, 1020, 867, 847, 812, 766, 728, 642 cm^{-1}.

Anal. Calcd for $C_{26}H_{36}Si$: C, 82.91; H, 9.63. Found: C, 82.78; H, 9.69.

1,1-Dimethyl-2,3:4,5:6,7-tris(bicyclo[2.2.2]octeno)germacycloheptatriene (2b). In the same manner as described above for the synthesis of **2a**, dibromide **3** (99.6 mg, 0.208 mmol) was dilithiated and treated with dichlorodimethylgermane (0.12 mL, 191 mg, 1.1 mmol) in THF (10 mL) at −78 °C. After being stirred for 30 min at −78 °C, the mixture was warmed to room temperature, evaporated under reduced pressure, and extracted with benzene (2 mL × 3). The residue from evaporation of the extract was then washed thoroughly with *n*-hexane. A residual solid from evaporation of the hexane washings was purified by passing though an alumina column to give **2b** (24.3mg, 27.7%) as colorless crystals after recrystallization from acetonitrile–benzene. A single crystal was grown as described above: mp 280–282 °C (dec) (sealed tube); sublimes at about 200 °C; ^{1}H NMR (270 MHz, C_6D_6, 25 °C) δ 2.75 (br s, 6H), 1.6–0.9 (br m, 24H), 0.3 (br s, 6H; this signal split into two peaks at δ 0.37 (3H) and –0.05 (3H) when measured in THF-d_8 at −50 °C with the frequency of 90 MHz[20]); ^{13}C NMR (67.8 MHz, C_6D_6, 25 °C) δ 148.3, 142.6, 140.9, 34.0, 33.5, 33.2, 27 −25 (br) (the methyl carbons were not observed at this temperature due to broadening, and were observed at −50°C in THF–d_8 with 22.5 MHz frequency as two signals at δ −2.3 and −6.9[21]); IR (KBr) 2946, 2857, 1552, 1467, 1453, 1224, 1144, 1017, 867, 810, 602 cm^{-1}.

Anal. Calcd for $C_{26}H_{36}Ge$: C, 74.15; H, 8.62. Found: C, 73.86; H, 8.42.

1,1-Dimethyl-2,3:4,5:6,7-tris(bicyclo[2.2.2]octeno)stannacycloheptatriene (2c). Similarly, dibromide **3** (101 mg, 0.211 mmol) was dilithiated and treated with dichlorodimethylstannane (220 mg, 1.00 mmol) in THF (9 mL) at −78°C. After being stirred for 30 min at −78 °C, the reaction mixture was warmed to room temperature and evaporated. The crude product was purified by chromatography over alumina and repeated recrystallizations by slow diffusion of acetonitrile to the benzene solution to give **2c** (17.0 mg, 17.2%) as colorless crystals. A single crystal was grown as described above: mp >285 °C; ^{1}H NMR (270 MHz, C_6D_6, 25 °C) δ 2.70 (br s, 6H), 1.6–1.1 (br m, 24H), 0.31 (s, 3H) 0.19 (s, 3H); ^{13}C NMR (67.8 MHz, C_6D_6) δ 151.7, 144.5, 141.9, 35.7, 34.4, 33.6,

27.4, 27.2, 26.8, 25.9, 25.6, 25.5, –8.6, –14.2; IR (KBr) 2912, 2856, 1557, 1451, 1330, 1179, 1153, 1015, 868, 809 cm^{-1}.

Anal. Calcd for $C_{26}H_{36}Sn$: C, 66.83; H, 7.77. Found: C, 67.22; H, 7.72.

X-ray Crystallography on 2a–c. Data for compounds **2a–c** were collected on a Rigaku AFC7R diffractometer with graphite monochromated CuKα radiation and a 12 kW rotating anode generator. Crystal data for **2a** are as follows: $C_{26}H_{36}Si$; space group P_{nma} ; a = 14.258(3) Å, b = 16.029(2) Å, c = 9.386(2) Å; V = 2145.0(5) $Å^3$; Z = 4; D_{calc} = 1.166 g/cm^3; μ(CuKα) = 9.94 cm^{-1}; total of 1858 reflections within 2θ = 120.1° and $I > 3\sigma(I)$. The final R factor was 4.0 % (R_W = 4.6%). Crystal data for **2b** are as follows: $C_{26}H_{36}Ge$; space group P_{nma}; a = 14.291(4) Å, b = 16.080(3) Å, c = 9.380(4) Å; V = 2155(1) $Å^3$; Z = 4; D_{calc} = 1.298 g/cm^3; μ(CuKα) = 19.57 cm^{-1}; total of 1868 reflections within 2θ = 120.1° and $I > 3\sigma(I)$. The final R factor was 4.2 % (R_W = 4.9%). Crystal data for **2c** are as follows: $C_{26}H_{36}Sn$; space group P_{nma}; a = 14.922(4) Å, b = 16.044(2) Å, c = 9.370(4) Å; V = 2243(1) $Å^3$; Z = 4; D_{calc} = 1.383 g/cm^3; μ(CuKα) = 91.01 cm^{-1}; total of 1939 reflections within 2θ = 120.1° and $I > 3\sigma(I)$. The final R factor was 4.2 % (R_W = 5.0%). All of these structures were solved by heavy-atom Patterson methods and expanded using Fourier techniques.[22] The non-hydrogen atoms were refined anisotropically. Hydrogen atoms were refined isotropically except for the methyl hydrogen of **2c**, whose positions were geometrically calculated and fixed. Crystallographic data, i.e., atomic coordinate, anisotropic displacement parameters, bond lengths, and bond angles of **2a–c** are given in Tables 3–6, 7-10 and 11-14 respectively. The numbering system is also shown respectively.

Table 3. Atomic Coordinates and Equivalent Isotropic Temperature Factors for **2a**

Atom	X/*a*	Y/*b*	Z/*c*	*B*eq
Si(1)	0.02299(6)	0.2500	0.26850(9)	2.92(2)
C(1)	-0.0577(1)	0.3408(1)	0.2758(2)	2.94(5)
C(2)	-0.1194(1)	0.3490(1)	0.3841(2)	2.82(5)
C(3)	-0.1309(1)	0.2925(1)	0.5050(2)	2.77(4)
C(4)	-0.0647(2)	0.4099(2)	0.1670(3)	3.72(6)
C(5)	-0.1661(2)	0.4118(2)	0.1093(3)	4.81(7)
C(6)	-0.0462(2)	0.4935(2)	0.2412(3)	4.91(7)
C(7)	-0.1784(2)	0.4277(1)	0.3742(3)	3.49(5)
C(8)	-0.2334(2)	0.4253(2)	0.2338(3)	4.50(7)
C(9)	-0.1126(2)	0.5033(2)	0.3673(3)	4.78(7)
C(10)	-0.1466(2)	0.3287(1)	0.6521(2)	3.38(5)
C(11)	-0.0674(2)	0.2981(1)	0.7496(3)	3.73(6)
C(12)	-0.2404(2)	0.2980(2)	0.7134(3)	4.21(6)
C(13)	0.1056(3)	0.2500	0.4238(4)	4.3(1)
C(14)	0.0908(3)	0.2500	0.0981(4)	4.6(1)
C(1*)	-0.0577(1)	0.1592(1)	0.2758(2)	2.94(5)
C(2*)	-0.1194(1)	0.1510(1)	0.3841(2)	2.82(5)
C(3*)	-0.1309(1)	0.2075(1)	0.5050(2)	2.77(4)
C(4*)	-0.0647(2)	0.0901(2)	0.1670(3)	3.72(6)
C(5*)	-0.1660(2)	0.0882(2)	0.1093(3)	4.81(7)
C(6*)	-0.0462(2)	0.0065(2)	0.2412(3)	4.91(7)
C(7*)	-0.1784(2)	0.0723(1)	0.3742(3)	3.49(5)
C(8*)	-0.2334(2)	0.0747(2)	0.2338(3)	4.50(7)
C(9*)	-0.1126(2)	-0.0033(2)	0.3673(3)	4.78(7)
C(10*)	-0.1466(2)	0.1713(1)	0.6521(2)	3.38(5)
C(11*)	-0.0674(2)	0.2019(1)	0.7496(3)	3.73(6)
C(12*)	-0.2404(2)	0.2020(2)	0.7134(3)	4.21(6)
H(1)	-0.023(2)	0.402(1)	0.087(3)	4.4(6)
H(2)	-0.176(2)	0.359(2)	0.066(3)	6.1(8)
H(3)	-0.169(2)	0.453(2)	0.038(3)	5.8(7)
H(4)	0.011(2)	0.495(2)	0.277(3)	5.0(7)
H(5)	-0.057(2)	0.537(2)	0.169(3)	5.4(6)
H(6)	-0.221(1)	0.434(1)	0.454(2)	3.0(5)
H(7)	-0.282(2)	0.383(2)	0.241(3)	5.2(6)
H(8)	-0.268(2)	0.476(2)	0.222(3)	6.1(7)
H(9)	-0.078(2)	0.508(2)	0.458(3)	5.4(7)
H(10)	-0.147(2)	0.555(2)	0.358(3)	5.6(7)
H(11)	-0.149(1)	0.389(1)	0.648(2)	3.1(5)
H(12)	-0.003(2)	0.318(2)	0.717(3)	5.0(6)
H(13)	-0.078(1)	0.319(1)	0.848(3)	3.8(5)
H(14)	-0.289(2)	0.319(2)	0.656(3)	5.1(6)
H(15)	-0.248(1)	0.318(1)	0.815(2)	3.2(5)
H(16)	0.054(3)	0.2500	0.011(4)	6(1)
H(17)	0.127(2)	0.301(2)	0.090(3)	8.9(10)
H(18)	0.078(3)	0.2500	0.515(6)	8(1)
H(19)	0.135(3)	0.299(2)	0.443(4)	12(1)

(Table 3. Continued)

Atom	X/*a*	Y/*b*	Z/*c*	*B*eq
H(1*)	-0.023(2)	0.098(1)	0.087(3)	4.4(6)
H(2*)	-0.176(2)	0.141(2)	0.066(3)	6.1(8)
H(3*)	-0.169(2)	0.047(2)	0.038(3)	5.8(7)
H(4*)	0.011(2)	0.005(2)	0.277(3)	5.0(7)
H(5*)	-0.057(2)	-0.037(2)	0.169(3)	5.4(6)
H(6*)	-0.221(1)	0.066(1)	0.454(2)	3.0(5)
H(7*)	-0.282(2)	0.117(2)	0.241(3)	5.2(6)
H(8*)	-0.268(2)	0.024(2)	0.222(3)	6.1(7)
H(9*)	-0.078(2)	-0.008(2)	0.458(3)	5.4(7)
H(10*)	-0.147(2)	-0.055(2)	0.358(3)	5.6(7)
H(11*)	-0.149(1)	0.111(1)	0.648(2)	3.1(5)
H(12*)	-0.003(2)	0.182(2)	0.717(3)	5.0(6)
H(13*)	-0.078(1)	0.181(1)	0.848(3)	3.8(5)
H(14*)	-0.289(2)	0.181(2)	0.656(3)	5.1(6)
H(15*)	-0.248(1)	0.182(1)	0.815(2)	3.2(5)
H(17*)	0.127(2)	0.199(2)	0.090(3)	8.9(10)
H(19*)	0.135(3)	0.201(2)	0.443(4)	12(1)

Table 4. Anisotropic Temperature Factors for **2a**

Atom	*U*11	*U*22	*U*33	*U*12	*U*13	*U*23
Si(1)	0.0377(5)	0.0378(5)	0.0355(5)	0.0000	0.0025(4)	0.0000
C(1)	0.044(1)	0.031(1)	0.037(1)	-0.0043(9)	-0.002(1)	0.0017(10)
C(2)	0.046(1)	0.026(1)	0.035(1)	0.0006(10)	-0.005(1)	-0.0016(9)
C(3)	0.039(1)	0.032(1)	0.034(1)	0.0017(9)	0.0001(10)	-0.0011(10)
C(4)	0.057(2)	0.043(1)	0.041(1)	-0.005(1)	0.002(1)	0.009(1)
C(5)	0.075(2)	0.066(2)	0.042(2)	0.002(2)	-0.012(1)	0.010(2)
C(6)	0.078(2)	0.038(1)	0.070(2)	-0.015(1)	-0.007(2)	0.012(1)
C(7)	0.055(2)	0.035(1)	0.042(1)	0.008(1)	-0.001(1)	0.001(1)
C(8)	0.055(2)	0.055(2)	0.061(2)	0.008(1)	-0.012(1)	0.006(2)
C(9)	0.084(2)	0.030(1)	0.067(2)	0.003(1)	-0.016(2)	-0.001(1)
C(10)	0.059(1)	0.033(1)	0.037(1)	0.004(1)	0.001(1)	-0.004(1)
C(11)	0.062(2)	0.041(1)	0.039(1)	0.001(1)	-0.005(1)	-0.007(1)
C(12)	0.058(2)	0.063(2)	0.040(1)	0.009(1)	0.006(1)	-0.003(1)
C(13)	0.050(2)	0.068(3)	0.045(2)	0.0000	-0.006(2)	0.0000
C(14)	0.053(2)	0.078(3)	0.043(2)	0.0000	0.009(2)	0.0000

Table 5. Observed Bond Lengths of **2a**

Bond Length(Å)		Bond Length(Å)	
Si(1)-C(1)	1.857(2)	Si(1)-C(1)	1.857(2)
Si(1)-C(14)	1.869(4)	Si(1)-C(13)	1.875(4)
C(1)-C(2)	1.350(3)	C(1)-C(4)	1.509(3)
C(2)-C(3)	1.461(3)	C(2)-C(7)	1.518(3)
C(3)-C(3)	1.363(4)	C(3)-C(10)	1.514(3)
C(4)-C(5)	1.543(4)	C(4)-C(6)	1.534(4)
C(5)-C(8)	1.528(4)	C(6)-C(9)	1.524(4)
C(7)-C(8)	1.534(3)	C(7)-C(9)	1.535(4)
C(10)-C(11)	1.533(3)	C(10)-C(12)	1.536(3)
C(11)-C(11)	1.543(4)	C(12)-C(12)	1.538(5)

Table 6. Observed Bond Angles of **2a**

Bond Angles(deg)		Bond Angles(deg)	
C(1)-Si(1)-C(1)	103.2(1)	C(1)-Si(1)-C(14)	110.6(1)
C(1)-Si(1)-C(13)	111.2(1)	C(1)-Si(1)-C(14)	110.6(1)
C(1)-Si(1)-C(13)	111.2(1)	C(13)-Si(1)-C(14)	109.9(2)
Si(1)-C(1)-C(2)	120.6(2)	Si(1)-C(1)-C(4)	126.2(2)
C(2)-C(1)-C(4)	113.2(2)	C(1)-C(2)-C(3)	126.6(2)
C(1)-C(2)-C(7)	113.3(2)	C(3)-C(2)-C(7)	120.0(2)
C(2)-C(3)-C(3)	128.3(1)	C(2)-C(3)-C(10)	119.2(2)
C(3)-C(3)-C(10)	112.5(1)	C(1)-C(4)-C(5)	108.3(2)
C(1)-C(4)-C(6)	108.8(2)	C(5)-C(4)-C(6)	107.7(2)
C(4)-C(5)-C(8)	108.9(2)	C(4)-C(6)-C(9)	109.6(2)
C(2)-C(7)-C(8)	108.3(2)	C(2)-C(7)-C(9)	108.7(2)
C(8)-C(7)-C(9)	107.3(2)	C(5)-C(8)-C(7)	109.8(2)
C(6)-C(9)-C(7)	109.3(2)	C(3)-C(10)-C(11)	108.2(2)
C(3)-C(10)-C(12)	110.3(2)	C(11)-C(10)-C(12)	108.4(2)
C(10)-C(11)-C(11)	108.6(1)	C(10)-C(12)-C(12)	108.7(1)

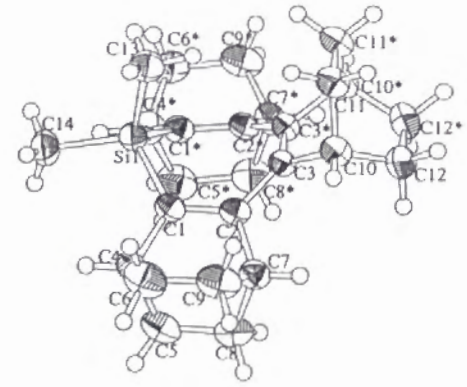

Table 7. Atomic Coordinates and Equivalent Isotropic Temperature Factors for **2b**

Atom	X/*a*	Y/*b*	Z/*c*	*B*eq
Ge(1)	0.02716(4)	0.2500	0.26865(5)	3.41(1)
C(1)	-0.0575(2)	0.3430(2)	0.2774(3)	3.42(7)
C(2)	-0.1195(2)	0.3493(2)	0.3848(3)	3.23(7)
C(3)	-0.1305(2)	0.2922(2)	0.5067(3)	3.12(6)
C(4)	-0.0658(2)	0.4124(2)	0.1695(4)	4.11(8)
C(5)	-0.1661(3)	0.4124(3)	0.1109(4)	5.10(10)
C(6)	-0.0498(3)	0.4955(2)	0.2447(4)	5.33(10)
C(7)	-0.1804(2)	0.4269(2)	0.3761(4)	3.75(7)
C(8)	-0.2344(3)	0.4240(3)	0.2345(4)	4.83(9)
C(9)	-0.1161(3)	0.5029(2)	0.3709(4)	5.15(10)
C(10)	-0.1445(2)	0.3282(2)	0.6540(3)	3.76(7)
C(11)	-0.0645(3)	0.2982(2)	0.7502(3)	4.06(8)
C(12)	-0.2377(3)	0.2979(2)	0.7164(4)	4.46(8)
C(13)	0.1111(4)	0.2500	0.4312(6)	4.8(1)
C(14)	0.0960(5)	0.2500	0.0904(6)	5.5(2)
C(1*)	-0.0575(2)	0.1570(2)	0.2774(3)	3.42(7)
C(2*)	-0.1195(2)	0.1507(2)	0.3848(3)	3.23(7)
C(3*)	-0.1305(2)	0.2078(2)	0.5067(3)	3.12(6)
C(4*)	-0.0658(2)	0.0876(2)	0.1695(4)	4.11(8)
C(5*)	-0.1661(3)	0.0876(3)	0.1109(4)	5.10(10)
C(6*)	-0.0498(3)	0.0045(2)	0.2447(4)	5.33(10)
C(7*)	-0.1804(2)	0.0731(2)	0.3761(4)	3.75(7)
C(8*)	-0.2344(3)	0.0760(3)	0.2345(4)	4.83(9)
C(9*)	-0.1161(3)	-0.0029(2)	0.3709(4)	5.15(10)
C(10*)	-0.1445(2)	0.1718(2)	0.6540(3)	3.76(7)
C(11*)	-0.0645(3)	0.1018(2)	0.7502(3)	4.06(8)
C(12*)	-0.2377(3)	0.1021(2)	0.7164(4)	4.46(8)
H(1)	-0.022(2)	0.407(2)	0.094(3)	4.6(8)
H(2)	-0.178(2)	0.362(2)	0.057(4)	6.7(10)
H(3)	-0.170(2)	0.453(2)	0.038(4)	5.8(9)
H(4)	0.010(2)	0.496(2)	0.275(3)	4.8(8)
H(5)	-0.060(2)	0.536(2)	0.174(4)	7(1)
H(6)	-0.224(2)	0.431(2)	0.456(3)	4.8(8)
H(7)	-0.279(2)	0.377(2)	0.241(3)	4.0(7)
H(8)	-0.269(2)	0.473(2)	0.223(3)	4.7(8)
H(9)	-0.081(2)	0.509(2)	0.461(4)	5.9(9)
H(10)	-0.150(2)	0.552(2)	0.362(3)	4.9(8)
H(11)	-0.143(2)	0.386(2)	0.649(3)	2.9(6)
H(12)	-0.009(2)	0.321(2)	0.711(4)	5.4(9)
H(13)	-0.076(2)	0.319(2)	0.851(3)	4.8(8)
H(14)	-0.293(2)	0.321(2)	0.651(4)	5.8(9)
H(15)	-0.245(2)	0.318(2)	0.822(3)	4.3(7)
H(16)	0.110(3)	0.290(2)	0.494(4)	10(1)
H(17)	0.168(3)	0.2500	0.404(5)	5(1)
H(18)	0.078(4)	0.282(4)	0.037(6)	19(2)
H(19)	0.140(6)	0.2500	0.109(9)	14(3)

(Table 7. Continued)

Atom	X/*a*	Y/*b*	Z/*c*	*B*eq
H(1*)	-0.022(2)	0.093(2)	0.094(3)	4.6(8)
H(2*)	-0.178(2)	0.138(2)	0.057(4)	6.7(10)
H(3*)	-0.170(2)	0.047(2)	0.038(4)	5.8(9)
H(4*)	0.010(2)	0.004(2)	0.275(3)	4.8(8)
H(5*)	-0.060(2)	-0.036(2)	0.174(4)	7(1)
H(6*)	-0.224(2)	0.069(2)	0.456(3)	4.8(8)
H(7*)	-0.279(2)	0.123(2)	0.241(3)	4.0(7)
H(8*)	-0.269(2)	0.027(2)	0.223(3)	4.7(8)
H(9*)	-0.081(2)	-0.009(2)	0.461(4)	5.9(9)
H(10*)	-0.150(2)	-0.052(2)	0.362(3)	4.9(8)
H(11*)	-0.143(2)	0.114(2)	0.649(3)	2.9(6)
H(12*)	-0.009(2)	0.179(2)	0.711(4)	5.4(9)
H(13*)	-0.076(2)	0.171(2)	0.851(3)	4.8(8)
H(14*)	-0.293(2)	0.179(2)	0.651(4)	5.8(9)
H(15*)	-0.245(2)	0.182(2)	0.822(3)	4.3(7)
H(16*)	0.110(3)	0.210(2)	0.494(4)	10(1)
H(18*)	0.078(4)	0.218(4)	0.037(6)	19(2)

Table 8. Anisotropic Temperature Factors for **2b**

Atom	*U*11	*U*22	*U*33	*U*12	*U*13	*U*23
Ge(1)	0.0467(3)	0.0440(3)	0.0388(3)	0.0000	0.0023(3)	0.0000
C(1)	0.054(2)	0.041(2)	0.035(2)	-0.010(1)	0.000(1)	0.004(1)
C(2)	0.050(2)	0.031(2)	0.042(2)	0.002(1)	-0.007(1)	0.001(1)
C(3)	0.047(2)	0.036(2)	0.035(2)	0.004(1)	0.000(1)	0.000(1)
C(4)	0.064(2)	0.048(2)	0.044(2)	-0.006(2)	0.003(2)	0.007(2)
C(5)	0.080(3)	0.068(3)	0.045(2)	-0.001(2)	-0.015(2)	0.009(2)
C(6)	0.084(3)	0.047(2)	0.071(3)	-0.015(2)	-0.008(2)	0.012(2)
C(7)	0.060(2)	0.036(2)	0.046(2)	0.009(2)	-0.002(2)	0.000(2)
C(8)	0.067(2)	0.056(2)	0.061(2)	0.002(2)	-0.014(2)	0.008(2)
C(9)	0.096(3)	0.034(2)	0.066(2)	0.003(2)	-0.014(2)	0.000(2)
C(10)	0.068(2)	0.035(2)	0.039(2)	0.004(2)	0.000(2)	-0.003(2)
C(11)	0.066(2)	0.046(2)	0.042(2)	0.002(2)	-0.006(2)	-0.006(2)
C(12)	0.064(2)	0.065(2)	0.041(2)	0.006(2)	0.006(2)	-0.005(2)
C(13)	0.051(3)	0.073(4)	0.057(3)	0.0000	-0.002(3)	0.0000
C(14)	0.064(4)	0.092(5)	0.053(3)	0.0000	0.012(3)	0.0000

Table 9. Observed Bond Lengths of **2b**

Bond	Length(Å)	Bond	Length(Å)
Ge(1)-C(1)	1.926(3)	Ge(1)-C(1)	1.926(3)
Ge(1)-C(13)	1.940(6)	Ge(1)-C(14)	1.940(6)
C(1)-C(2)	1.346(4)	C(1)-C(4)	1.511(4)
C(2)-C(3)	1.474(4)	C(2)-C(7)	1.525(4)
C(3)-C(3)	1.359(6)	C(3)-C(10)	1.511(4)
C(4)-C(5)	1.534(5)	C(4)-C(6)	1.528(5)
C(5)-C(8)	1.528(5)	C(6)-C(9)	1.521(6)
C(7)-C(8)	1.537(5)	C(7)-C(9)	1.530(5)
C(10)-C(11)	1.534(5)	C(10)-C(12)	1.535(5)
C(11)-C(11)	1.550(7)	C(12)-C(12)	1.539(7)

Table 10. Observed Bond Angles of **2b**

Bond	Angles(deg)	Bond	Angles(deg)
C(1)-Ge(1)-C(1)	102.0(2)	C(1)-Ge(1)-C(13)	110.8(1)
C(1)-Ge(1)-C(14)	110.8(1)	C(1)-Ge(1)-C(13)	110.8(1)
C(1)-Ge(1)-C(14)	110.8(1)	C(13)-Ge(1)-C(14)	111.3(3)
Ge(1)-C(1)-C(2)	120.2(2)	Ge(1)-C(1)-C(4)	126.5(2)
C(2)-C(1)-C(4)	113.2(3)	C(1)-C(2)-C(3)	127.2(3)
C(1)-C(2)-C(7)	113.4(3)	C(3)-C(2)-C(7)	119.4(3)
C(2)-C(3)-C(3)	128.5(2)	C(2)-C(3)-C(10)	119.0(2)
C(3)-C(3)-C(10)	112.5(2)	C(1)-C(4)-C(5)	108.3(3)
C(1)-C(4)-C(6)	108.9(3)	C(5)-C(4)-C(6)	107.8(3)
C(4)-C(5)-C(8)	109.0(3)	C(4)-C(6)-C(9)	109.5(3)
C(2)-C(7)-C(8)	108.0(3)	C(2)-C(7)-C(9)	108.2(3)
C(8)-C(7)-C(9)	107.4(3)	C(5)-C(8)-C(7)	109.8(3)
C(6)-C(9)-C(7)	109.7(3)	C(3)-C(10)-C(11)	108.6(3)
C(3)-C(10)-C(12)	110.0(3)	C(11)-C(10)-C(12)	108.8(3)
C(10)-C(11)-C(11)	108.3(2)	C(10)-C(12)-C(12)	108.6(2)

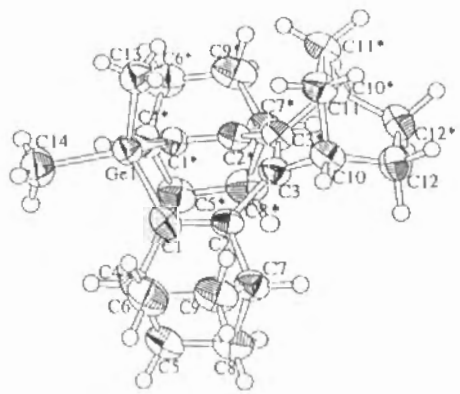

Table 11. Atomic Coordinates and Equivalent Isotropic Temperature Factors for **2c**

Atom	X/*a*	Y/*b*	Z/*c*	*Beq*
Sn(1)	0.03366(3)	0.2500	0.27179(5)	3.44(1)
C(1)	-0.0589(3)	0.3491(3)	0.2825(5)	3.3(1)
C(2)	-0.1192(3)	0.3509(3)	0.3880(5)	3.06(10)
C(3)	-0.1272(3)	0.2921(3)	0.5096(5)	3.00(10)
C(4)	-0.0707(4)	0.4197(4)	0.1760(6)	4.3(1)
C(5)	-0.1654(5)	0.4146(4)	0.1172(6)	5.2(2)
C(6)	-0.0602(5)	0.5026(4)	0.2560(8)	5.9(2)
C(7)	-0.1820(4)	0.4252(3)	0.3817(5)	3.8(1)
C(8)	-0.2323(4)	0.4217(4)	0.2381(6)	5.1(1)
C(9)	-0.1257(5)	0.5047(4)	0.3805(7)	5.6(2)
C(10)	-0.1391(4)	0.3284(3)	0.6578(5)	3.6(1)
C(11)	-0.0619(4)	0.2974(3)	0.7509(5)	4.1(1)
C(12)	-0.2275(4)	0.2970(4)	0.7212(5)	4.6(1)
C(13)	0.1241(6)	0.2500	0.4484(10)	4.9(2)
C(14)	0.1043(7)	0.2500	0.072(1)	6.4(3)
C(1*)	-0.0589(3)	0.1509(3)	0.2825(5)	3.3(1)
C(2*)	-0.1192(3)	0.1491(3)	0.3880(5)	3.06(10)
C(3*)	-0.1272(3)	0.2079(3)	0.5096(5)	3.00(10)
C(4*)	-0.0707(4)	0.0803(4)	0.1760(6)	4.3(1)
C(5*)	-0.1654(5)	0.0854(4)	0.1172(6)	5.2(2)
C(6*)	-0.0602(5)	-0.0026(4)	0.2560(8)	5.9(2)
C(7*)	-0.1820(4)	0.0748(3)	0.3817(5)	3.8(1)
C(8*)	-0.2323(4)	0.0783(4)	0.2381(6)	5.1(1)
C(9*)	-0.1257(5)	-0.0047(4)	0.3805(7)	5.6(2)
C(10*)	-0.1391(4)	0.1716(3)	0.6578(5)	3.6(1)
C(11*)	-0.0619(4)	0.2026(3)	0.7509(5)	4.1(1)
C(12*)	-0.2275(4)	0.2030(4)	0.7212(5)	4.6(1)
H(1)	-0.031(3)	0.419(3)	0.096(5)	3.0(9)
H(2)	-0.177(4)	0.363(3)	0.064(6)	5(1)
H(3)	-0.162(4)	0.451(3)	0.048(6)	5(1)
H(4)	0.002(6)	0.499(5)	0.281(8)	8(1)
H(5)	-0.074(5)	0.553(5)	0.193(8)	9(1)
H(6)	-0.229(3)	0.426(3)	0.452(5)	4(1)
H(7)	-0.271(3)	0.377(3)	0.241(5)	3.0(10)
H(8)	-0.271(4)	0.467(4)	0.237(6)	5(1)
H(9)	-0.099(4)	0.513(3)	0.477(6)	5(1)
H(10)	-0.172(5)	0.547(4)	0.385(7)	8(1)
H(11)	-0.136(3)	0.381(3)	0.660(5)	2.5(9)
H(12)	-0.008(4)	0.322(3)	0.710(5)	4(1)
H(13)	-0.070(4)	0.314(4)	0.845(6)	6(1)
H(14)	-0.276(3)	0.316(3)	0.671(5)	4(1)
H(15)	-0.233(4)	0.315(4)	0.817(6)	5(1)
H(16)	0.189(8)	0.2500	0.43(1)	11.2(8)
H(17)	0.1163	0.2983	0.5040	6.0260
H(18)	0.051(6)	0.2500	0.02(1)	7(1)
H(19)	0.1408	0.2983	0.0653	7.7231

(Table 11. Continued)

Atom	X/*a*	Y/*b*	Z/*c*	*B*eq
H(1*)	-0.031(3)	0.081(3)	0.096(5)	3.0(9)
H(2*)	-0.177(4)	0.137(3)	0.064(6)	5(1)
H(3*)	-0.162(4)	0.049(3)	0.048(6)	5(1)
H(4*)	0.002(6)	0.001(5)	0.281(8)	8(1)
H(5*)	-0.074(5)	-0.053(5)	0.193(8)	9(1)
H(6*)	-0.229(3)	0.074(3)	0.452(5)	4(1)
H(7*)	-0.271(3)	0.123(3)	0.241(5)	3.0(10)
H(8*)	-0.271(4)	0.033(4)	0.237(6)	5(1)
H(9*)	-0.099(4)	-0.013(3)	0.477(6)	5(1)
H(10*)	-0.172(5)	-0.047(4)	0.385(7)	8(1)
H(11*)	-0.136(3)	0.119(3)	0.660(5)	2.5(9)
H(12*)	-0.008(4)	0.178(3)	0.710(5)	4(1)
H(13*)	-0.070(4)	0.186(4)	0.845(6)	6(1)
H(14*)	-0.276(3)	0.184(3)	0.671(5)	4(1)
H(15*)	-0.233(4)	0.185(4)	0.817(6)	5(1)
H(17*)	0.1163	0.2017	0.5040	6.0260
H(19*)	0.1408	0.2017	0.0653	7.7231

Table 12. Anisotropic Temperature Factors for **2c**

Atom	*U*11	*U*22	*U*33	*U*12	*U*13	*U*23
Sn(1)	0.0448(3)	0.0482(3)	0.0377(3)	0.0000	0.0021(2)	0.0000
C(1)	0.049(3)	0.040(3)	0.036(3)	-0.004(2)	-0.004(2)	0.006(2)
C(2)	0.054(3)	0.027(2)	0.035(2)	0.002(2)	-0.007(2)	-0.001(2)
C(3)	0.048(3)	0.037(2)	0.029(2)	0.001(2)	0.001(2)	-0.002(2)
C(4)	0.073(4)	0.049(3)	0.041(3)	-0.007(3)	0.000(3)	0.018(3)
C(5)	0.084(4)	0.073(4)	0.040(3)	0.002(4)	-0.016(3)	0.014(3)
C(6)	0.106(5)	0.045(3)	0.075(4)	-0.012(4)	-0.015(4)	0.019(3)
C(7)	0.066(3)	0.038(3)	0.041(3)	0.009(3)	-0.008(2)	0.000(2)
C(8)	0.066(4)	0.070(4)	0.059(4)	0.010(3)	-0.021(3)	0.005(3)
C(9)	0.118(6)	0.034(3)	0.061(4)	0.003(4)	-0.019(4)	-0.003(3)
C(10)	0.069(3)	0.035(3)	0.032(2)	0.003(3)	-0.003(2)	-0.006(2)
C(11)	0.074(4)	0.049(3)	0.032(3)	-0.001(3)	-0.006(3)	-0.006(2)
C(12)	0.069(4)	0.073(4)	0.032(3)	0.012(3)	0.006(3)	-0.006(3)
C(13)	0.058(5)	0.062(5)	0.068(5)	0.0000	-0.011(4)	0.0000
C(14)	0.058(6)	0.125(9)	0.061(5)	0.0000	0.015(5)	0.0000

Table 13. Observed Bond Lengths of **2c**

Bond Length(Å)		Bond Length(Å)	
Sn(1)-C(1)	2.108(5)	Sn(1)-C(1)	2.108(5)
Sn(1)-C(13)	2.135(9)	Sn(1)-C(14)	2.145(9)
C(1)-C(2)	1.337(7)	C(1)-C(4)	1.520(7)
C(2)-C(3)	1.484(6)	C(2)-C(7)	1.517(7)
C(3)-C(3)	1.350(9)	C(3)-C(10)	1.516(6)
C(4)-C(5)	1.518(9)	C(4)-C(6)	1.536(9)
C(5)-C(8)	1.515(9)	C(6)-C(9)	1.522(10)
C(7)-C(8)	1.543(7)	C(7)-C(9)	1.527(8)
C(10)-C(11)	1.529(7)	C(10)-C(12)	1.532(8)
C(11)-C(11)	1.52(1)	C(12)-C(12)	1.51(1)

Table 14. Observed Bond Angles of **2c**

Bond Angles(deg)		Bond Angles(deg)	
C(1)-Sn(1)-C(1)	97.9(3)	C(1)-Sn(1)-C(13)	112.2(2)
C(1)-Sn(1)-C(14)	111.3(2)	C(1)-Sn(1)-C(13)	112.2(2)
C(1)-Sn(1)-C(14)	111.3(2)	C(13)-Sn(1)-C(14)	111.4(4)
Sn(1)-C(1)-C(2)	119.5(4)	Sn(1)-C(1)-C(4)	127.4(4)
C(2)-C(1)-C(4)	113.0(5)	C(1)-C(2)-C(3)	127.4(4)
C(1)-C(2)-C(7)	113.8(4)	C(3)-C(2)-C(7)	118.7(4)
C(2)-C(3)-C(3)	129.5(2)	C(2)-C(3)-C(10)	117.9(4)
C(3)-C(3)-C(10)	112.6(3)	C(1)-C(4)-C(5)	107.8(5)
C(1)-C(4)-C(6)	108.3(4)	C(5)-C(4)-C(6)	108.6(5)
C(4)-C(5)-C(8)	109.8(5)	C(4)-C(6)-C(9)	109.1(5)
C(2)-C(7)-C(8)	107.8(4)	C(2)-C(7)-C(9)	108.5(5)
C(8)-C(7)-C(9)	107.0(5)	C(5)-C(8)-C(7)	109.5(5)
C(6)-C(9)-C(7)	109.9(5)	C(3)-C(10)-C(11)	108.0(4)
C(3)-C(10)-C(12)	109.3(4)	C(11)-C(10)-C(12)	108.7(4)
C(10)-C(11)-C(11)	108.9(3)	C(10)-C(12)-C(12)	109.2(3)

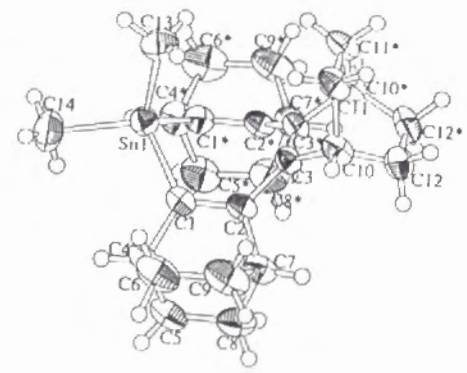

Variable Temperature NMR Measurements. The ^{1}H NMR spectrum (90 MHz) was measured for **2a** in THF–d_8 at the temperature range of –40 °C to 10 °C, for **2b** in THF–d_8 at the temperature range of –30 °C to 40 °C, and for **2c** in nitrobenzene–d_5 at the temperature range of –55 °C to 100 °C.

Total line-shape analyses were conducted at the five points near the coalescence temperature as shown Figure 4–6. The rate constants were determined as follows: **2a**, $k = 77 \pm 10$ sec^{-1} at T = 253.1 K; $k = 115 \pm 10$ sec^{-1} at T = 256.2 K (coalescence temperature); $k = 143 \pm 10$ sec^{-1} at T= 258.1 K; $k = 225 \pm 25$ sec^{-1} at T = 263.1 K; $k = 590 \pm 60$ sec^{-1} at T = 273.1 K: **2b**, $k = 46 \pm 4$ sec^{-1} at T = 278.1 K; $k = 77 \pm 3$ sec^{-1} at T = 283.1 K (coalescence temperature); $k = 145 \pm 15$ sec^{-1} at T = 288.1 K; $k = 210 \pm 20$ sec^{-1} at T = 293.1 K; $k = 350 \pm 50$ sec^{-1} at T = 298.1 K: **2c**, $k = 25 \pm 3$ sec^{-1} at T = 343 K; $k = 37 \pm 2$ sec^{-1} at T = 348 K (coalescence temperature); $k = 61 \pm 4$ sec^{-1} at T = 353 K; $k = 100 \pm 10$ sec^{-1} at T = 358 K; $k = 143 \pm 20$ sec^{-1} at T = 363 K. Activation parameters were obtained from the plot of ln k against 1/T by the conventional method.

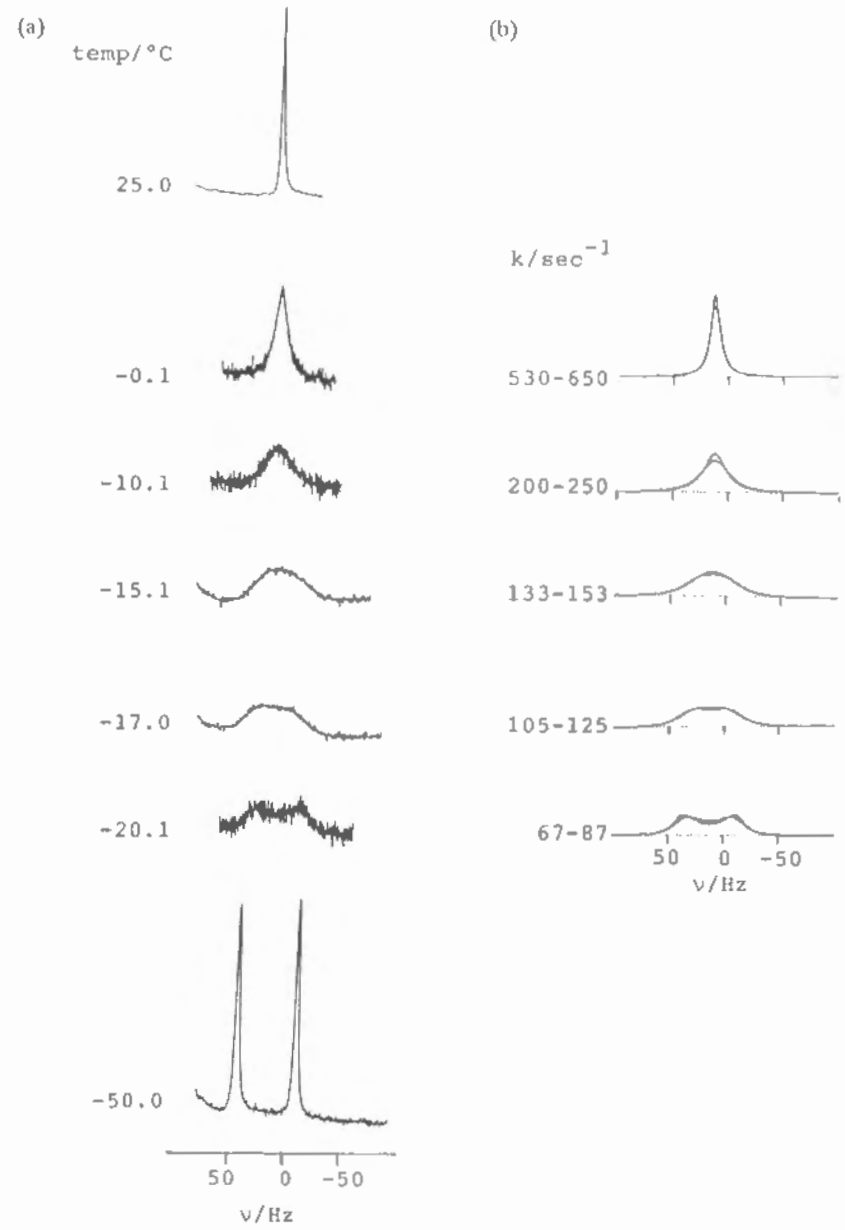

Figure 4. (a) Experimental and (b) simulated spectra for ^{1}H NMR (90 MHz) signals of methyl protons of silepin **2a** in THF–d_8

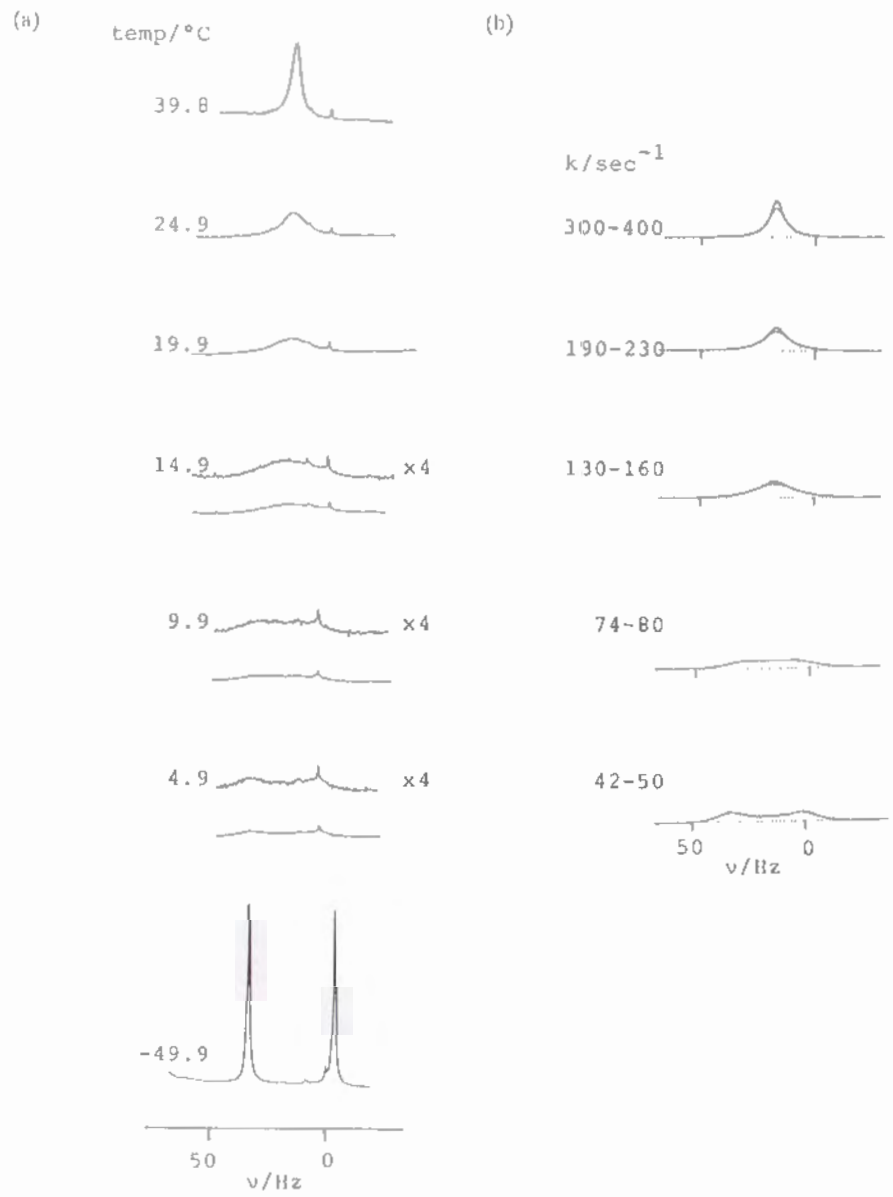

Figure 5. (a) Experimental and (b) simulated spectra for ^{1}H NMR (90 MHz) signals of methyl protons of germepin **2b** in THF–*d*8

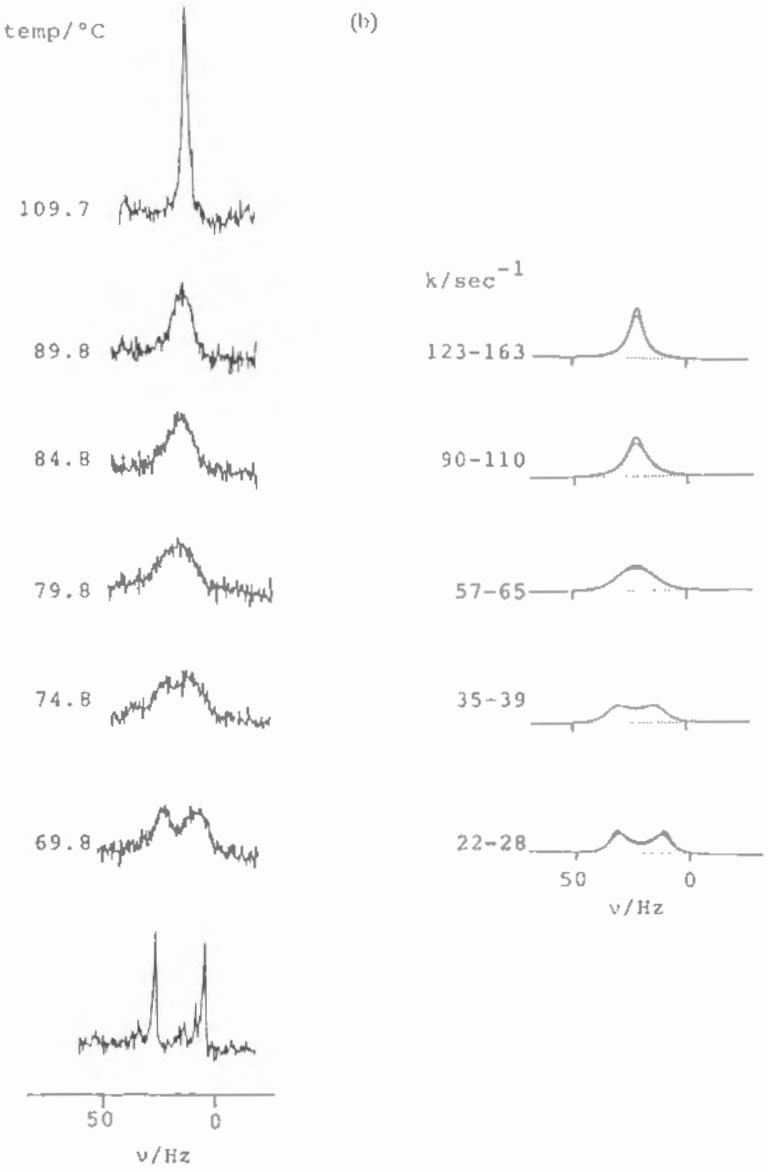

Figure 6. (a) Experimental and (b) simulated spectra for ^{1}H NMR (90 MHz) signals of methyl protons of stannepin **2c** in THF–*d*8

References and Notes

(1) (a) Birkofer, L.; Haddad, H. *Chem. Ber.* **1969**, *102*, 432–434; **1972**, *105*, 2101–2103. (b) Birkofer, L.; Haddad, H; Zamarlik, H. *J. Organomet. Chem.* **1970**, *25*, C57–C58. (c) Corey, J. Y.; Dueber, M.; Bichlmeir, B. *J. Organomet. Chem.* **1971**, *26*, 167–173. (d) Ishikawa, M.; Fuchikami, T.; Kumada, M. *Tetrahedron Lett.* **1976**, 1299–1302. (e) Birkofer, L.; Haddad, H. *Chem. Ber.* **1977**, *110*, 3314–3318. (f) Corey, J. Y.; Farrell. R. L. *J. Organomet. Chem.* **1978**, *153*, 15–23. (g) Ishikawa, M.; Fuchikami, T.; Kumada, M. *J. Organomet. Chem.* **1978**, *162*, 223–238. (h) Birkofer, L.; Haddad, H. *J. Organomet. Chem.* **1979**, *164*, C17–C19.

(2) (a) Andrianof, K. A.; Volkava, L. M.; Derazari, N. V.; Chumaeskii, N. A. *Khim. Geterotskil. Soedin.* **1967**, 435; *Chem. Abstr.* **1967**, *67*, 10869c. (b) Corey, J. Y.; Corey, E. R. *Tetrahedron Lett.* **1972**, 4669–4672.

(3) (a) Cartledge, F. K.; Mollére, P. D. *J. Organomet. Chem.* **1971**, *26*, 175–181. (b) Barton, T. J.; Volz, W. E.; Johnson, J. L. *J. Org. Chem.* **1971**, *36*, 3365–3367. (c) Barton, T. J.; Kippenhan, Jr., R. C.; Nelson, A. J. *J. Am. Chem. Soc.* **1974**, *96*, 2272–2273.

(4) (a) Nakadaira, Y.; Sato, R.; Sakurai, H. *Organometallics* **1991**, *10*, 435–442. (b) Nakadaira, Y.; Sato, R.; Sakurai, H. *J.Organomet. Chem.* **1992**, *441*, 411–417.

(5) (a) Leusink, A. J.; Noltes, J. G.; Budding, H. A.; van der Kerk, G. J. M. *Recl. Trav. Chim. Pays-Bas*. **1964**, *83*, 1036–1038. (b) Leusink, A. J.; Budding, H. A.; Noltes, J. G. *J. Organomet.Chem.* **1970**, *24*, 375–386.

(6) Corey, J. Y.; Deuber, M.; Malaidza, M. *J. Organomet.Chem.* **1972**, *36*, 49–60.

(7) Olah, G. A.; Rasul, G.; Heiliger, L.; Bausch, J; Prakash, G. K. S*J. Am. Chem. Soc.* **1992**, *114*, 7737–7742.

(8) Sugihara, Y.; Yagi, T.; Murata, I. *J. Am. Chem. Soc.* **1992**, *114*, 1479–1481, and references are cited therein.

(9) An X-ray structural analysis of the metallepin has only been reported for *Sb*-chlorobenzo[*d*]stibepine: Ashe III, A. J.; Goossen, L.; Kampf, J. W.; Konishi, H. *Angew. Chem. Int. Ed. engl.* **1992**, *31*, 1642–1643. Also the previous works on the heterepins containing Group 15 and 16 elements are surveyed therein.

(10) (a) Komatsu, K.; Akamatsu, H.; Jinbu, Y.; Okamoto, K. *J. Am. Chem. Soc.* **1988**, *110*, 633–634. (b) Komatsu, K.; Aonuma, S.; Jinbu, Y.; Tsuji, R.; Hirosawa, C.; Takeuchi, K. *J. Org. Chem.* **1991**, *56*, 195–203. (c) Aonuma, S.; Komatsu, K.; Takeuchi, K. *Chem. Lett*. **1991**, 767–770. (d) Komatsu, K.; Akamatsu, H.; Aonuma, S.; Jinbu, Y.; Maekawa, N.; Takeuchi, K. *Tetrahedron* **1991**, *47*, 6951–6766. (e) Komatsu, K. *Pure Appl. Chem*. **1993**, *65*, 73–80.

(11) (a) The benzene derivative: Komatsu, K.; Jinbu, Y.; Gillete, G. R.; West, R. *Chem. Lett.* **1988**, 2029–2032. (b) The cyclooctatetraene derivative: Komatsu, K.; Nishinaga, T.; Aonuma, S.; Hirosawa, C.; Takeuchi, K.; Lindner, H. J.; Richter, J. *Tetrahedron Lett.* **1991**, *32*, 6767–6770. (c) A cation radical of the cyclooctatetraene derivative: Nishinaga, T.; Komatsu, K.; Sugita, N.; Lindner, H. J.; Richter, J. *J. Am. Chem. Soc.* **1993**, *115*, 11642–11643. (d) The tropylium ion derivative: Kagayama, A.; Komatsu, K.; Nishinaga, T.; Takeuchi, K.; Kabuto, C. *J. Org. Chem.* **1994**, *59*, 4999–5004. (e) The cyclopentadiene derivative: Komatsu, K.; Nishinaga, T.; Takeuchi, K.; Lindner, H. J.; Richter, J. *J. Org. Chem.* in press.

(12) Andrieux, C. P.; Merz, A.; Savéant, J. -M. *J. Am. Chem. Soc.* **1985**, *107*, 6097–6103 and references are cited therein. See also Garst, J. F.; Barbas, J. T. *J. Am. Chem. Soc.* **1974**, *96*, 3239–3246.

(13) An attempted dilithiation by the use of *n*-BuLi at −78 °C was not successful affording an inseparable complex mixture.

(14) It is supposed that dimethylstannylene, $(CH_3)_2Sn$, was split off through the metallacycloheptatriene/metallanorcaradiene equilibrium shown below. Similar cleavage was observed for the case of silepin derivative: ref. 3b. However, the fate of $(CH_3)_2Sn$ was not clarified even by careful examination of the product mixture. The rate of formation of benzene **4** was estimated from the change in ^1H NMR spectrum: the rate followed the first-order kinetics and the rate constant was 2.8×10^{-4} sec^{-1}.

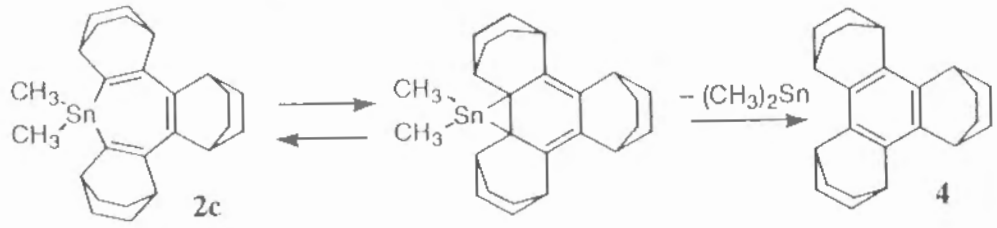

(15) MOPAC 6.0.

(16) Reflecting the less orderly transition-state structure resulting from the longer C–M bond, a gradual increase in $\Delta S^{\ddagger}$ is observed in the sequence; **6**, **2a**, **2b**, **2c**.

(17) Aonuma, S.; Komatsu, K.; Takeuchi, K. *Chem. Lett.* **1989**, 2107–2110.

(18) Schulman, J. M.; Disch, R. L.; Sabio, M. L. *J. Am. Chem. Soc.* **1982**, *104*, 3785–3788.

(19) Suffert, J. *J. Org. Chem.* **1989**, *54*, 509–510.

(20) The chemical shift was corrected with reference to the signal of α-methylene of THF (δ 3.58) as a standard.

(21) The chemical shift was corrected with reference to the signal of α-methylene carbon of THF-*d*8 (δ 67.4) as a standard.

(22) TeXsan: Crystal Structure Analysis Package, Molecular, Structure Corporation (1992).

Chapter 6

A Novel Carbodication Composed of Two Tris(bicyclo[2.2.2]octeno)tropylium Units Connected by a Triple Bond: Synthesis, Structure, and Properties

Abstract

Bis{tris(bicyclo[2.2.2]octeno)tropyliumyl}acetylene dication **3**, which is the first example of the acetylene having two tropylium-ion units at both ends, has been synthesized by stepwise introduction of the tris(bicyclo[2.2.2]octeno)cycloheptatrienyl unit to acetylene followed by hydride abstraction. The results of X-ray crystallography indicated that the two tropylium rings are twisted with each other by the angle of 44° and the tropylium ring is slightly bent into a boat form. The dication **3** was neutralized in 50% aqueous acetonitrile via two steps at the p*H* values of 7.0 and 11.5, which correspond to the pK_{R^+} values of the dication and the half-neutralized monocation, respectively. Thus, the dication **3** is 6 pK_{R^+} unit destabilized compared with the corresponding monocation (pK_{R^+} 13.0) due to the intramolecular electrostatic repulsion of the positive charge. The cyclic voltammetry indicated that the dication **3** undergoes two reversible one-electron reductions consecutively in dichloromethane. The electrochemical reduction of **3** as well as chemical reduction with zinc powder in dichloromethane-acetonitrile afforded a blue solution of the corresponding cation radical $\mathbf{3}^{\cdot+}$, but not the diradical, as shown by ESR experiments.

Introduction

The tropylium ion tri-annelated with bicyclo[2.2.2]octene framework, **1**, was found to exhibit remarkably high thermodynamic stability (pK_{R^+} 13.0) due to both inductive and σ-conjugative effects of the rigid σ-frameworks.[1] However effects of the substituent at the 7-position have not been examined except for the 7-methyl derivative **2**: the 7-methyl substituent in **2** was found to destabilize the cation by 0.6 pK_{R^+} unit [1] in spite of its electron donating ability. This destabilization was attributed to the possible distortion of the tropylium ring from planarity due to severe steric congestion generated between the methyl group and bridgehead hydrogens.

1

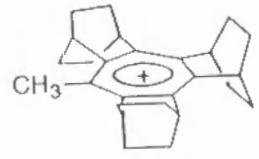

2

Based on these results, we have designed the dication **3** having two units of monocation **1** at both sides of acetylene, for which we could expect the effects of π-conjugative interaction without much steric congestion. As to the parent tropylium ion substituted with an ethynyl group, the arylethynyl derivatives **4** are known,[2] but there has been no report on the dication with two tropylium units at both sides of acetylene. The present chapter describes the synthesis of dication **3** as the first example of such dications, together with its structural, thermodynamic, and electrochemical properties.

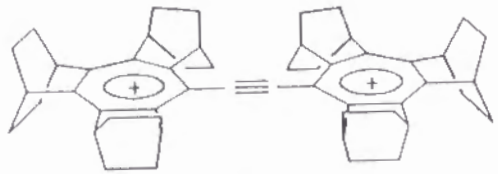

3

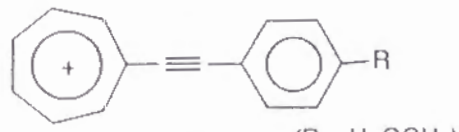

4

Results and Discussion

Synthesis. Synthesis of dication **3** was carried out as shown in Scheme 1. Reaction of cation **1** with (trimethylsilyl)ethynyllithium followed by desilylation afforded the ethynylcycloheptatriene **6** in 50% yield. Lithiation of **6** and repeated reaction with **1** gave dicycloheptatrienylacetylene **7** in 41% yield. Direct hydride abstraction from **7** using a trityl salt resulted in formation of dication **3** in nearly 32% yield accompanied by serious contamination with unremovable impurity. However the hydride abstraction by the use of two equiv of dichlorodicyano-*p*-benzoquinone (DDQ) and anion exchange with trityl hexafluoroantimonate yielded desired dication salt, **3**·2SbF_6^-, in 59% yield as yellow needles, which are analytically pure and stable under air.

Scheme 1

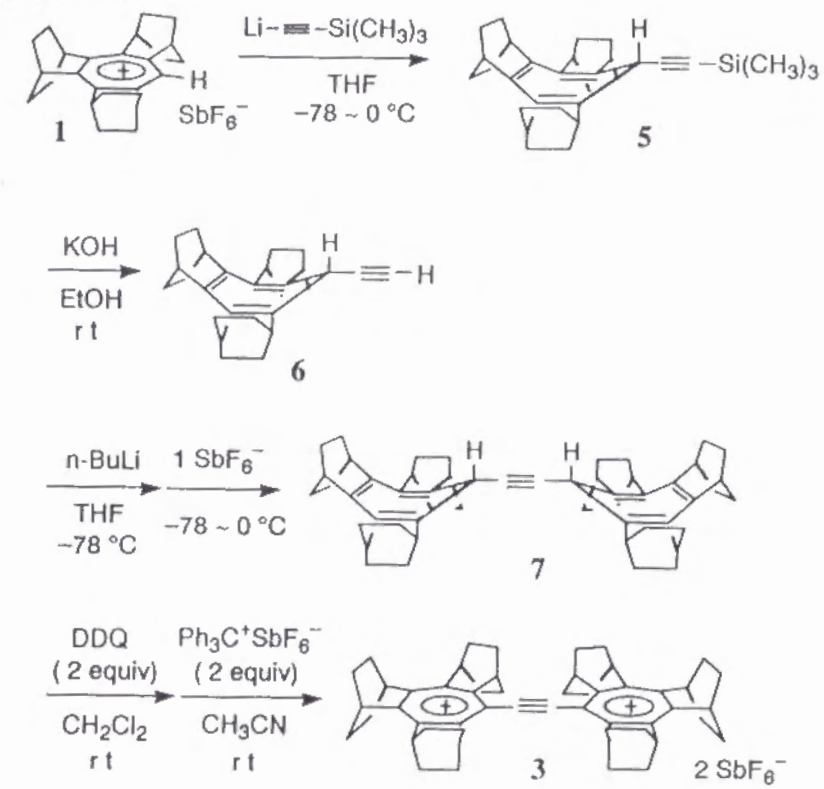

Spectral Properties. Dication **3** was fully characterized by the spectral data shown in Table 1. Also shown are those of monocation **1** for comparison.

The ^{1}H NMR chemical shifts of **3** are generally similar to those of **1** except a signal for one of the bridgehead protons, which extends over in front of the triple bond and is thus deshielded by 0.37 ppm compared with the rest of bridgehead protons. The presence of a triple bond is evidenced by the ^{13}C NMR signal at δ 104.7 ppm. In the electronic spectrum the longest wavelength absorption exhibits a bathochromic shift by about 80 nm as compared with **1**, indicating the π-conjugative effect between the two tropylium units and the acetylenic π-systems.[3]

Structure. It is of particular interest to examine the relative geometry of the two π-systems conjugatively connected to both sides of a triple bond. When we assume that a π-system is conjugated with only one set of p-orbitals of the triple bond, the two π-systems would take the conformation either coplanar (**A**) or perpendicular (**B**) to each other. On the other hand, there might not be any specifically favored orientation for the two π-systems if the cylindrically symmetric structure of the π-clouds is considered more significant for the triple bond (**C**).

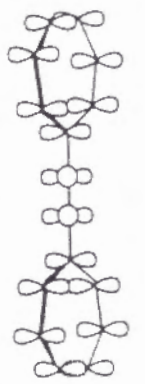

A

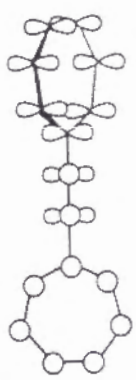

B

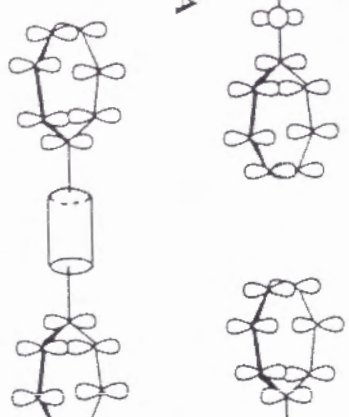

C

Table 1. Spectral Data for the SbF_6^- Salts of **3** and **1**

	^{1}H NMR δ / ppm (CD_3CN, 270 MHz)			^{13}C NMR δ / ppm (CD_3CN, 67.8 MHz)				IR ν / cm^{-1}			UV-vis λ_{max} / nm (log ε)
Compd	⁻CH⁻⁺	CH	CH_2	⁻CH⁻⁺	≡C–	CH	CH_2		(KBr)		(CH_3CN)
3 ·2SbF_6^-	——	4.46	2.07	167.8	104.7	40.9	24.7 [a]	2947	2871	1617	282 (4.83)
		(4 H)	(24 H)	166.9		36.9		1457	1455	1365	386 (4.39)
		4.09	1.51	164.0		36.7		1327	1276	1172	
		(8H)	(24 H)	135.6				1139	1029	815	
								657			
1 ·SbF_6^- [b]	8.55	4.13	2.03	168.3	——	42.7	25.0	2951	2873	1625	256 (4.71)
	(1 H)	(2 H)	(12 H)	166.0		36.6	24.8	1458	1420	1320	308 (4.01)
		4.07	1.43	163.9		36.1	24.7	1270	1245	1173	
		(2 H)	(12 H)	144.2				1040	1025	814	
		3.56						658			
		(2 H)									

[a] Three signals are supposedly overlapping as judged from the signal intensity. [b] Data from Ref.1.

In the case of diphenylacetylene, MO calculations using CNDO (or INDO) indicated that the energy difference between the coplanar and the perpendicular geometries is negligibly small, i.e., 0.7 kcal mol^{-1} (or 0.4 kcal mol^{-1} by INDO), with the perpendicular geometry being slightly more stable;[4] however, the experimental results from X-ray crystallography and UV spectroscopy on diphenylacetylene, and from measurement of dipole moment of bis(3-chlorophenyl)-acetylene all indicated that the two benzene rings are in a coplanar geometry both in solid state and in solution.[4]

Thus we carried out the X-ray crystallography on a single crystal of **3**·2SbF_6^-. Unfortunately, the small size of the crystal and disorder in SbF_6^- anion prevented us from obtaining a sufficiently low R factor to allow detailed discussion on the precise structure (R = 0.117). Also it was found that two benzene molecules (from recrystallization solvent) were contained in the crystal of **3**·2SbF_6^-. However, the discussion on general structural features of the whole molecule could be made safely. The observed structure is shown in Figure 1. It reveals that the two seven-membered rings are rotated with each other with the dihedral angle of the mean planes being 44°.

We also conducted semiempirical MO calculations (AM1) for ditropyliumylacetylene dication (**8**) as a simplified model. The results indicated that as the dihedral angle between the two seven-membered rings changes from 0° (coplanar) to 90° (perpendicular) the heat of formation exhibits a very slight decrease in a monotonous way, the energy difference between the coplanar and the perpendicular models being quite minute (0.15 kcal mol^{-1}). Thus, there seems to be almost no energy barrier for ring rotation in **8**. The experimentally observed

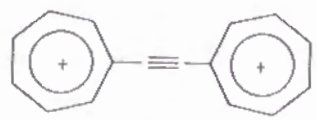

8

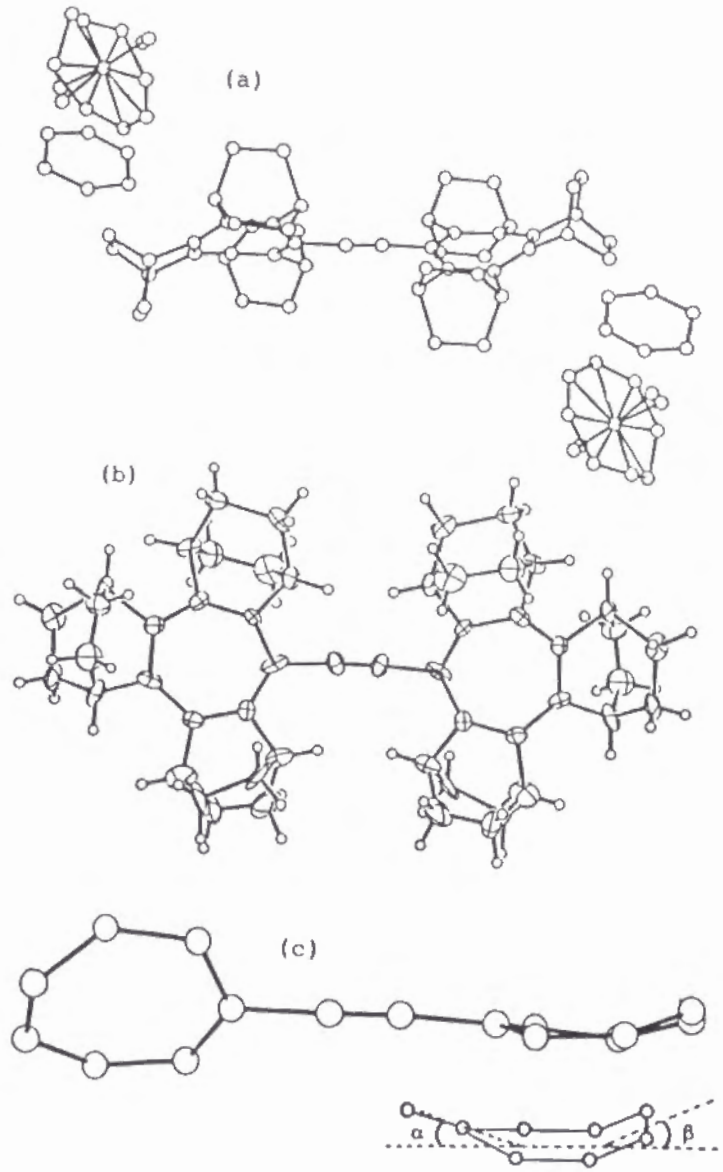

Figure 1. X-ray crystal structures. (a) The structure of **3**·2SbF_6^-·2C_6H_6: the six F atoms in SbF_6^- anion could not be precisely located due to the disorder and are represented by twelve atoms; hydrogen atoms are deleted for clarity. (b) Top view of the dication **3**. (c) Side view of the central ditropyliumylacetylene framework: the dihedral angle between the bow and the central portion (α) is 10.9° and the angle between the stern and the central portion (β) is 18.7°.

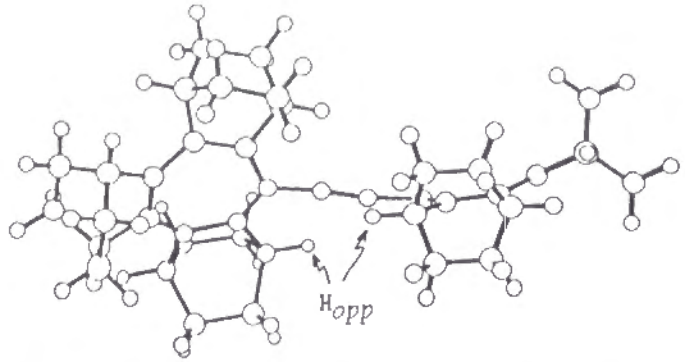

Figure 2. The AM1 calculated structure of the dication **3**.

geometry of the two π-systems in **3** could be considered as the result of a compromise between the conjugative stabilization in a coplanar geometry and the repulsive interaction between the two cationic moieties. Also the steric repulsion between the bridgehead hydrogens of the two tropylium units opposite to each other (marked as H_{opp} in Figure 2; see below) may be contributing.

Another structural feature to be noticed in the X-ray structure of **3** is that the tropylium ring is not planar but somewhat folded to a boat form as shown in Figure 1(c). This unexpected feature is presumably due to steric congestion caused by surrounding bicyclic frameworks, though such effect should be smaller than that in the methyl derivative **2**.[5]

The AM1 calculations conducted for the optimized structure of **3** gave the result quite similar to the X-ray structure as shown in Figure 2 with the twisting angle between the two tropylium units being 53°.

Thermodynamic Stability. In order to examine the thermodynamic stability of the dication having such characteristic π-conjugation, the pK_{R+} value of **3** was measured by spectrophotometric titration in 50% aqueous acetonitrile. The hydrolysis was found to occur via two steps as shown in Figure 3.

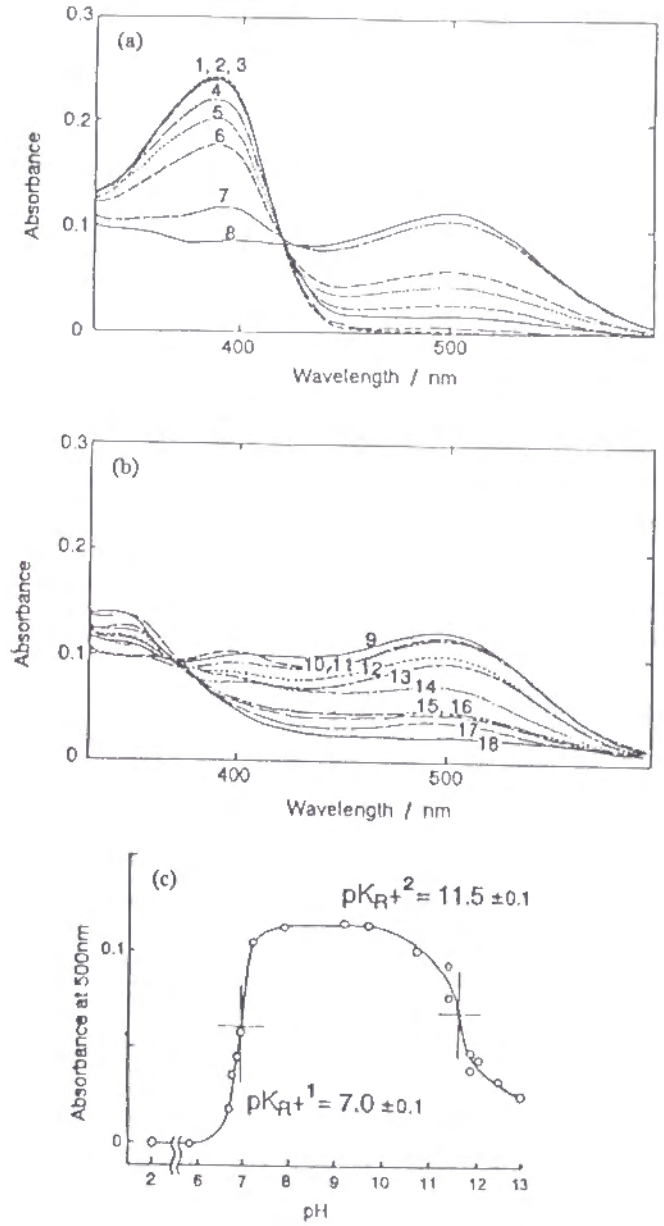

Figure 3. The pK_{R+} measurement of $3 \cdot 2SbF_6^-$ (9×10^{-6} M) in 50% aqueous acetonitrile: dependence of the UV–vis spectra upon p*H* . (a) Spectrum 1, p*H* 2.2; 2, 5.4; 3, 6.6; 4, 6.7; 5, 6.8; 6, 6.9; 7, 7.2; 8, 7.4. (b) Spectrum 9, p*H* 7.9; 10, 9.2; 11, 9.7; 12, 10.7; 13, 11.3; 14, 11.4; 15, 11.9; 16, 12.1; 17, 12.4; 18, 13.0. (c) Plot of the absorbance at 500 nm against p*H*.

As the p*H* value of the solution was increased from 2 to 8, the color of the solution changed from yellow to red and the UV–vis spectrum exhibited decrease in absorption at 386 nm with concomitant appearance of new absorption at 500 nm. As the p*H* was increased further, the red color faded and was gone away at the p*H* value larger than 12. These color changes corresponding to the change in p*H* were completely reversible.

From the plot of the absorbance at 500 nm against p*H* (Figure 3(c)), the pK_{R+} values of original dication **3** and the half-neutralized monocation were determined as 7.0±0.1 and 11.5±0.1, respectively. Compared with cations **1** (pK_{R+} 13.0)[1] and **2** (pK_{R+} 12.4),[1] the stability of dication **3** is lowered by 5–6 pK_{R+} units, while that of the half-neutralized monocation is not so much different from that of **2**. Apparently, the destabilization of **3** is ascribed to the electrostatic repulsion between the two positively charged units. Upon neutralization, there appear to be formed isomeric mixtures of monocationic alcohols **3**-OH and then the diols **3**-$(OH)_2$. From the considerable bathochromic shift of the visible absorption of the half-neutralized monocation (λ_{max} 500 nm), it is supposed that, upon the first neutralization, the hydroxide ion attacks not only the ethynyl-substituted carbon but also the other carbons of the tropylium ring to give the monocation with extended π-conjugation as shown in Scheme 2.[6]

Red-Ox Behavior. In contrast to cations **1** and **2**, which were reduced irreversibly upon cyclic voltammetry (CV),[1] dication **3** exhibited two reversible reduction waves at –0.49 and –0.66 V vs Ag/Ag^+ as shown in Figure 4, with the first reduction potential lower than monocation **1** by 0.6 V upon comparison of the peak potentials. Thus dication **3** is supposed to give consecutively the cation radical and the neutral species both of which can persist in solution.

When the ESR spectrum was measured under the electrolytic conditions

Scheme 2

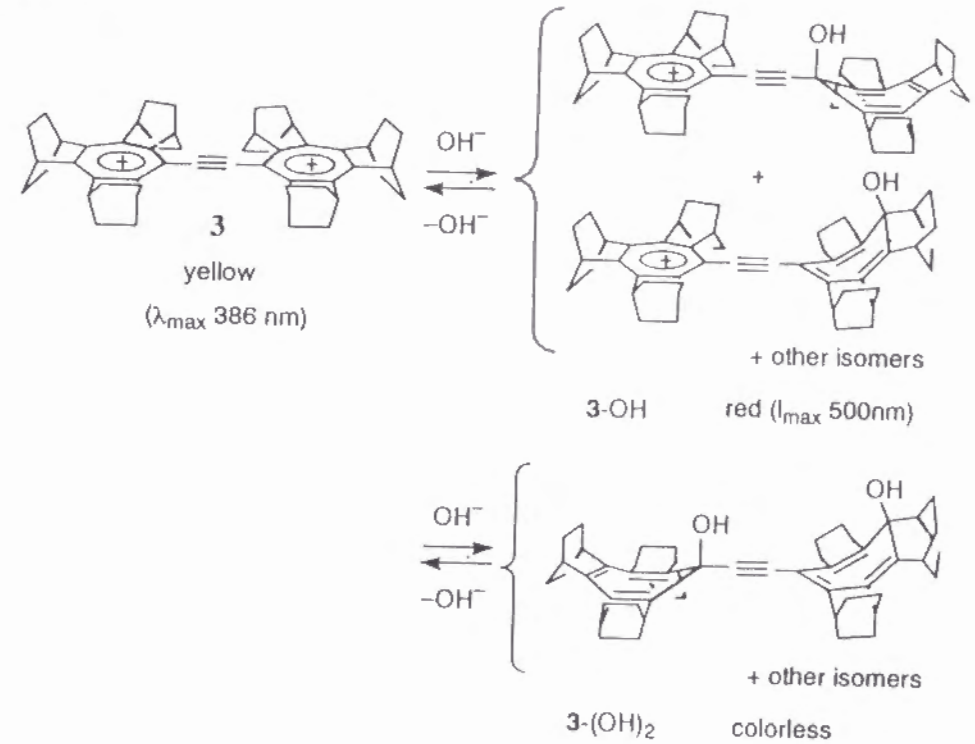

with the potential changed stepwise by 0.1 V from –0.1 V to –1.0 V vs Ag/Ag^+, a strong single-line signal with a peak-to-peak width of 0.3 mT, shown in Figure 5(a), began to appear at the potential of –0.4 V and kept almost the same intensity over the potential ranging to –1.0 V. The feature of this signal[7] remained the same at the whole potential range and the signal persisted at room temperature under argon atmosphere for at least 15 min after the cathodic current was cut off. During the electrolysis, the color of the solution in a region close to the working electrode turned to dark blue. Even after the exhaustive reduction with the potential over –1.0 V, there was observed no sign for generation of a triplet diradical, such as a $\Delta m = 2$ signal at the half-field (~160 mT) or any fine structure for the sample solution frozen to a glass at –120 °C (Figure 5(b)). From these results, the single-line signal is considered as due to the cation radical $\mathbf{3}^{\cdot+}$. The

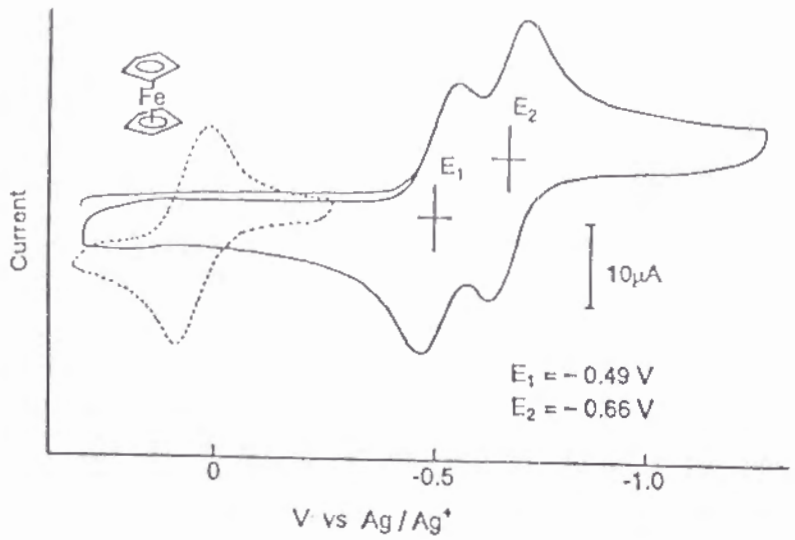

Figure 4. Cyclic voltammogram of $\mathbf{3}\cdot 2SbF_6^-$ in dichloromethane: sample, 0.3 mM; supporting electrolyte, tetrabutylammonium perchlorate (0.1 M); scan rate, 100 mV s^{-1}. (Dotted line is the voltammogram of ferrocene added as an internal standard after the measurement.)

two-electron reduced product appears to form a closed-shell molecule although no spectral study could be made because of its extreme instability.

Dication **3** was also chemically reduced by zinc powder in dichloromethane-acetonitrile (9:1) to generate a dark blue solution, which exhibited the ESR signal identical to that in Figure 5(a) and the electronic absorption at λ_{max} 597 nm.[8] This solution also did not show any evidence for a triplet diradical by the same ESR experiment as described above. Although the cation radical $\mathbf{3}^{\cdot+}$ was stable in solution, it seemed to decompose by evaporation of the solvent under high vacuum since no blue color was regenerated by dissolution of the residue in the same solvent transferred by vacuum distillation.

In an attempt to obtain more information about the structure of the fully reduced product, the reaction of **3** with zinc powder was conducted in acetonitrile-THF (1:1).[9] In the previous work, zinc powder in acetonitrile was shown to

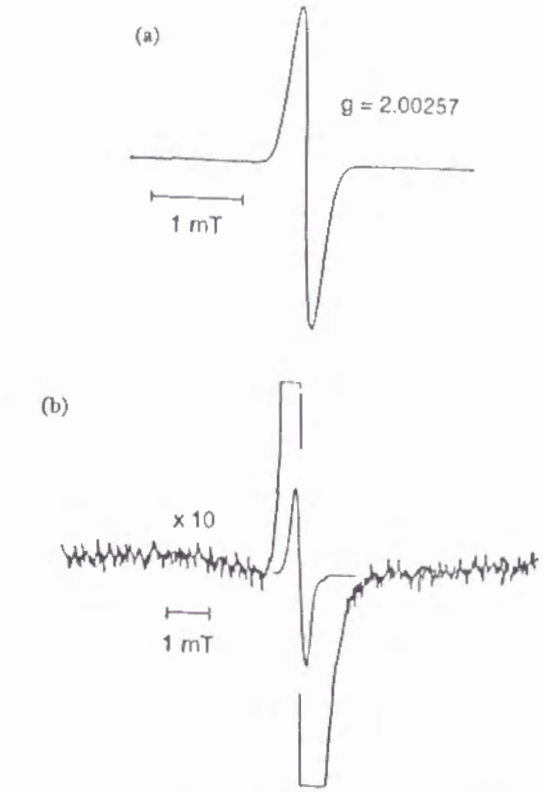

Figure 5. ESR spectra of the cation radical $\mathbf{3}^{\cdot+}$ generated by electrolysis in dichloromethane recorded at (a) room temperature and (b) at -120 °C.

reduce *t*-butyltropylium ion,[10a] which has the reduction potential[10b] about 0.1 V higher (less negative) than that for the second reduction step for the dication **3**. The color of the solution changed to dark blue and then to red with formation of dark red precipitates suggesting the formation of new species, possibly the fully reduced one. This red material did not show any ESR signal, but the definite determination of its structure was hampered by its ready decomposition or polymerization as deduced from its weak and broad ^{13}C NMR spectrum.

Thus, the solvent polarity was found to strongly affect the reduction pathway of the dication **3**. Studies on the one- and two-electron reduction processes for the similar dications having a *para*- or *meta*-phenylene spacer instead of a triple bond are discussed in the next chapter.

In summary, the first derivative of ditropyriumylacetylene dication was synthesized, and was found to be considerably destabilized as compared with the corresponding monocation. The X-ray crystallography indicated that the two seven-membered ring are twisted by 44°. Upon one-electron reduction, the dication is reduced stepwise affording a stable cation radical, but the fully reduced species could not be characterized.

Experimental Section

General Procedures. Melting points were determined on a Yamato MP-21 apparatus and are uncorrected. Elemental analysis was performed by Micro-analytical Center, Kyoto University, Kyoto. NMR spectra were recorded on JEOL GSX270 (270 MHz for ^{1}H and 67.8 MHz for ^{13}C NMR) or on JEOL FX90 (90 MHz for ^{1}H) spectrometers using Me_4Si as an internal standard. IR spectra were taken on Perkin Elmer 1640 spectrometer. UV–vis spectra were taken on Hitachi 200–10 spectrometer. ESR spectra were recorded on JEOL PE–2X or on JES–SRE2X spectrometer. Mass spectrum was taken on JEOL JMS–SG spectrometer. Cyclic voltammograms were obtained by the use of a Hokuto–Denko HA104 potentiostat, a HB107A function generator, a Hitachi 057 X–Y recorder, and a three-electrode cell composed of platinum wire working and counter electrodes and a Ag/0.01 M $AgNO_3$ (acetonitrile) reference electrode. The observed potential was corrected with reference to ferrocene ($E_{1/2}$ +0.083 V) added as an internal standard after each measurement. A Sartorius 4503MP6 microbalance was employed for weighing samples less than 1 mg.

THF was freshly distilled from sodium benzophenone ketyl before use. dichloromethane and acetonitrile were refluxed and distilled over P_2O_5 under nitrogen. All reactions where anhydrous conditions were required were

conducted under an atmosphere of argon or nitrogen. Medium-pressure liquid chromatography (MPLC) was carried out using silica gel 60 (E. Merk, particle size 0.040–0.063 mm, 230–400 mesh ASTM) as a stationary phase and hexane as an eluent. Commercial tetrabutylammonium perchlorate was recrystallized from hexane and ethyl acetate. 1,2:3,4:5,6-tris(bicyclo[2.2.2]octeno)tropylium hexafluoroantimonate ($\mathbf{1}\cdot SbF_6^-$)[1b] and trityl hexafluoroantimonate ($Ph_3C^+SbF_6^-$)[11] were prepared following the literature procedure.

7-(trimethylsilylethynyl)-1,2:3,4:5,6-tris(bicyclo[2.2.2]octeno)cyclo-heptatriene (5). A solution of 1.6 M *n*-BuLi in hexane (0.19 mL, 0.30 mmol) was added dropwise to a stirred solution of (trimethylsilyl)acetylene (0.037 mL, 0.025 g, 0.26 mmol) in THF (4 mL) at −78 °C, and the resulting mixture was stirred for 1 h at −78 °C and for 0.5 h at 0 °C. Then, the mixture was cooled to −78 °C again, and a suspension of $\mathbf{1}\cdot SbF_6^-$ (82 mg, 0.14 mmol) in THF (3 mL) was slowly added. After stirring for 1 h at −78 °C, the mixture was slowly warmed to room temperature over 0.5 h, evaporated under reduced pressure, and extracted with ether. The ethereal solution was evaporated to give 78 mg of a pale yellow powder, which was shown to contain about 50 mg (0.12 mmol, 81% yield) of **5** by ^{1}H NMR analysis. Separation of the crude product by the use of MPLC afforded **5** (33 mg, 54%) as an unstable white powder, which decomposed slowly in solid state under vacuum and more rapidly in $CDCl_3$:[12] mp 151-162 °C (dec); ^{1}H NMR($CDCl_3$, 270 MHz) δ 2.88 (br s, 6 H), 2.48 (s, 1 H), 1.70-1.25 (m, ≥24 H), 0.19 (s, 9 H); ^{13}C NMR ($CDCl_3$, 67.8 MHz)[13] δ 31.7, 31.3, 27.5, 26.6, 26.4, 26.3, 25.8, 0.3; IR (KBr) 2174 (C≡C, m) cm^{-1}.

7-ethynyl-1,2:3,4:5,6-tris(bicyclo[2.2.2]octeno)cycloheptatriene (6). The crude product from the above reaction containing 36 mg (0.086 mmol) of **5** was dissolved in 10 mL of ethanol. To this solution was added dropwise a 0.1 M

solution of KOH in ethanol (12 mL) at room temperature. The solution was stirred for 3 h with occasional heating to reflux under nitrogen. The solution was evaporated under reduced pressure and extracted with ether. The ethereal solution was evaporated to give 35 mg of a pale yellow powder, which was shown to contain about 25 mg (0.071 mmol, 83 % yield) of **6** by ^{1}H NMR analysis. Separation with MPLC afforded **6** (15 mg, 50%) as a white powder, which was as unstable as **5**: mp 92-97 °C (dec); ^{1}H NMR ($CDCl_3$, 270 MHz) δ 2.90, 2.88 (br s x 2, 6 H), 2.55 (δ, J =2.4 Hz, 1 H), 1.70–1.25 (m, ≥25 H); ^{13}C NMR ($CDCl_3$, 67.8 MHz)[13] δ 31.8, 31.3, 29.7, 26.6, 26.4, 26.2, 25.8; IR (KBr) 3320 (C≡C–H, s), 2119 (C≡C, w) cm^{-1}.

Anal. Calcd for $C_{27}H_{32}$: C, 90.95; H, 9.05. Found: C, 89.14; H, 9.32.[12]

Bis{2,3:4,5:6,7-tris(bicyclo[2.2.2]octeno)cycloheptatrien-1-yl}acetylene (7). To a solution of the crude product from the above reaction containing 22 mg (0.062 mmol) of **6** in THF (4 mL) was added dropwise a 1.5 M solution of n-BuLi in hexane (0.050 mL, 0.075 mmol) at −78 °C, and the resulting mixture was stirred for 1 h at −78 °C, and for 10 min at 0 °C. Then, the mixture was cooled again to −78 °C, and a suspension of **1**·SbF_6^- (47 mg, 0.083 mmol) in THF (3 mL) was added slowly. The mixture was stirred for 0.5 h at −78 °C, and was slowly warmed to room temperature over 1 h. The solution was evaporated under reduced pressure and extracted with ether (4 mL x 4) and benzene (8 mL). The organic solution was evaporated and the residue separated by MPLC to yield 20 mg (48%) of **7** and 10 mg (45%) of unchanged **6**. The compound **7** was more stable than its precursors **5** and **6**, but slowly decomposed in $CDCl_3$ solution: mp 112-113 °C (dec); ^{1}H NMR ($CDCl_3$, 90 MHz) δ 3.17 (br s, 4 H), 2.91 (br s, 8 H), 2.70 (s, 2 H), 1.70-1.21 (br m, ≥48 H); ^{13}C NMR ($CDCl_3$, 67.8 MHz)[13] δ 32.0, 31.4, 27.6, 26.7, 26.4, 25.8, 24.3; MS m/z 686 (M^+).

Anal. Calcd for $C_{52}H_{62}$: C, 90.90; H, 9.10. Found: C, 90.10; H, 9.01.[12]

Bis{tris(bicyclo[2.2.2]octeno)tropyliumyl}acetylene Hexafluoroantimonate (3·2SbF_6^-). (a) A Method Using DDQ. A solution of DDQ (21 mg, 0.091 mmol) in dichloromethane (2 mL) was added dropwise to a stirred solution of **7** (29 mg, 0.042 mmol) in dichloromethane (6 mL) to give a dark red solution. After stirring for 0.5 h at room temperature, the solution was concentrated to *ca.* 2 mL. To this solution was added ether (15 mL) to cause the formation of black precipitates, which were collected by filtration and dried under vacuum to give 52 mg of a black powder. This product was dissolved in 15 mL of acetonitrile, and to this solution was added dropwise a solution of $Ph_3C^+SbF_6^-$ (44 mg, 0.093 mmol) in 2 mL of acetonitrile with stirring at room temperature. The resulting orange-yellow solution was evaporated and the residue redissolved in 1.5 mL of dichloromethane-acetonitrile (2:1). To this solution was added ether (15 mL) to cause the formation of yellow precipitates, which were collected by filtration and dried under vacuum to give crude **3**·2SbF_6^- as a yellow powder (39 mg). Recrystallization by slow diffusion of ethyl acetate into a saturated solution of the crude product in dichloromethane yielded **3**·2SbF_6^- as pale yellow needles (28 mg, 59%): mp 218–221 °C (dec). The spectral data are shown in Table 1.

Anal. Calcd for $C_{52}H_{60}F_{12}Sb_2$: C, 54.00; H, 5.23. Found: C, 53.75; H, 5.44%.

A single crystal of **3**·2SbF_6^-·2C_6H_6 for X-ray crystallography was obtained by slow diffusion of benzene into a saturated solution of **3**·SbF_6^- in dichloromethane.

(b) A Direct Method Using Trityl Hexafluoroantimonate. A solution of $Ph_3C^+SbF_6^-$ (17 mg, 0.036 mmol) in dichloromethane (2 mL) was added dropwise to a stirred solution of **7** (12 mg, 0.017 mmol) in dichloromethane (5 mL) to yield a dark green solution. After stirring for 10 min at room temperature, the solution was concentrated to *ca.* 1 mL. To this solution was added ether (10 mL) to cause the formation of orange precipitates, which were collected by

filtration and dried under vacuum to give an orange powder (7 mg) which contained $\mathbf{3}\cdot 2SbF_6^-$ as a major component and some impurity as shown by ^1H NMR. Recrystallization by slow diffusion of ethyl acetate into a saturated solution of the crude product in dichloromethane did not improve the purity.

X-ray Crystallography. A pale yellow crystal with small sizes of 0.07 x 0.2 x 0.5 mm, which were cut from the cracked crystals, was used for the data collection on a Rigaku automated four circle diffractometer (AFC5PR), equipped with a rotating anode (45 kV, 200 mA), using graphite-monochromated Mo-Kα radiation (λ=0.71069 Å). Crystal data are as follows; a = 10.760(4) Å, b = 30.041(10) Å, c = 19.674(6) Å, V = 6360(5) Å^3, the space group = Iba2(No. 45), Z=4 for $C_{52}H_{60}\cdot 2SbF_6\cdot 2C_6H_6$, D_{calcd}=1.371 g cm^{-3}, μ(MoKα)=9.23 cm^{-1}. A Low temperature equipment was used to maintain the stability of crystal (120 K). The ω scan mode with a scan rate of 1 ° min^{-1} was employed with a scan range, 1.2 + 0.30 tan θ. A total of 3464 reflections within 2θ=54.7 ° were collected. Lp correction and the empirical absorption correction using the psi-scan method were applied.

The structure was solved by the direct method combined with the heavy atom method. In an asymmetric unit, one SbF_6^- anion, a half moiety of cation and one benzene solvent molecule are included. Although F atoms were found disorderly, the cation molecule and benzene molecules were found in the definite positions. The full-matrix least-squares refinement gave the reasonable decrease by introducing anisotropic temperature factor for Sb atom. However, all carbon atoms could not refined anisotropically. Finally carbon atoms of seven-membered ring were refined anisotropically and all hydrogens were included in the calculated positions. The final cycle of refinement was carried out using 1711 observed reflections within I>2σ(I) converged to the final $R = \Sigma \| |F_o| - |F_c| | / \Sigma |F_o|$ value of 0.117 and $Rw = [(\Sigma_w(|F_o| - |F_c|)^2/\Sigma_w F_o^2)]^{1/2}$ of 0.112. The

maximum and minimum peaks on the final difference Fourier map correspond to 1.09 and –2.41 eÅ^{-3}, respectively. The relatively high R value and structural parameters of a low accuracy were caused by the poor quality and small size of the crystal as well as the disorder of SbF_6^- anion. All computations were performed using Rigaku Texsan software package system (TEXRAY Structure Analysis Package, Molecular Structure Corporation, 1985). Crystallographic data, i.e., atomic coordinate, anisotropic displacement parameters, bond lengths, and bond angles are given in Tables 2–5 respectively.

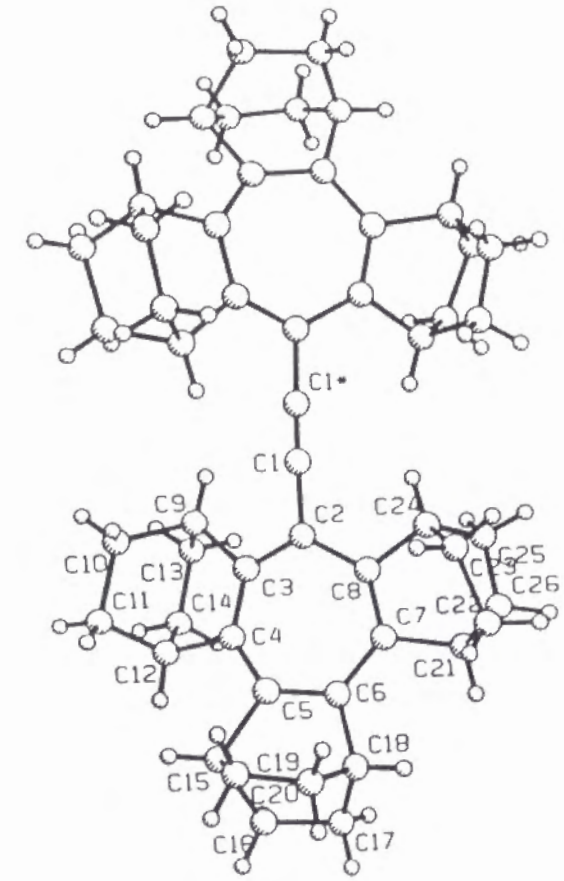

Table 2. Atomic Coordinates and Equivalent Isotropic Temperature Factors for **3**·2SbF_6^-

Atom	X/*a*	Y/*b*	Z/*c*	*B*(EQ)
Sb	0.79178(13)	0.129007(49)	0.50000	4.67(8)
F(1)	0.6123(54)	0.1140(17)	0.5316(27)	11(2)
F(2)	0.7000(46)	0.0948(13)	0.5692(23)	6(1)
F(3)	0.7939(44)	0.0768(13)	0.4469(22)	5(1)
F(4)	0.7730(52)	0.1796(14)	0.5436(24)	9(1)
F(5)	0.8094(55)	0.1785(18)	0.4305(32)	6(1)
F(6)	0.7215(78)	0.1665(23)	0.4385(41)	8(2)
F(7)	0.7934(52)	0.0847(16)	0.4293(24)	7(1)
F(8)	0.8536(50)	0.0913(17)	0.5524(25)	7(1)
F(9)	0.8692(46)	0.1663(13)	0.5750(25)	10(1)
F(10)	0.6198(89)	0.1421(27)	0.4597(46)	17(3)
F(11)	0.9670(31)	0.1296(11)	0.4829(50)	10.4(9)
F(12)	0.9343(39)	0.1202(13)	0.5602(23)	12(1)
C(1)	0.0256(21)	0.01518(71)	0.4300(16)	4.3
C(2)	0.1022(27)	0.05617(95)	0.4253(16)	4.5
C(3)	0.1790(17)	0.06216(65)	0.4813(12)	2.3
C(4)	0.2513(19)	0.10118(67)	0.4981(23)	4.0
C(5)	0.2492(23)	0.14248(81)	0.4659(14)	3.5
C(6)	0.2229(23)	0.15038(85)	0.3968(14)	3.5
C(7)	0.1684(28)	0.12016(89)	0.3487(16)	4.6
C(8)	0.1018(27)	0.08194(82)	0.3638(16)	4.2
C(9)	0.1818(22)	0.02706(92)	0.5330(15)	4.6
C(10)	0.1435(26)	0.04720(83)	0.6044(17)	4.4
C(11)	0.2350(30)	0.0906(10)	0.6239(16)	5.5
C(12)	0.3216(20)	0.09741(94)	0.5653(16)	4.3
C(13)	0.3352(33)	0.0135(11)	0.5422(19)	8.1
C(14)	0.4141(34)	0.0560(11)	0.5578(20)	7.2
C(15)	0.2703(21)	0.18637(77)	0.5116(20)	4.8
C(16)	0.3908(21)	0.2093(10)	0.4713(16)	5.7
C(17)	0.3521(31)	0.2158(10)	0.3962(19)	6.7
C(18)	0.2359(26)	0.19968(97)	0.3780(18)	5.5
C(19)	0.1566(37)	0.2253(12)	0.4240(24)	8.0
C(20)	0.1669(27)	0.21552(78)	0.4898(20)	5.7
C(21)	0.1672(37)	0.1303(12)	0.2751(19)	7.5
C(22)	0.0392(33)	0.1387(12)	0.2505(26)	9.3
C(23)	-0.0429(43)	0.0996(10)	0.2822(19)	9.2
C(24)	0.0325(31)	0.0636(10)	0.3066(17)	5.9
C(25)	0.1261(43)	0.0544(14)	0.2484(22)	8.9
C(26)	0.2032(40)	0.0914(12)	0.2374(20)	8.8
C(61)	0.5329(58)	0.2173(19)	0.1524(31)	14(2)
C(62)	0.4825(45)	0.1770(14)	0.1770(26)	11(1)

(Table 2. Continued)

Atom	X/*a*	Y/*b*	Z/*c*	*B*(EQ)
C(63)	0.5566(65)	0.1600(18)	0.2377(38)	15(2)
C(64)	0.6639(56)	0.1841(18)	0.2529(30)	13(2)
C(65)	0.7190(50)	0.2204(17)	0.2270(30)	11(1)
C(66)	0.6427(46)	0.2427(14)	0.1752(27)	11(1)
H(1)	0.0547	0.0548	0.6027	8.4
H(2)	0.1501	0.0235	0.6375	8.4
H(3)	0.1868	0.1177	0.6258	6.2
H(4)	0.2813	0.0865	0.6615	6.2
H(5)	0.3484	-0.0076	0.5805	10.0
H(6)	0.3651	-0.0049	0.5023	10.0
H(7)	0.4675	0.0606	0.5102	10.4
H(8)	0.4763	0.0519	0.5878	10.4
H(9)	0.4223	0.2332	0.4864	7.6
H(10)	0.4606	0.1852	0.4663	7.6
H(11)	0.3606	0.2465	0.3874	9.1
H(12)	0.4150	0.2009	0.3655	9.1
H(13)	0.1706	0.2555	0.4155	9.3
H(14)	0.0686	0.2191	0.4116	9.3
H(15)	0.0897	0.2048	0.5025	5.4
H(16)	0.1781	0.2454	0.5084	5.4
H(17)	0.0009	0.1689	0.2676	10.8
H(18)	0.0248	0.1425	0.2011	10.8
H(19)	-0.0967	0.1092	0.3170	8.9
H(20)	-0.0990	0.0873	0.2456	8.9
H(21)	0.1762	0.0292	0.2610	9.5
H(22)	0.0833	0.0462	0.2065	9.5
H(23)	0.1995	0.0984	0.1881	9.1
H(24)	0.2862	0.0837	0.2470	9.1

Table 3. Anisotropic Temperature Factors for $3 \cdot 2SbF_6^-$

Atom	*U*11	*U*22	*U*33	*U*12	*U*13	*U*23
Sb	0.04794(90)	0.06057(97)	0.0721(14)	0.0008(12)	0.0047(31)	0.0065(26)
F(1)	0.203(26)					
F(2)	0.090(12)					
F(3)	0.084(20)					
F(4)	0.095(17)					
F(5)	0.064(12)					
F(6)	0.118(18)					
F(7)	0.088(26)					
F(8)	0.101(16)					
F(9)	0.107(16)					
F(10)	0.112(36)					
F(11)	0.087(12)					
F(12)	0.195(34)					
C(1)	0.049(22)	0.045(20)	0.048(21)	-0.015(17)	-0.011(18)	0.014(15)
C(2)	0.040(22)	0.092(20)	0.022(27)	0.025(18)	0.010(24)	-0.049(20)
C(3)	0.016(14)	0.046(12)	0.031(28)	0.0091(97)	0.014(14)	0.015(11)
C(4)	0.052(18)	0.056(14)	0.020(20)	0.009(10)	0.083(47)	0.037(40)
C(5)	-0.012(19)	0.084(15)	0.065(22)	0.006(11)	-0.002(15)	-0.002(15)
C(6)	0.053(17)	0.071(15)	0.004(21)	0.004(16)	0.014(19)	0.009(16)
C(7)	0.078(20)	0.071(20)	0.012(24)	-0.025(16)	0.028(19)	-0.009(17)
C(8)	0.083(19)	0.060(18)	0.023(24)	-0.002(16)	-0.007(20)	-0.004(17)
C(9)	0.0584					
C(10)	0.063(15)					
C(11)	0.074(11)					
C(12)	0.0474(86)					
C(13)	0.105(15)					
C(14)	0.092(13)					
C(15)	0.0629(88)					
C(16)	0.079(12)					
C(17)	0.094(12)					
C(18)	0.0665(90)					
C(19)	0.111(14)					
C(20)	0.084(10)					
C(21)	0.090(11)					
C(22)	0.108(14)					
C(23)	0.102(13)					
C(24)	0.0613(91)					
C(25)	0.114(14)					
C(26)	0.112(13)					
C(61)	0.168(20)					
C(62)	0.132(17)					
C(63)	0.182(23)					
C(64)	0.149(19)					
C(65)	0.147(17)					
C(66)	0.133(15)					

Table 4. Observed Bond Lengths of $3 \cdot 2SbF_6^-$

	Bond Length(Å)		Bond Length(Å)
SB - F1	2.078(56)	C8 - C24	1.457(38)
SB - F2	1.972(43)	C9 - C10	1.585(38)
SB - F3	1.884(37)	C9 - C13	1.709(40)
SB - F4	1.759(41)	C10 - C11	1.678(39)
SB - F5	2.030(55)	C11 - C12	1.497(37)
SB - F6	1.819(71)	C12 - C14	1.600(39)
SB - F7	1.925(47)	C13 - C14	1.563(44)
SB - F8	1.669(46)	C15 - C16	1.669(35)
SB - F9	2.031(47)	C15 - C20	1.480(34)
SB - F10	2.051(92)	C16 - C17	1.546(41)
SB - F11	1.916(37)	C17 - C18	1.389(37)
SB - F12	1.956(42)	C18 - C19	1.463(47)
C1 - C1	1.066(39)	C19 - C20	1.331(49)
C1 - C2	1.484(34)	C21 - C22	1.481(46)
C2 - C3	1.390(32)	C21 - C26	1.437(48)
C2 - C8	1.436(37)	C22 - C23	1.596(45)
C3 - C4	1.445(26)	C23 - C24	1.435(41)
C3 - C9	1.465(31)	C24 - C25	1.551(50)
C4 - C5	1.393(35)	C25 - C26	1.403(44)
C4 - C12	1.527(48)	C61 - C62	1.413(57)
C5 - C6	1.408(35)	C61 - C66	1.476(63)
C5 - C15	1.611(37)	C62 - C63	1.524(70)
C6 - C7	1.438(37)	C63 - C64	1.396(68)
C6 - C18	1.533(37)	C64 - C65	1.340(59)
C7 - C8	1.386(33)	C65 - C66	1.470(60)
C7 - C21	1.479(43)		

Table 5. Observed Bond Angles of $3 \cdot 2SbF_6^-$

	Bond Angles(deg)		Bond Angles(deg)
F1 - SB - F2	38.3(16)	F9 - SB - F12	46.7(16)
F1 - SB - F3	89.8(19)	F10 - SB - F11	144.9(39)
F1 - SB - F4	86.2(22)	F10 - SB - F12	165.3(28)
F1 - SB - F5	116.5(22)	F11 - SB - F12	48.4(30)
F1 - SB - F6	86.9(29)	C1 - C1 - C2	175.5(25)
F1 - SB - F7	94.3(21)	C1 - C2 - C3	112.8(27)
F1 - SB - F8	92.2(23)	C1 - C2 - C8	119.9(26)
F1 - SB - F9	106.5(19)	C3 - C2 - C8	126.9(28)
F1 - SB - F10	47.0(24)	C2 - C3 - C4	127.3(26)
F1 - SB - F11	165.8(23)	C2 - C3 - C9	118.0(22)
F1 - SB - F12	121.2(20)	C4 - C3 - C9	114.5(25)
F2 - SB - F3	87.4(17)	C3 - C4 - C5	127.6(31)
F2 - SB - F4	93.2(18)	C3 - C4 - C12	113.8(26)
F2 - SB - F5	153.4(22)	C5 - C4 - C12	117.9(23)
F2 - SB - F6	125.1(28)	C4 - C5 - C6	126.3(29)

(Table 5. Continued)

	Bond Angles(deg)		Bond Angles(deg)
F2 - SB - F7	98.2(19)	C4 - C5 - C15	118.2(28)
F2 - SB - F8	54.5(19)	C6 - C5 - C15	115.4(23)
F2 - SB - F9	89.5(19)	C5 - C6 - C7	127.7(25)
F2 - SB - F10	85.1(29)	C5 - C6 - C18	112.2(25)
F2 - SB - F11	128.3(26)	C7 - C6 - C18	119.2(26)
F2 - SB - F12	84.4(19)	C6 - C7 - C8	126.4(27)
F3 - SB - F4	172.7(23)	C6 - C7 - C21	121.2(26)
F3 - SB - F5	103.6(23)	C8 - C7 - C21	112.1(29)
F3 - SB - F6	98.7(28)	C2 - C8 - C7	128.8(29)
F3 - SB - F7	12.6(18)	C2 - C8 - C24	116.6(25)
F3 - SB - F8	76.9(18)	C7 - C8 - C24	114.3(28)
F3 - SB - F9	149.0(19)	C3 - C9 - C10	109.6(20)
F3 - SB - F10	87.5(26)	C3 - C9 - C13	105.4(20)
F3 - SB - F11	84.2(21)	C10 - C9 - C13	104.3(22)
F3 - SB - F12	102.3(18)	C9 - C10 - C11	110.3(21)
F4 - SB - F5	72.9(23)	C10 - C11 - C12	107.2(23)
F4 - SB - F6	75.0(26)	C4 - C12 - C11	111.7(20)
F4 - SB - F7	162.2(22)	C4 - C12 - C14	106.6(24)
F4 - SB - F8	109.3(25)	C11 - C12 - C14	110.6(26)
F4 - SB - F9	38.3(20)	C9 - C13 - C14	110.6(22)
F4 - SB - F10	85.4(29)	C12 - C14 - C13	108.3(26)
F4 - SB - F11	101.0(23)	C5 - C15 - C16	100.5(24)
F4 - SB - F12	85.0(21)	C5 - C15 - C20	102.5(23)
F5 - SB - F6	30.2(26)	C16 - C15 - C20	101.7(23)
F5 - SB - F7	91.1(24)	C15 - C16 - C17	107.3(22)
F5 - SB - F8	151.2(25)	C16 - C17 - C18	116.4(29)
F5 - SB - F9	92.7(17)	C6 - C18 - C17	110.9(26)
F5 - SB - F10	71.6(29)	C6 - C18 - C19	107.7(28)
F5 - SB - F11	77.4(25)	C17 - C18 - C19	100.5(27)
F5 - SB - F12	115.8(21)	C18 - C19 - C20	116.0(33)
F6 - SB - F7	87.2(29)	C15 - C20 - C19	118.3(33)
F6 - SB - F8	175.5(30)	C7 - C21 - C22	111.3(38)
F6 - SB - F9	108.2(26)	C7 - C21 - C26	109.6(28)
F6 - SB - F10	41.3(28)	C22 - C21 - C26	102.7(34)
F6 - SB - F11	106.6(34)	C21 - C22 - C23	105.2(30)
F6 - SB - F12	144.4(27)	C22 - C23 - C24	111.8(34)
F7 - SB - F8	88.5(22)	C8 - C24 - C23	105.3(25)
F7 - SB - F9	154.5(21)	C8 - C24 - C25	107.8(27)
F7 - SB - F10	82.1(27)	C23 - C24 - C25	104.7(32)
F7 - SB - F11	82.6(27)	C24 - C25 - C26	110.9(34)
F7 - SB - F12	109.7(20)	C21 - C26 - C25	113.9(41)
F8 - SB - F9	76.3(23)	C62 - C61 - C66	130.2(53)
F8 - SB - F10	136.7(32)	C61 - C62 - C63	110.8(46)
F8 - SB - F11	73.9(28)	C62 - C63 - C64	115.2(54)
F8 - SB - F12	38.9(17)	C63 - C64 - C65	135.0(63)
F9 - SB - F10	123.0(25)	C64 - C65 - C66	112.8(52)
F9 - SB - F11	73.7(27)	C61 - C66 - C65	115.0(45)

The pK_{R+} Determination. For the preparation of a sample solution, each 0.5 mL portion of the stock solution, prepared by dissolving 2 mg of **3**·2SbF_6^- in acetonitrile (5 mL), was pipetted out and made up to 20 mL by adding H_2O (0.5 mL) and acetonitrile–H_2O (1:1). The sample solution with higher basicity or acidity were made by addition of 1 to 3 drops of either 0.01 N, 0.1 N, 1 N, and 2 N NaOH, or 0.1 N, 1 N, and 3 N HCl. The UV–vis spectrum of the sample solution was recorded using a 1-cm quartz cell. Immediately after recording the spectrum, the pH of each sample solution was determined on a Horiba M–8S p*H* meter. The observed absorbance at 500 nm was plotted against pH to give a two-step titration curve, and each midpoint was taken as the pK_{R+} value (Figure 3(c)).

ESR Measurement. (a) Electrolytic Reduction. An originally made electrolytic cell was used (see Figure 9 of Chapter 3, p.53). The cell consisted of a 5-mm o.d. Pyrex glass tube (length, 65 mm) which was connected to a 3-mm o.d. tube (length, 40 mm) at the bottom and a 20-mm o.d. tube (length, 40 mm) at the top. A platinum wire (diameter, 0.5 mm) reaching the bottom, which was shielded with a polyethylene tube except at the bottom part, served as a working electrode, while a coiled gold wire (diameter, 0.5 mm) placed in an upper part served as a counter electrode. A reference electrode ($Ag/AgNO_3$) was also inserted into an upper part together with a capillary polyethylene tube for the purpose of introducing an argon gas.

A solution of **3**·2SbF_6^- (3.7 mg, 0.0032 mmol) in 5 mL of a 0.1 M solution of tetrabutylammonium perchlorate in dichloromethane was placed in this cell. The solution was electrolyzed after bubbling with argon for a few minutes, and then the ESR spectrum was recorded.

(b) Chemical Reduction with Zinc Powder. A 9-mm o.d. Pyrex glass tube having a 5-mm o.d. ESR sample tube (length, 300 mm) as a side arm was used, which was connectable to a vacuum line. In the 9-mm tube was placed

$3 \cdot 2SbF_6^-$ (2.9 mg, 0.0025 mmol) together with a short capillary tube containing zinc powder (3.3 mg, 0.050 mmol), and the tube was evacuated to 10^{-4} mmHg. A solvent (1.0 mL) placed in a flask connected to a vacuum line was degassed and dried by repeating the freeze-pump-thaw cycle for three times over CaH_2, and then transferred to the 9-mm tube by vacuum distillation. After sealing off the 9-mm tube, $3 \cdot 2SbF_6^-$ was dissolved in the solvent and thoroughly mixed with zinc powder, and the ESR spectrum was recorded immediately.

UV–vis Measurements of Cation Radical $3^{\cdot+}$. A vacuum-proof quartz cell (cell path, 1 mm) was used, which was connected to a Pyrex glass tube having side arms.[14] In one side arm was placed $3 \cdot 2SbF_6^-$ (0.584 mg, 5.05×10^{-4} mmol) together with a small capillary tube containing zinc powder (1.0 mg, 0.015 mmol) and the tube was evacuated to 10^{-4} mmHg. The solvent (3.0 mL) was degassed and dried as described above, and transferred into another side arm by vacuum distillation. After sealing off the glass tube, $3 \cdot 2SbF_6^-$ was dissolved and mixed well with zinc, and the UV–vis spectrum was recorded immediately.

References and Notes

(1) (a) Komatsu, K.; Akamatsu, H.; Jinbu, Y.; Okamoto, K. *J. Am. Chem. Soc.* **1988**, *110*, 633. (b) Komatsu, K.; Akamatsu, H.; Aonuma, S.; Jinbu, Y.; Maekawa, N.; Takeuchi, K. *Tetrahedron* **1991**, *47*, 6951.

(2) Jutz, C.; Voithenleitner, F. *Chem. Ber.* **1964**, *97*, 1337.

(3) In comparison, the (propyn-1-yl)tropylium derivative **9** exhibited the longest-wavelength absorption in acetonitrile at λ_{max} 348 nm (log ε 3.99), which is in-between those of **3** and **1**: A. Kagayama and K. Komatsu, unpublished results.

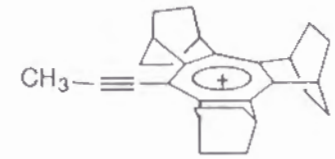

9

(4) Liberles, A.; Matlosz, B. *J. Org. Chem.* **1971**, *36*, 2710.

(5) In this connection it is desirable to have the X-ray crystal structures of the monocations **1** and **2**. However, we have not succeeded in obtaining single crystals of the salts of these cations.

(6) It might be considered that the first neutralization might cause the hydroxide-ion attack at the ethynyl carbon to give a tautomeric mixture of monocations A and B, which might also explain the considerable bathochromic shift. However, the completely neutralized species formed by further neutralization of A and/or B should still maintain a heptafulvene-type partial structure, and should be colored as supposed from the yellow color observed for the corresponding heptafulvene derivative: Aonuma, S.; Komatsu, K.; Maekawa, N.; Takeuchi, K. *Chem. Lett.* **1991**, 767. This is against our present experimental observation.

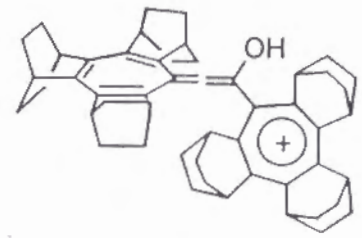

A

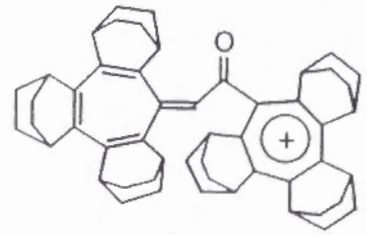

B

On the other hand, one might argue that some isomers of the completely neutralized form 3-$(OH)_2$ in Scheme 2 should also be colored now that the π-conjugated monocation 3-OH is red-colored. We consider

that the coloration in **3**-OH arises from the intramolecular charge-transfer type interaction, that is, the transition from HOMO localized at the ethynylcycloheptatriene moiety to considerably low LUMO localized at the tropylium ring. In contrast, the fully neutralized species **3**-$(OH)_2$ are simply composed of two cycloheptatriene rings connected by an acetylenic bond, and the π-π^* transition band is not necessarily in the visible range.

(7) Even by all the efforts such as application of lower modulation width and/or lowering the concentration, no hyperfine structure was observed probably due to too many small couplings with the interacting protons present in the bicyclic frameworks.

(8) The molar extinction coefficient (ε) was calculated as 3.7×10^4 assuming that the cation radical $\mathbf{3}^{\cdot+}$ was formed quantitatively.

(9) THF was added so as to increase the solubility of the formed species.

(10) (a) Okamoto, K.; Komatsu, K.; Sakaguchi, O. *Bull. Chem. Soc. Jpn.* **1974**, *47*, 2431. (b) The reduction peak potential for *t*-butyltropylium ion was determined as –0.61 V vs $Ag/AgNO_3$ in acetonitrile (Okamoto, K.; Takeuchi, K.; Komatsu, K.; Kubota, Y.; Ohara, R.; Arima, M.; Takahashi, K.; Waki, Y.; Shirai, S. *Tetrahedron* **1983**, *39*, 4011), while that for **3** was found to be –0.49 V in acetonitrile (nearly one-step, two-electron reduction).

(11) Thummel, R. P.; Chayangkoon, P. *J. Org. Chem.* **1983**, *48*, 596.

(12) No satisfactory elemental analysis was obtained because of the instability.

(13) Only the aliphatic CH, CH_2, and CH_3 carbons were recorded. Weaker signals for fully substituted carbons could not be observed due to the decomposition during the measurement.

(14) Okamoto, K.; Kitagawa, T.; Takeuchi, K.; Komatsu, K.; Kinoshita, T.; Aonuma, S.; Nagai, M.; Miyabo, A. *J.Org. Chem.* **1990**, *55*, 996-1002.

Chapter 7

Syntheses, Properties, and Redox Behaviors of 7-Phenyl-1,2:3,4:5,6tris(bicyclo[2.2.2]octeno)-tropylium Ion and the Dications Composed of Two 1,2:3,4:5,6-Tris(bicyclo[2.2.2]octeno)tropylium Units Connected by *para*- and *meta*-Phenylene Spacers

Abstract

The stable carbodications composed of two tris(bicyclo[2.2.2]octeno)-tropylium units connected by a *para*-phenylene (**7**) and a *meta*-phenylene spacer (**8**) were synthesized, together with the corresponding monocation having a 7-phenyl substituent (**6**) as a reference compound, and their properties were fully characterized. The pK_{R+} values of **6**, **7**, and **8** were determined in 50% *aq.* acetonitrile to be 12.0, 11.5, and 10.4, respectively. The 7-phenyl substituent, which is supposedly nearly perpendicular to the tropylium ring, destabilizes the cation by 1 p*K* unit. The two cation units at the *para*-phenylene positions in **7** were neutralized simultaneously, but those in **8** were neutralized stepwise; the pK_{R+} value for the half-neutralized monocation was 12.2. Upon one-electron reduction monocation **6** gave a stable free radical persisting in solution at room temperature. *para*-Phenylene-connected dication **7** did not give any radical species but instead gave a closed-shell hydrocarbon upon one-step, two-electron reduction. In the case of *meta*-phenylene-connected dication **8**, two very closely spaced reduction steps were observed upon cyclic voltammetry, and the resulting fully reduced species was identified as a triplet diradical by low-temperature ESR.

Introduction

Tropylium ion **1**, annelated with three bicyclo[2.2.2]octene units, is highly stabilized by the inductive and σ-π conjugative effects of the rigid bicyclic σ-frameworks.[1] As the substituent at the 7-position, both simple alkyl and unsaturated groups were shown to destabilize cation **1**.[2] However, it is of interest to construct a carbodication by connecting two molecules of **1** at the 7-position with a π-conjugative spacer and examine how the thermodynamic stability would be changed and how the whole π-system would behave upon consecutive one-electron reduction processes.

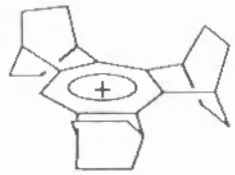

1

Dications **2**,[3] **3**,[4] and **4** [5] are typical examples of carbodications having Hückel aromatic systems connected by a phenylene spacer. However, except for the pK_{R+} data measured for **4**, there have been no specific data regarding either the redox or thermodynamic properties of these dications.

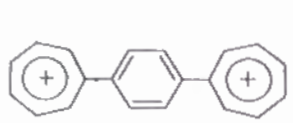

2

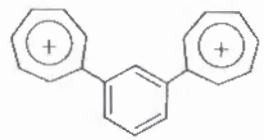

3

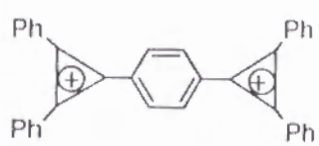

4

In the previous chapter, dication **5** was synthesized, which has a triple bond as a spacer, and its behavior upon one-electron reduction was examined.[6]

Radical cation $\mathbf{5}^{\cdot+}$ was smoothly produced and appeared stable in solution, but the product of further reduction, which was considered to be a closed-shell species (a cummulene), was highly unstable and could not be identified spectroscopically. In the present chapter are described the synthesis and properties, particularly the redox behavior, of dications having *para*- (**7**) and *meta*-phenylene spacers (**8**), as well as the corresponding phenyl-substituted monocation **6** as 'a reference compound.

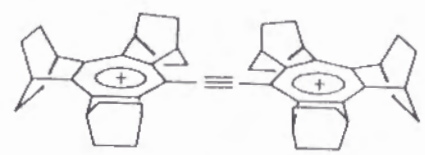

5

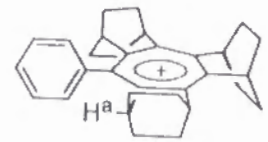

6

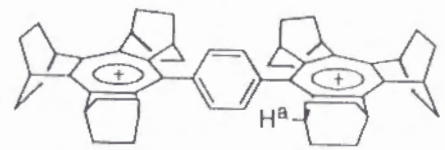

7

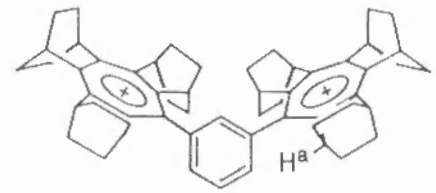

8

Results and Discussion

Synthesis. Syntheses of cations **6**, **7**, and **8** were carried out as shown in Scheme 1.[7] The reaction of cation **1** with phenyllithium gave cycloheptatriene **9**, and subsequent hydride abstraction with trityl cation smoothly afforded phenylated monocation **6**, though the latter reaction was unusually slow. Similarly, addition of cation **1** to the (cycloheptatrienylphenyl)lithiums generated from **10** and **11** afforded di(cycloheptatrienyl)benzenes **12** and **13**. However, in contrast to the corresponding intermediates in the syntheses of **6** and parent *meta*- and *para*-phenylenebis(tropylium ion) **2** and **3**,[3,4] **12** did not react with trityl cation even at

Scheme 1

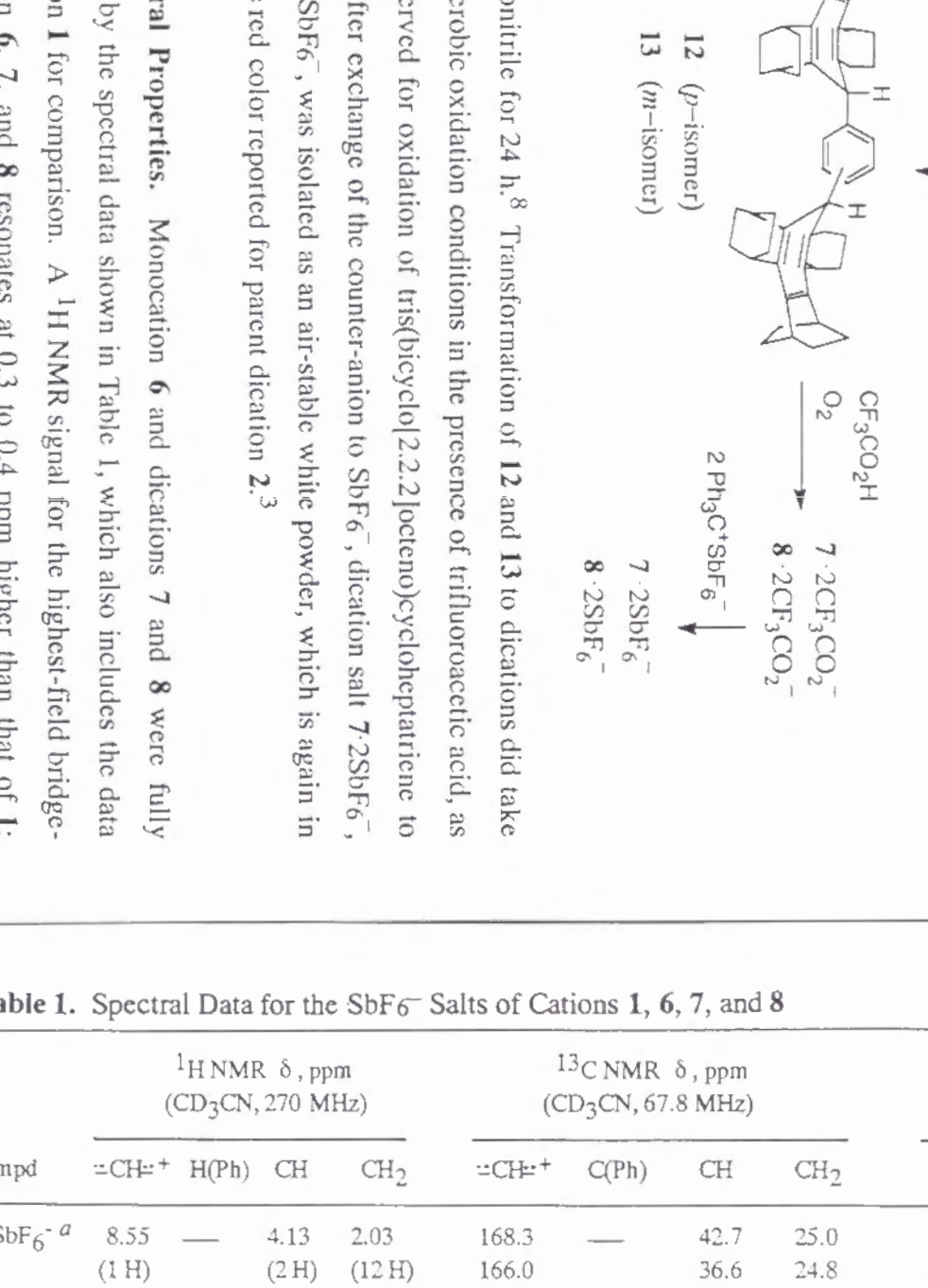

80 °C in acetonitrile for 24 h.[8] Transformation of **12** and **13** to dications did take place under aerobic oxidation conditions in the presence of trifluoroacetic acid, as has been observed for oxidation of tris(bicyclo[2.2.2]octeno)cycloheptatriene to cation **1**.[1b] After exchange of the counter-anion to SbF_6^-, dication salt **7**·$2SbF_6^-$, as well as **8**·$2SbF_6^-$, was isolated as an air-stable white powder, which is again in contrast to the red color reported for parent dication **2**.[3]

Spectral Properties. Monocation **6** and dications **7** and **8** were fully characterized by the spectral data shown in Table 1, which also includes the data for monocation **1** for comparison. A ^{1}H NMR signal for the highest-field bridgehead proton in **6**, **7**, and **8** resonates at 0.3 to 0.4 ppm higher than that of **1**;

Table 1. Spectral Data for the SbF_6^- Salts of Cations **1**, **6**, **7**, and **8**

	^{1}H NMR δ, ppm (CD_3CN, 270 MHz)				^{13}C NMR δ, ppm (CD_3CN, 67.8 MHz)				IR ν, cm^{-1}			UV-vis λ_{max} nm (log ε)
Compd	=CH–$^+$	H(Ph)	CH	CH_2	=CH–$^+$	C(Ph)	CH	CH_2	(KBr)			(CH_3CN)
1 ·SbF_6^- [a]	8.55 (1 H)	—	4.13 (2 H) 4.07 (2 H) 3.56 (2 H)	2.03 (12 H) 1.43 (12 H)	168.3 166.0 163.9 144.2	—	42.7 36.6 36.1	25.0 24.8 24.7	2951 1458 1270 1040 658	2873 1420 1245 1025	1625 1320 1173 814	256 (4.71) 308 (4.01)
6 ·SbF_6^- [b]	—	7.55 (2 H) 7.26 (3 H)	4.09 (2 H) 4.06 (2 H) 3.17 (2 H)	2.09- 1.44 (24 H)	165.98 164.10 163.32 155.43	140.94 129.41 128.63 126.39	38.72 36.15 35.95	24.20 24.07 23.90	3010 1474 1298 819	2946 1456 1137 706	2870 1328 1031 656	260 (4.67) 314 (3.92)
7 ·$2SbF_6^-$	—	7.46 (4 H)	4.14 (4 H) 4.11 (4 H) 3.24 (4 H)	2.10 (24 H) 1.49 (24 H)	166.20 165.31 164.67 155.10	142.12 128.63	39.73 36.95 36.64	24.80 24.60 24.60	3010 1475 1326 1031	2946 1460 1298 817	2870 1339 1136 656	261 (4.98) 314 (4.23)
8 ·$2SbF_6^-$	—	7.82 (1 H) 7.48 (2 H) 7.18 (1 H)	4.10 (4 H) 4.07 (4 H) 3.25 (4 H)	1.93 (24 H) 1.40 (24 H)	166.02 165.34 164.76 154.62	143.00 131.44 127.82 125.52	39.80 36.96 36.64	24.75 24.59 24.46	3010 1617 1365 1172 815	2947 1457 1327 1139 657	2871 1455 1276 1029	260 (4.96) 316 (4.24)

[a] Data from Ref.1. [b] NMR spectra were measured in $CDCl_3$.

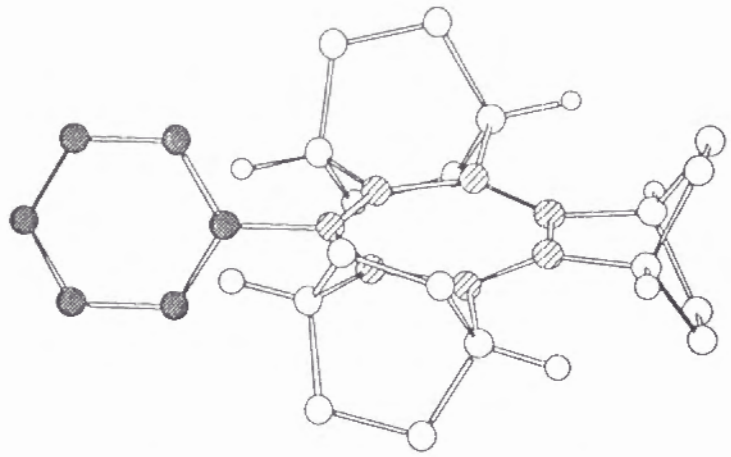

Figure 1. AM1 calculated structure of cation **6**. The methylene and phenyl hydrogens are omitted for clarity. The dihedral angle between the phenyl and tropylium rings is 83.0°.

the shift implies that this signal corresponds to the proton (H^a) that sticks out in front of the phenyl ring in the shielding zone. Thus, the benzene ring at the 7-position of these cations is believed to be nearly perpendicular to the plane of the tropylium ring. The results of semiempirical MO calculations with AM1 for cation **6** indicate that the two aromatic rings are twisted by 83.0°, as shown in Figure 1. Apparently, there is no π-conjugation between the phenyl and tropylium rings. The absence of conjugation is reflected in the UV absorptions of **6**, **7**, and **8**, which exhibit only slight bathochromic shift compared with **1**. There is no further bathochromic shift for dications **7** and **8** as compared with **6**; the extinction coefficients of the dications are twice as large as those of monocation **6**.

Thermodynamic Stability. As a measure of the thermodynamic stability, the pK_R+ values of the cations were determined spectrophotometrically in 50% aqueous acetonitrile. As expected because of the inductive effect of the phenyl substituent, monocation **6** (pK_R+ 12.0 ± 0.2)[9] is less stabilized than **1**[1] by 1.0 pK unit. In the case of dication **7**, which has a *para*-phenylene spacer, the two cation

units behave independently of each other and are neutralized almost simultaneously (eq. 1) at pH 11.5 (± 0.2)[9], which is taken as the pK_R+ value. That this value is 0.5 pK unit lower than the value for **6** reflects destabilization due to the through-bond electrostatic repulsion of the two positively charged units. In comparison, two cationic units in dication **8** located at *meta*-phenylene positions were neutralized in two-steps (eq. 2) at pH 10.4 (± 0.3)[9] and 12.2 (± 0.2),[9] values which correspond to the pK_R+ of the dication and the half-neutralized monocation, respectively. Thus, dication **8** itself is even more destabilized than *para*-phenylene-connected dication **7** by 1.1 pK unit, whereas the half-neutralized monocation of **8** is almost as stable as monocation **6**.

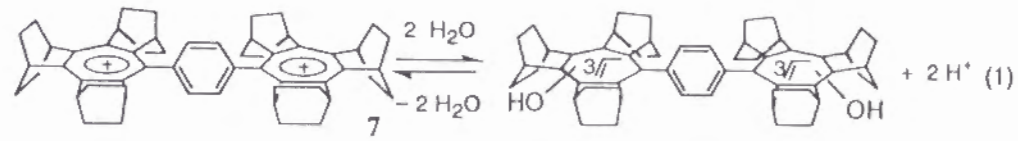

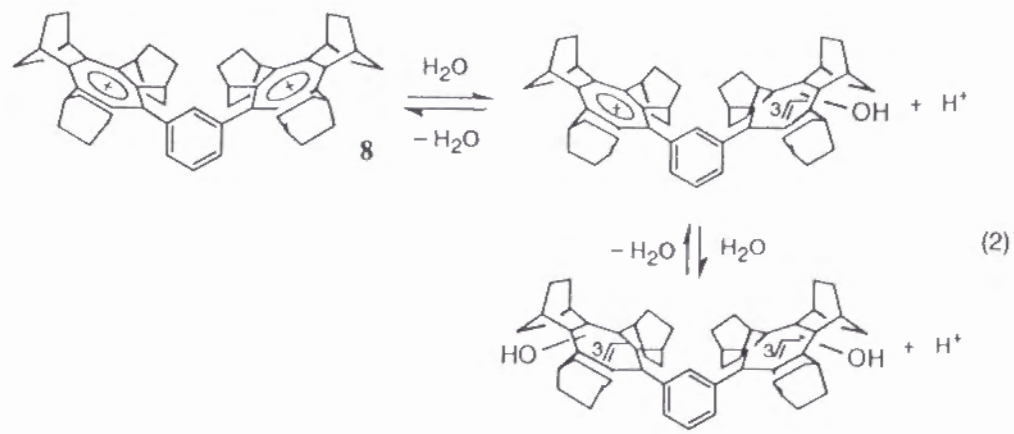

Red-Ox Behavior. Reflecting its extraordinarily high stability, monocation **1**, as well as its 7-methyl derivative, hardly undergoes one-electron reduction; its cathodic peak potential (E_{pc}) in acetonitrile is −1.12 V vs Ag/Ag^+ (−1.09 V for the 7-methyl derivative)[1a] upon cyclic voltammetry (CV), as compared with −0.51 V for the parent tropylium ion.[1b] The reduction was irreversible for these cations under the conditions of CV measurement at a scan rate of 0.1 V s^{-1}. In contrast, 7-phenyl derivative **6** in acetonitrile exhibited a well-defined reversible redox wave at $E_{1/2}$ −1.12 V (E_{pc} −1.15 V), as shown in Figure 2(a). This clearly indicates the generation of a free radical, which is stabilized by severe steric hindrance for dimerization and also by the lack of any hydrogen atom that could be abstracted from the radical; abstraction of a bridgehead hydrogen of the bicyclic framework, that is at the α-position of the alkyl group, is prevented by Bredt's rule. In accordance, a strong single-line ESR signal[10] with a peak-to-peak width of 0.3 mT (g = 2.0023) was observed upon electrolytic reduction of cation **6** at −1.5 V in CH_2Cl_2 and was found to persist at least for 0.5 h at room temperature after the cathodic current was cut off.

It is of particular interest to examine the behavior of dications **7** and **8** upon one- and two-electron reductions and to clarify the fate of fully reduced species. The CV of **7** in acetonitrile exhibited the voltammogram shown in Figure 2(b). A single cyclic scan exhibited a characteristic feature with an anodic peak positively shifted by about 0.5 V from the cathodic peak. The cathodic peak (E_{pc} −1.01 V) is in the potential range comparable to those of related cations **1** and **6** and apparently corresponds to a one-step, two-electron reduction. Therefore the anomalous voltammogram must have arisen from the anodic shift due to the extra energy required upon oxidation of the completely reduced species back to dication **7**. One possible cause for this extra energy requirement could be some structural change from the reduced form to the dication. Since no ESR signal was observed even upon extensive electrolytic reduction, the reduced species from **7** can not

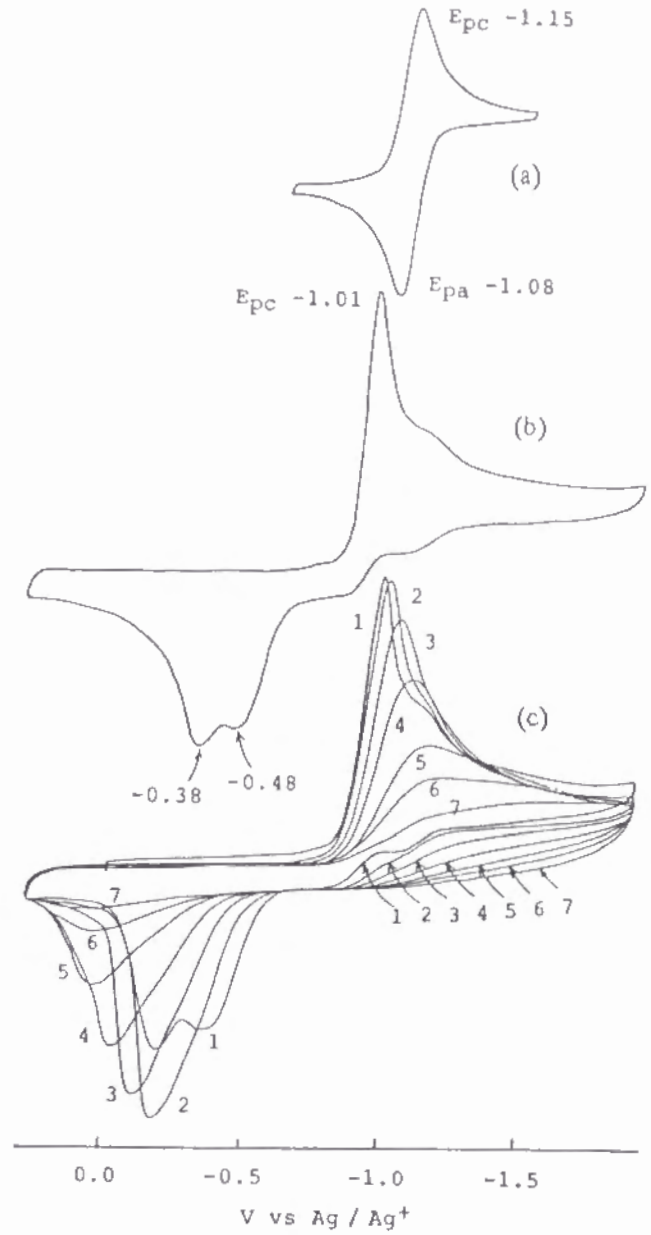

Figure 2. Cyclic voltammograms of (a) monocation **6** (0.5 mM), (b) dication **7** (0.5 mM) (the first cyclic scan), (c) dication **7** (the first to seventh scans; the number of scan is shown in the figure). All voltammograms were obtained in acetonitrile containing $Bu_4N^+ClO_4^-$ (0.1 M) as a supporting electrolyte; scan rate, 0.1 V s^{-1}.

have any unpaired spin. It is assumed that the two free radicals generated at the *para*-positions prefer to form closed-shell covalent molecule **16**, which would readily relax into boat form **17** (Scheme 2). Because of the rigid bicyclic frameworks surrounding the seven-membered ring, the boat form is much more stable than the planar structure, which involves severe steric repulsion between the bridgehead- and *ortho*-hydrogens.[11] Thus, considerable energy is required to transform boat structure **17** back to planar radical cation **14**, and this energy could be the origin of the unusual positive shift of the anodic peak in the voltammogram. A similar potential shift associated with change in molecular geometry has typically been observed upon reduction of azacyclooctatetraene derivatives and cyclooctatetraene.[12]

Scheme 2

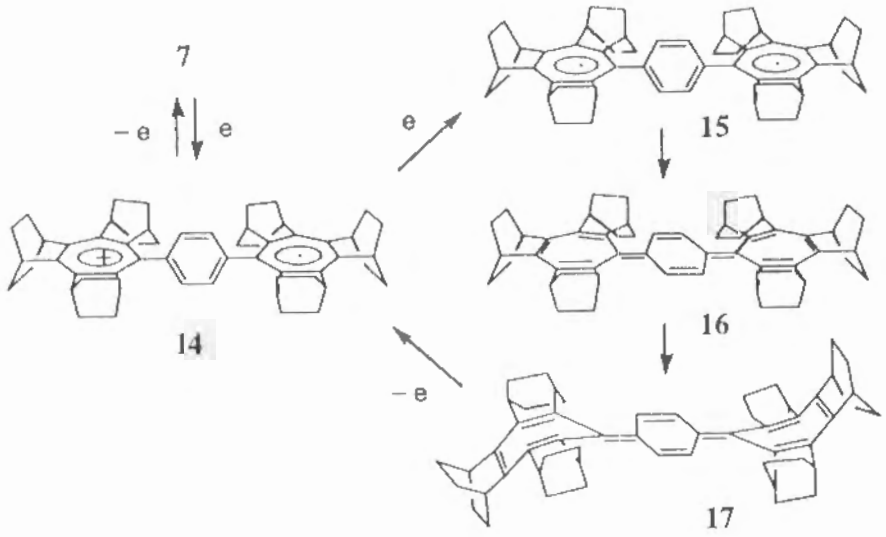

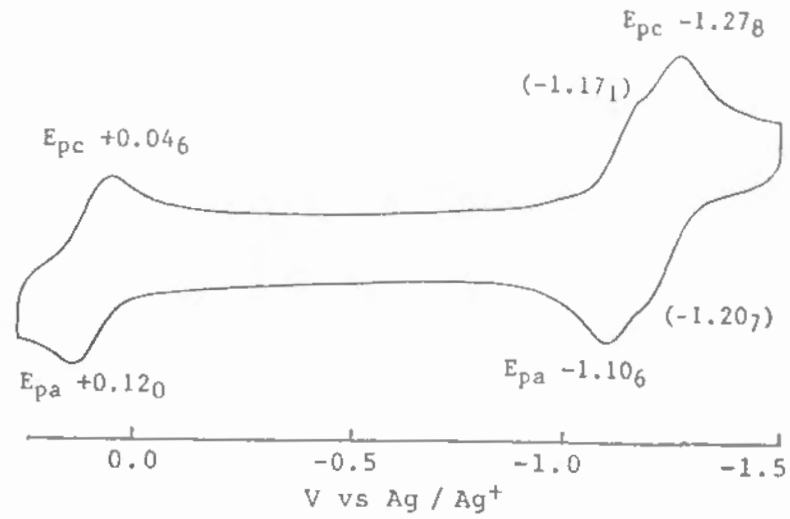

Figure 3. Cyclic voltammogram of dication **8** (0.5 mM) in dichloromethane containing $Bu_4N^+ClO_4^-$ (0.1 M) as a supporting electrolyte, with ferrocene (0.5 mM) added as an internal standard ($E_{1/2}$, +0.083 V vs Ag/Ag^+); scan rate, 0.1 V s^{-1}.

On each repeated cycle, the voltammogram of **7** exhibited a gradual decrease in peak currents, as shown in Figure 2(c). After electrolysis at a constant potential of −1.5 V, the working electrode was found to be coated with a film of red-brown solid, which was barely soluble in common organic solvents. This material is believed to have been formed by polymerization or decomposition of presumably unstable hydrocarbon **17**, although the spectroscopic examination of its structure was hampered by its insolubility.

In contrast to dication **7**, *meta*-phenylene-connected dication **8** is expected to give a non-Kékule type electronic structure upon two-electron reduction. Dication **8** in dichloromethane exhibited the voltammogram shown in Figure 3. The voltammogram is characterized by barely separated two-step reduction waves at $E_{1/2}$ −1.14 and −1.24 V vs Ag/Ag^+, which are completely reversible. Thus, electron transfer to **8** is believed to occur without much structural change to yield

the corresponding radical cation and diradical consecutively, in contrast to the case of **7**. The ESR spectrum measured upon electrolytic reduction of **8** in acetonitrile–THF (1:4) at a potential of −1.5 V showed a single-line signal (g = 2.0026), which was analogous to that of the 7-phenylated monoradical obtained from **6**. When the solution was solidified at −120 °C, there was observed an ESR signal with a fine structure typical for a triplet diradical with zero-field splitting parameters D = 0.0054 cm^{-1} and E < 0.0001 cm^{-1}, as shown in Figure 4.[13] Thus, two-electron reduction of dication **8** generates diradical **18**, which can not be transformed into a closed-shell structure.

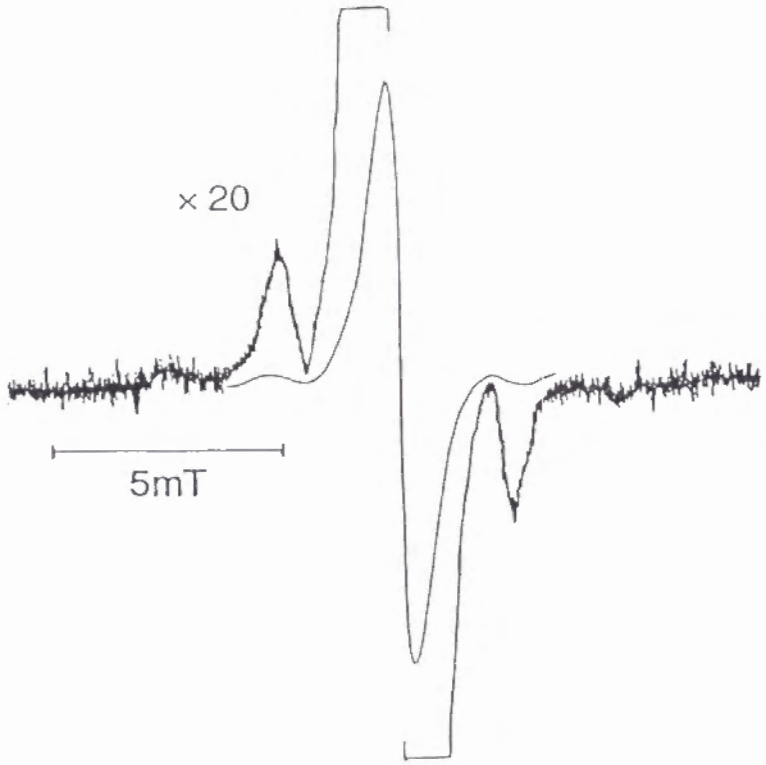

Figure 4. ESR spectrum of diradical $\mathbf{8}^{2\cdot}$ measured at −120 °C in frozen THF–acetonitrile (1:4).

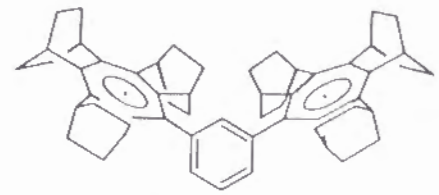

18

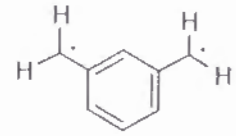

19

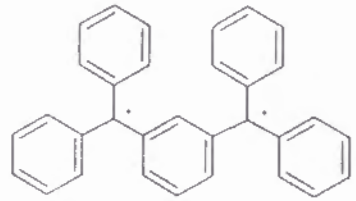

20

By comparison of reported D values for *m*-xylylene (**19**, D=0.011 cm^{-1})[14] and Schlenk's hydrocarbon (**20**, 0.008 cm^{-1}),[15] the distance between two radical centers in **18** is estimated as 8 Å, compared to 6 Å for **19** and 7 Å for **20**. This value seems to be in good agreement with structure **18**, in which each of the two spins is completely delocalized in each one of the seven-membered rings.

Experimental Section

General Procedures. Melting points were determined on a Yamato MP–21 apparatus and are uncorrected. Elemental analysis was performed by Micro-analytical Center, Kyoto University, Kyoto. NMR spectra were recorded on JEOL GSX270 (270 MHz for ^{1}H and 67.8 MHz for ^{13}C NMR) or on JEOL FX90 (90 MHz for ^{1}H) spectrometers using Me_4Si as an internal standard. IR spectra were taken on Perkin Elmer 1640 spectrometer. UV-vis spectra were taken on Hitachi 200–10 spectrometer. ESR spectra were recorded on JEOL PE–2X or on JES–SRE2X spectrometer. Mass spectrum was taken on JEOL JMS–SG

spectrometer. Cyclic voltammograms were obtained by the use of a Hokuto–Denko HA104 potentiostat, a HB107A function generator, a Hitachi 057 X–Y recorder, and a three-electrode cell composed of platinum wire working and counter electrodes and a Ag/0.01 M $AgNO_3$ (acetonitrile) reference electrode. The observed potential was corrected with reference to ferrocene ($E_{1/2}$ +0.083 V) added as an internal standard after each measurement. A Sartorius 4503MP6 microbalance was employed for weighing samples less than 1 mg.

THF was freshly distilled from sodium benzophenone ketyl before use. dichloromethane and acetonitrile were refluxed and distilled over P_2O_5 under nitrogen. All reactions where anhydrous conditions were required were conducted under an atmosphere of argon or nitrogen. Medium-pressure liquid chromatography (MPLC) was carried out using silica gel 60 (E. Merk, particle size 0.040–0.063 mm, 230–400 mesh ASTM) as a stationary phase and hexane as an eluent. Commercial tetrabutylammonium perchlorate was recrystallized from hexane and ethyl acetate. 1,2:3,4:5,6-tris(bicyclo[2.2.2]octeno)tropylium hexafluoroantimonate (**1**·SbF_6^-)[1b] and trityl hexafluoroantimonate ($Ph_3C^+SbF_6^-$)[16] were prepared following the literature procedure.

7-Phenyl-1,2:3,4:5,6-tris(bicyclo[2.2.2]octeno)tropylium Hexafluoroantimonate (6·SbF_6^-). A solution of 2.0 M PhLi in hexane (0.15 mL, 0.30 mmol) was added dropwise to a stirred suspension of salt **1**·SbF_6^- (56.4 mg, 0.0994 mmol) in THF (1 mL) at −78 °C. The mixture was stirred for 10 min at −78 °C and slowly warmed to room temperature over 15 min. After being treated with water, the mixture was extracted with diethyl ether. The extract was washed with aqueous sodium chloride, dried, and evaporated to dryness. Separation by medium pressure liquid chromatography (MPLC) over silica gel 60 (Merck Co.) with hexane as the eluent yielded 7-phenyl-1,2:3,4:5,6-tris(bicyclo[2.2.2]-octeno)cycloheptatriene (**9**) (31.3 mg, 77.1%) as a white powder: mp 94-118 °C

(gradual decomposition); ^{1}H NMR ($CDCl_3$, 90 MHz;) δ 7.00 (br s, 5H, Ph), 4.32 (s, ^{1}H, cycloheptatrienyl-H), 2.88 (br s, 2H, bridgehead CH), 2.67 (br s, 4H, bridgehead CH), 1.73–0.30 (m, 24H, CH_2); ^{13}C NMR ($CDCl_3$, 22.5 MHz) δ 143.74 (s), 138.64 (s), 135.08 (s), 133.69 (s), 126.94 (d), 126.52 (d), 124.96 (d), 54.75 (d), 38.42 (d), 31.59 (d), 31.45 (d), 28.21 (t), 26.48 (t), 26.16 (t), 25.91 (t), 25.67 (t; two signals overlapped); UV (cyclohexane) λ_{max} 275 nm (log ε 3.82); MS *m/z* 408 (M^+).

A solution of trityl hexafluoroantimonate (125 mg, 0.261 mmol) in acetonitrile (1.8 mL) was added dropwise to a stirred solution of cycloheptatriene **9** (106 mg, 0.260 mmol) in dichloromethane (1.5 mL). The resulting yellow-orange solution was heated at 50 °C for 20 h. The color became pale yellow. The solution was evaporated to dryness, and the residual solid was reprecipitated from dichloromethane (0.5 mL) / diethyl ether (16 mL) to give salt **6**·SbF_6^- as a white powder (98.3 mg, 58.8%); mp >300 °C.

Anal. Calcd for $C_{31}H_{35}F_6Sb$: C, 57.87; H, 5.48. Found: C, 57.93; H, 5.44. For the spectral data, see Table 1.

***p*-Phenylenebis{tris(bicyclo[2.2.2]octeno)tropylium} Hexafluoroantimonate (7·2SbF_6^-).** A solution of *p*-bromophenyllithium was prepared by addition of 1.5 M butyllithium in hexane (1.0 mL, 1.5 mmol) to a stirred solution of *p*-dibromobenzene (328 mg, 1.39 mmol) in THF (1 mL) at −78 °C. To a stirred suspension of **1**·SbF_6^- (96.5 mg, 0.231 mmol) in THF (1 mL) at −78 °C was added a solution of 1.0 mL of *p*-bromophenyllithium (0.8 mmol), and the mixture stirred for 7 min at −78 °C. After being warmed to room temperature, the mixture was worked up and separated by MPLC in the manner described above for the preparation of cycloheptatriene **9** to give 7-(*p*-bromophenyl)-1,2:3,4:5,6-tris-(bicyclo[2.2.2]octeno)cycloheptatriene (**10**) (101 mg, 89.5%) as a white powder; mp 128–135 °C (gradual decomposition); ^{1}H NMR ($CDCl_3$, 270 MHz) δ 7.10 (d,

2H, Ar-H), 6.82 (d, 2H, Ar-H), 4.23 (s, 1H, cycloheptatrienyl-H), 2.88 (br s, 2H, bridgehead CH), 2.70 (br s, 2H, bridgehead CH), 2.60 (br s, 2H, bridgehead CH), 1.71–0.38 (m, 24H, CH_2); ^{13}C NMR ($CDCl_3$, 67.8 MHz) δ 142.80, 138.83, 134.65, 133.99, 130.17, 129.50, 128.23, 54.21, 38.33, 31.56, 31.46, 28.13, 26.42, 26.07, 25.97, 25.73, 25.63.

Anal. Calcd for $C_{31}H_{35}Br$: C, 76.37; H, 7.24. Found: C, 76.10; H, 7.47.

To a stirred solution of *p*-(bromophenyl)cycloheptatriene **10** (103 mg, 0.211 mmol) in THF (1.5 mL) at –78 °C was added 1.53 M butyllithium in hexane (0.15 mL, 0.23 mmol). To this solution was added a suspension of **1**·SbF_6^- (179 mg, 0.315 mmol) in THF (1.5 mL), and the mixture was stirred at –78 °C for 15 min. After being warmed to room temperature, the mixture was worked up as described above to give a crude product and unchanged **1**·SbF_6^-. Thorough washing of this mixture with acetonitrile (4 mL) in an ultrasonic bath afforded *p*-bis{2,3:4,5:6,7-tris-(bicyclo[2.2.2]octeno)cycloheptatrien-1-yl}benzene (**12**) (100 mg, 64.3%) as a barely soluble white powder; mp 275-280 °C; ^1H NMR ($CDCl_3$, 270 MHz) δ 6.63 (s, 4H, Ar-H), 4.20 (s, 2H, cycloheptatrienyl-H), 2.81 (br s, 4H, bridgehead CH), 2.67 (br s, 4H, bridgehead CH), 2.54 (br s, 4H, bridgehead CH), 1.59 – 0.56 (m, 48H, CH_2); ^{13}C NMR ($CDCl_3$, 67.8 MHz) δ 138.99, 138.34, 135.18, 133.78, 125.37, 54.50, 38.80, 31.63, 31.56, 27.87, 26.57, 26.21, 25.93, 25.75, 25.44.

To a solution of *p*-dicycloheptatrienylbenzene **12** (52.0 mg, 0.0703 mmol) in dichloromethane (4 mL) was added trifluoroacetic acid (0.30 g, 2.6 mmol), and oxygen gas was bubbled in for a few seconds. The solution was stirred in a stoppered flask at room temperature for 3 days, after which period a pale brown suspension resulted. The mixture was evaporated to dryness, re-dissolved in dichloromethane (2 mL), and stirred magnetically. To this solution was added a 0.11 M solution of trityl hexafluoroantimonate in dichloromethane, drop by drop, until the yellow-orange color of trityl cation began to remain in the solution, for

which total of 0.93 mL (0.10 mmol of the trityl cation) was required. After additional stirring for 10 min, the solvent was evaporated, and the residual yellowish solid was thoroughly washed, under sonification, successively with diethyl ether (5 mL) and with diethyl ether-dichloromethane (3 mL + 2 mL) to give salt **7**·$2SbF_6^-$ (61.8 mg, 72.5%) as an off-white powder; mp >300 °C.

Anal. Calcd for $C_{56}H_{64}F_{12}Sb_2$: C, 55.65; H, 5.34. Found: C, 55.60; H, 5.33. For the spectral data, see Table 1.

***m*-Phenylenebis{tris(bicyclo[2.2.2]octeno)tropylium} Hexafluoroantimonate (8·$2SbF_6^-$).** In the manner described for the preparation of the *para*-substituted compound, the reaction of **1**·SbF_6^- (262 mg, 0.462 mmol) and *m*-bromophenyllithium (1.82 mmol) afforded 7-(*m*-bromo-phenyl)-1,2:3,4:5,6-tris(bicyclo[2.2.2]octeno)cycloheptatriene (**11**) (153 mg, 68.0%) as a white powder; mp 137–143 °C; ^1H NMR ($CDCl_3$, 270 MHz) δ 7.11–6.86 (m, 4H, Ar-H), 4.28 (s, 1H, cycloheptatrienyl-H), 2.89 (br s, 2H, bridgehead CH), 2.71 (br s, 2H, bridgehead CH), 2.62 (br s, 2H, bridgehead CH), 1.72–0.38 (m, 24H, CH_2); ^{13}C NMR ($CDCl_3$, 67.8 MHz) δ 146.54, 138.90, 134.56, 134.13, 130.04, 128.14, 127.93, 125.68, 120.84, 54.34, 38.27, 31.54, 31.42, 28.17, 26.39, 26.12, 25.92, 25.64, 25.57.

Anal. Calcd for $C_{31}H_{35}Br$: C, 76.37; H, 7.24. Found: C, 76.14; H, 7.37.

By a method similar to the one described above, *m*-(bromophenyl)cycloheptatriene **11** (113 mg, 0.232 mmol) was transformed into *m*-bis{2,3:4,5:6,7-tris(bicyclo[2.2.2]octeno)cycloheptatrien-1-yl}benzene (**13**) (119 mg, 69.0%) as a barely soluble white powder; mp 247–249 °C; ^1H NMR ($CDCl_3$, 270 MHz) δ 6.79 (s, 1H, Ar-H), 6.61–6.54 (m, 3H, Ar-H), 4.15 (s, 2H, cycloheptatrienyl-H), 2.82 (br s, 4H, bridgehead CH), 2.68 (br s, 4H, bridgehead CH), 2.54 (br s, 4H, bridgehead CH), 1.62–0.51 (m, 48H, CH_2); ^{13}C NMR ($CDCl_3$, 67.8 MHz) δ

141.31, 138.36, 134.78, 133.49, 126.41, 124.78, 123.83, 55.14, 38.58, 31.71, 31.57, 27.72, 26.57, 26.50, 26.05, 25.73, 25.67.

Anal. Calcd for $C_{56}H_{66}$: C, 91.00; H, 9.00. Found: C, 88.81; H, 8.92.[17]

In the manner described above, a solution of *m*-dicycloheptatrienylbenzene **13** (107 mg, 0.145 mmol) and trifluoroacetic acid in dichloromethane was stirred under oxygen for 3 days and then treated with trityl hexafluoroantimonate (136 mg, 0.283 mmol) to give salt $\mathbf{8}\cdot 2SbF_6^-$ (114 mg, 65.0%) as an off-white powder; mp >300 °C.

Anal. Calcd for $C_{56}H_{64}F_{12}Sb_2$: C, 55.65; H, 5.34. Found: C, 55.49; H, 5.45. For the spectral data, see Table 1.

The pK_{R^+} Determination. A p*H* 10 buffer solution was prepared by mixing 0.2 M glycine in 50% aqueous acetonitrile (25 mL) and 0.2 M NaOH in 50% aqueous acetonitrile (19 mL) and diluting with 50% acetonitrile to 100 mL.[18] For the preparation of a sample solution, each 0.5 mL portion of the stock solution, prepared by dissolving 2 to 3 mg of cation salt in acetonitrile (5 mL or 10 mL), was pipetted out and diluted to 20 mL with H_2O (0.5 mL) and the buffer solution prepared as described above. Sample solutions with higher acidity or basicity were made by addition of 1 to 3 drops of 10% HCl, H_2SO_4, or 10% NaOH. The UV–vis spectra of the sample solutions were recorded using a 1-cm quartz cell. Immediately after the spectrum was recorded, the p*H* of each sample solution was determined on a Horiba M-8S p*H* meter. The observed absorbance at the cation's characteristic absorption was plotted against p*H* to give the titration curve, whose midpoint was taken as the pK_{R^+} value.

ESR Measurement. Electrolytic reduction was carried out as described in Chapter 6,[6] using an originally made electrolytic cell in a 0.1 M solution of tetrabutylammonium perchlorate in dichloromethane.

References and Notes

(1) (a) Komatsu, K.; Akamatsu, H.; Jinbu, Y.; Okamoto, K. *J. Am. Chem. Soc.* **1988**, *110*, 633-634. (b) Komatsu, K.; Akamatsu, H.; Aonuma, S.; Jinbu, Y.; Maekawa, N.; Takeuchi, K. *Tetrahedron* **1991**, *47*, 6951.

(2) The corresponding 7-methyl derivative (Ref. 1) and the 7-(cycloheptatrienylethynyl) derivative (Ref. 6) showed pK_{R^+} values in 50% aqueous acetonitrile of 12.4 and 11.5, respectively, as compared with the value of 13.0 for cation **1**.

(3) Murray, R. W.; Kaplan, M. L. *Tetrahedron Lett*. **1965**, 2903.

(4) Murray, R. W.; Kaplan, M. L. *Tetrahedron Lett*. **1967**, 1307.

(5) Eicher, T.; Berneth, H. *Tetrahedron Lett*. **1973**, 2039.

(6) Kagayama, A.; Komatsu, K.; Nishinaga, T.; Takeuchi, K.; Kabuto, C. *J. Org. Chem*. **1994**, *59*, 4999.

(7) In the literature, parent dications **2** and **3** were prepared by the reaction of tropylium ion with dimetalated benzenes and the subsequent hydride abstraction (Ref. 3, 4). In the present work, we preferred stepwise introduction of the cycloheptatrienyl unit because of the rather limited amount of the tropylium ion **1** available.

(8) This inertness might be ascribed to the presence of bulky bicyclic frameworks on the second cycloheptatriene unit that sterically hinder the approach of the trityl cation.

(9) Rather large errors are due to the low solubility of these cations in 50% aqueous acetonitrile, which causes some fluctuation in absorbance of the UV spectra.

(10) In spite of various attempts such as reducing the modulation width and lowering the concentration, no hyperfine structure was observed, probably

because of the presence of too many hydrogens coupling with the unpaired electron.

(11) The molecular mechanics calculations by MM2(87) indicated that boat structure **17** in Scheme 2 is 96 kcal mol^{-1} more stable than structure **16**, in which the π-conjugated system is enforced to be planar.

(12) Anderson, L. B.; Hanson, J. F.; Kakihana, T.; Paquette, L. A. *J. Am. Chem. Soc.* **1971**, *93*, 161, and the references cited therein. There is also the "square scheme" proposed for describing redox reactions coupled with structural or chemical changes: Richards, T. C.; Geiger, W. E. *J. Am. Chem. Soc.* **1994**, *116*, 2028.

(13) Unfortunately, a search at lower fields for an absorption for the half-field ($\Delta m = 2$) transition was unsuccessful.

(14) Wright, B. B.; Platz, M. S. *J. Am. Chem. Soc.* **1983**, *105*, 628.

(15) Kothe, G.; Denkel, K.-H.; Sümmermann, W. *Angew. Chem., Int. Ed. Engl.* **1970**, *9*, 906.

(16) Thummel, R. P.; Chayangkoon, P. *J. Org. Chem.* **1983**, *48*, 596.

(17) No satisfactory elemental analysis was obtained because of the instability.

(18) Gomori, G. In *Methods in Enzymology*; Colowick, S. P.; Kaplan, N. O., Eds.; Academic Press: New York, 1955; Vol. 1, p 145.

Chapter 8

General Conclusion

In pursuit of novel electronic properties, cyclic π-systems surrounded by rigid σ-frameworks have been synthesized and their structures and properties investigated. It is of great interest to study steric and electronic effects of such rigid σ-frameworks on the π-systems. In the present work are described the cyclic π-systems ranging from five to eight-membered ring fully annelated with bicyclo-[2.2.2]octene (abbreviated as BCO). Their thermodynamic stability, structural properties, and redox behaviors were investigated in detail, and these results were theoretically interpreted by the use of molecular orbital and molecular mechanics calculations. In addition to the previous results of the benzene and tropylium ion fully annelated with BCO, such a structural modification was found to be remark-ably effective in stabilization of both the closed- and open-shell cyclooctatetraene derivatives having positive charge. The presence of σ–π conjugation in the hydrocarbon derived from the BCO pentamer was confirmed from its character-istic structural features. This structural modification with the bicyclic frameworks was also found to be useful in the synthesis and structural determination of a series of metallepins containing Group 14 elements. Novel dications composed of two tropylium ions fully annelated with BCO were newly synthesized and demonstrated interesting red-ox behaviors. The detailed results of the present thesis are summarized below.

In Chapter 2 is described the synthesis of tetrakis(bicyclo[2.2.2]octeno)-cyclooctatetraene (TBCOCOT) by reductive cyclization of the α,ω-dibromide of bicyclo[2.2.2]octene tetramer. The X-ray structural analysis of TBCOCOT showed that the central eight-membered ring has a tub structure. From the

variable-temperature ^{13}C NMR study, TBCOCOT was found to be fixed at this conformation in an NMR time scale even at the temperature up to 150 °C. This result gives the barrier for ring inversion to be larger than 24 kcal mol^{-1} at least. Molecular mechanics calculations indicated that the structure with a planar central ring is 53.9 kcal mol^{-1} less stable than the tub structure. Nevertheless, TBCOCOT was readily reduced by potassium in THF to the planar dianion $TBCOCOT^{2-}$ as shown by ^{1}H and ^{13}C NMR.

In Chapter 3, one- or two-electron oxidation of TBCOCOT was investigated. The results of cyclic voltammetry suggested that cation radical $TBCOCOT^{\cdot+}$ is stable at room temperature while the dication $TBCOCOT^{2+}$ is less stable but could be observed under appropriate conditions. The stable cation radical was generated by electrolytic or chemical oxidation of TBCOCOT in dichloromethane or in acetonitrile, and was observed by ESR. A dark green salt of $TBCOCOT^{\cdot+}$ $SbCl_6^-$ was successfully isolated as a stable single crystal, which allowed the first X-ray structure determination of the COT cation radical. Its structure was in good agreement with the previous theoretical prediction for the cation radical of the parent COT. The MNDO calculation using the X-ray structure was quite successful for interpretation of the electronic spectrum. Further one-electron oxidation of $TBCOCOT^{\cdot+}$ $SbCl_6^-$ by the use of SbF_5 in dichloromethane gave $TBCOCOT^{2+}$ as a single product, which is the first example of a COT dication stable in solution at room temperature. From a low-temperature ^{13}C NMR measurement, $TBCOCOT^{2+}$ was shown to be in a tub structure, which inverts rapidly ($\Delta G^{\ddagger}$(–35 °C) 10.8 ± 0.7 kcal mol^{-1}) despite the loss of aromatic stability in the non-planar structure.

In Chapter 4, intramolecular reductive cyclization was examined for the α,ω-dibromide of the BCO pentamer. The produced hydrocarbon was found to be a bicyclo[2.2.2]octane having two bis(bicyclo[2.2.2]octeno)cyclopentadiene rings spiro-connected at the vicinal carbons. The X-ray structure disclosed remarkable

elongation (1.627(4) Å) of the σ-bond connecting the two cyclopentadiene rings. Theoretical considerations based on both molecular mechanics and molecular orbital calculations on the hydrocarbon and on the related model compounds imply that the major contributing factor for this bond elongation is the σ-π interaction (C-C hyperconjugation) between the σ-bond and the dienyl π-systems in the cyclopentadiene rings. The elongated σ-bond was readily cleaved by potassium metal to give a cyclohexane substituted by two cyclopentadienide anions at the 1,4-positions.

In Chapter 5 are described the synthesis and properties of a series of 1,1-dimethyl-2,3:4,5:6,7-tris(bicyclo[2.2.2]octeno)metallacycloheptatrienes (metallepins) containing silicon, germanium and tin. The X-ray structure determination was conducted for the first time for these compounds, i.e., metallepins containing Group 14 elements, and indicated that the central seven-membered ring is in a boat form for all of these metallepins. As the effective size of the Group 14 metal atom increases, the dihedral angle between the base plane and the stern part of the boat form was found to increase for release of the inner angle strain. Variable-temperature NMR measurements indicated that the metallepin ring is rapidly inverting in solution. The energy barrier for ring inversion increases as the metal–carbon bond is elongated, reflecting the increasing instability of the planar transition-state structure due to the inner-angle strain. This implies that cyclic (p–d)π delocalization would not be operating or negligibly small if present. The UV absorption did not show much difference from that of the C-unsubstituted metallepins in spite of annelation with three BCO units, probably because of the more folded boat structure of the central seven-membered ring and less π-conjugation.

In Chapter 6 is described the bis{tris(bicyclo[2.2.2]octeno)tropyliumyl}-acetylene dication, which is the first example of the acetylene having two tropylium-ion units at both ends. This dication was synthesized by stepwise

introduction of the tris(bicyclo[2.2.2]octeno)cycloheptatrienyl unit to acetylene followed by hydride abstraction. The results of X-ray crystallography indicated that the two tropylium rings are twisted with each other by the angle of 44° and the tropylium ring is slightly bent into a boat form. The dication was neutralized in 50% aqueous acetonitrile via two steps at the p*H* values of 7.0 and 11.5, which correspond to the pK_{R^+} values of the dication and the half-neutralized monocation, respectively. Thus, the dication is 6 pK_{R^+} unit destabilized compared with the corresponding monocation (pK_{R^+} 13.0) due to the intramolecular electrostatic repulsion of the positive charge. The cyclic voltammetry indicated that the dication undergoes two reversible one-electron reductions consecutively in dichloromethane. The electrochemical or chemical reduction of the dication afforded a blue solution of the corresponding cation radical, but not the diradical.

In Chapter 7 are presented the synthesis and properties of the stable carbodications composed of two tris(bicyclo[2.2.2]octeno)tropylium units connected by *para*-phenylene and *meta*-phenylene spacer, together with the corresponding monocation having a 7-phenyl substituent as the reference compound. The pK_{R^+} values of these di- and monocations were determined as 11.5, 10.4, and 12.0 respectively. The 7-phenyl substituent which is supposedly in the conformation nearly perpendicular to the tropylium ring is destabilizing the cation by 1 pK_{R^+} unit. While the two cations at the *para*-phenylene positions were neutralized simultaneously, those at the *meta*- phenylene were neutralized stepwise giving the pK_{R^+} value of 12.2 for the half-neutralized monocation. Upon one-electron reduction, 7-phenyl monocation gave a stable free radical persisting in solution at room temperature, while the *para*-phenylene-connected dication did not give any radical species but a closed-shell hydrocarbon upon one-step, two-electron reduction. In the case of the *meta*-phenylene-connected dication, very closely spaced two reduction steps were observed upon cyclic

voltammetry and the resulting fully reduced species was identified as a triplet diradical by low-temperature ESR.

Thus, the present work revealed that the novel properties and unusual electronic states in cyclic π-systems, which would be hardly accomplished by other methods, can be attained by the use of σ–π interaction with rigid σ-frameworks. There is the significance in this study that the structural modification with hydrocarbons, which is a fundamental constituent of organic compounds, can endow new properties to the original π-systems, without a large perturbation in the electronic state such as the one brought about by introduction of a hetero atom into the π-systems. The experimental method developed in the present study could be applied to the synthesis of a larger cyclic π-systems or condensed aromatic π-systems annelated with rigid σ-frameworks. These new hydrocarbons are expected to have characteristic functionalities such as multiple-step electron-transfer, π-donor or π-acceptor ability, or specific complexation with certain metal ions.

List of Publications

1) Komatsu, K.; Nishinaga, T.; Aonuma, S.; Hirosawa, C.; Takeuchi, K.; Lindner, H. J.; Richter, J. *Tetrahedron Lett.* **1991**, *32*, 6767. (Chapter 2)

2) Nishinaga, T.; Komatsu, K.; Sugita, N.; Lindner H. J.; Richter, J. *J. Am. Chem. Soc.* **1993**, *115*, 11642. (Chapter 3)

3) Nishinaga, T.; Komatsu, K.; Sugita, N. *J. Chem. Soc., Chem. Commun.* **1994**, 2319. (Chapter 3)

4) Komatsu, K.; Nishinaga, T.; Takeuchi, K.; Lindner, H. J.; Richter, J. *J. Org. Chem.* **1994**, *59*, 7322. (Chapter 4)

5) Nishinaga, T.; Komatsu, K.; Sugita, N. *J. Org. Chem.* in press. (Chapter 5)

6) Kagayama, A.; Komatsu, K.; Nishinaga, T.; Takeuchi, K.; Kabuto, C. *J. Org. Chem.* **1994**, *59*, 4999. (Chapter 6)

7) Komatsu, K.; Nishinaga, T.; Maekawa, N.; Kagayama, A.; Takeuchi, K. *J. Org. Chem.* **1994**, *59*, 7316. (Chapter 7)

Acknowledgment

I wish to express my sincere gratitude to Professor Nobuyuki Sugita and Professor Ken'ichi Takeuchi for their encouragement and valuable guidance. I am deeply grateful to Associate Professor Koichi Komatsu for his inspiring suggestion and discussion throughout the course of this investigation. My thanks are also due to Associate Professor Tomomi Kinoshita, Dr. Toshikazu Kitagawa, Dr. Sadayuki Mori, Dr. Kiyoshi Kudo for their helpful advice. I would like to express my grateful acknowledgment to Professor Hans J. Lindner and Mr. Jens Richter of Technische Hochschule Darmstadt for X-ray crystallography of the cyclooctatetraene derivatives (Chapter 2, 3) and the bicyclo[2.2.2]octene-pentamer (Chapter 4), to Dr. Chizuko Kabuto for X-ray crystallography of the bis-tropylium derivative (Chapter 6), and to Professor Jun Yamauchi and Mr. Hideo Fujita of Kyoto University for ENDOR measurement (Chapter 3). Also, I am gratefully indebted to Dr. Syuji Aonuma, Dr. Chitaru Hirosawa, Mrs. Naoko Ohwada, nee Maekawa, and Mr. Akifumi Kagayama for their valuable collaboration. Finally, I would like to gratefully acknowledge the assistance and encouragement of my parents.